ISSN 0352-5139
J. Serb. Chem. Soc. Vol. 68, No. 11 (2003)

CONTENTS

Published by the Serbian Chemical Society, Karnegijeva 4/III,
P. O. Box 35-08, 11001 Belgrade, Serbia and Montenegro
Printed by the Faculty of Technology and Metallurgy, Karnegijeva 4,
P. O. Box 35-03, 11001 Belgrade, Serbia and Montenegro

J. Serb. Chem. Soc. 68(11)785–794(2003)
JSCS – 3098

UDC 547.992+547.324–31:541.63:66.025.252
Original scientific paper

Oxidative fragmentations of 5-hydroxy-1-oxo-5α-cholestan-3β-yl acetate

NATALIJA M. KRSTIĆ[a,*#], MIRA S. BJELAKOVIĆ[a], LJUBINKA B. LORENC[a,b#] and VLADIMIR D. PAVLOVIĆ[a,b#]

[a]*Center for Chemistry, ICTM, P. O. Box 473, 11001 Belgrade and* [b]*Faculty of Chemistry, University of Belgrade, Studentski trg 12-16, P. O. Box 158, 11001 Belgrade, Serbia and Montenegro*

(Received 22 May 2003)

Abstract: 5-Hydroxy-1-oxo-5α-cholestan-3β-yl acetate (**11**) was prepared in 5 steps starting from (*E*)-3β-acetoxy-5,10-seco-1(10)-cholesten-5-one (**6**). Treatment of the 1-oxo-5-hydroxy derivative **11** with lead tetraacetate (LTA) (under thermal or hypoiodite conditions) or with mercuric oxide/iodine (HgO/I_2) reagent resulted in the oxidative β-fragmentation of the C(5)–C(10) bond affording 1,5-dioxo-5,10-secocholest-10(19)-en-3β-yl acetate (**12**), in different yields, depending on the reagent. Also the stereochemistry of the 1β,6β-cyclization product **13**, formed by transannular cyclization of the 1,5-diketone **12** on silica gel, is discussed in this work.

Keywords: 5-Hydroxy-1-oxo-5α-cholestan-3β-yl acetate, 1,5-dioxo-5,10-secocholest-10(19)-en-3β-yl acetate, β-fragmentation, transannular cyclization.

INTRODUCTION

It is well known that the alkoxy radical ***i*** (generated by the oxidation of the 5-hydroxy steroids **1** and **2** with lead tetraacetate (LTA) under thermal or photolytic conditions or with hypoiodite-forming reagents) readily undergoes β-fragmentation involving scission of the C(5)–C(10) bond, to afford, *via* the C(10)-radical intermediate ***ii***, the diastereomeric (*Z*)- and (*E*)-1(10)-unsaturated 5,10-secosteroidal 5-ketones **3** and **4** in different proportions and, depending on the oxidant used, in high yield (Scheme 1).[1–3]

The direction of β-fragmentation in **1** and **2** to give exclusively the 5,10-secoketones **3** and **4** was explained by the stability of the tertiary C-radical intermediate ***ii***, due to the presence of the angular Me(19) group at the C(10)-radical center.

In accordance with such an explanation, it was anticipated that other 5-hydroxy steroids with similar structures and with the same reagents should react in the same way. However, when LTA oxidations (thermal and hypoiodite) of the 5-hydroxy-8,9-seco-8,9-diketone **5**, a

* Corresponding author. E-mail: nkrstic@chem.bg.ac.yu
# Serbian Chemical Society active member.

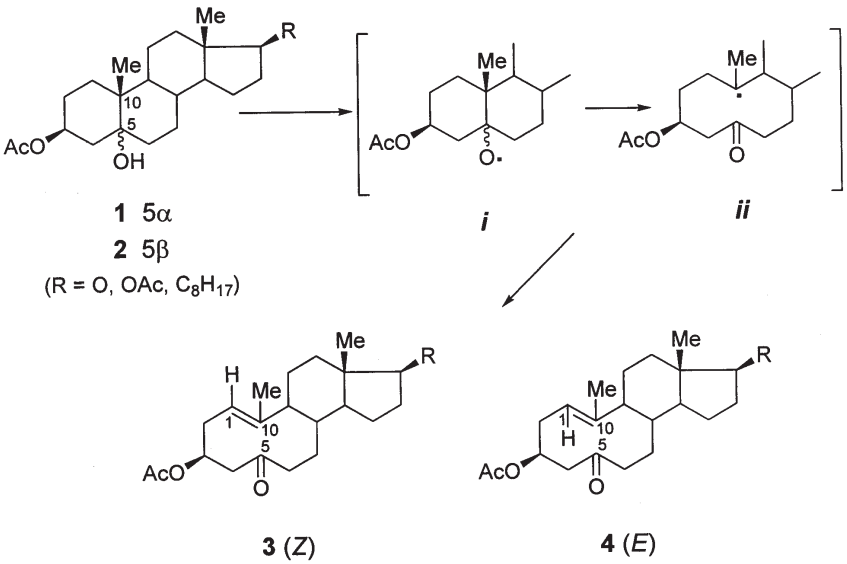

Scheme 1.

substrate with a polar oxo-group located at the α-position to the corresponding C(10)-radical center (type ***ii***), were performed under similar experimental conditions, the only obtained product was an unresolvable mixture of the 7-, 11- and 14-acetoxy derivatives arising from the competing acetoxylation of the α-positions next to the C(8)- and C(9)-oxo groups.

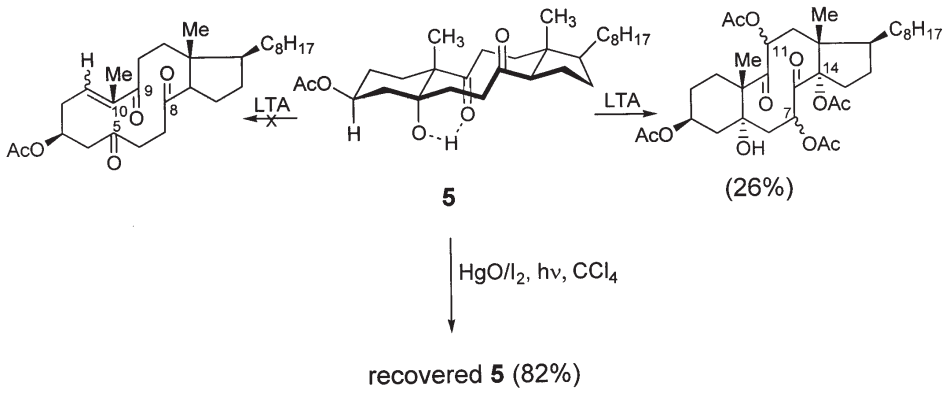

Scheme 2.

On the other hand, when the oxidative fragmentation of the C(5)–C(10) bond in compound **5** was attempted with HgO/I_2 reagent, practically all the starting material remained unchanged (recovery being ≈ 82 %, while the rest was an unresolvable mixture) (Scheme 2).[4]

The resistance of compound **5** to undergo oxidative β-fragmentation of its C(5)–C(10) bond was explained by strong hydrogen bonding between the 5-OH group and the 9-oxo

function. As a consequence of this interaction, the formation of the alkoxy radical was suppressed.

RESULTS AND DISCUSSION

In order to obtain more information concerning the influence of an oxo-group in the α-position to the C(10) on the oxidative fragmentation of the C(5)–C(10) bond, in the present work the possibility of inducing oxidative β-fragmentation of 5-hydroxy-1-oxo-5α-cholestan-3β-yl acetate (**11**) was investigated.

For the introduction of an oxygen function at the C(1)-position, the ten-membered ring containing (*E*)-3β-acetoxy-5,10-seco-1(10)-cholesten-5-one (**6**) was required. This compound was prepared from cholestane-3β,5α-diol 3-acetate according to the procedure given in Ref. 3. Substrate **11** was then synthesized in 5 steps, as shown in Scheme 3.

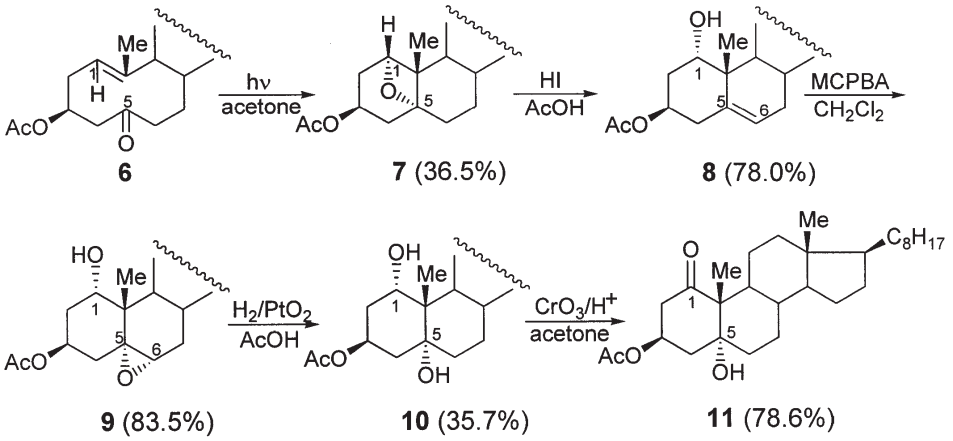

6 **7** (36.5%) **8** (78.0%)

9 (83.5%) **10** (35.7%) **11** (78.6%)

Scheme 3.

UV irradiation of **6** in acetone solution with a high pressure mercury lamp (TQ 150 Z2) afforded a photoproduct (Paterno-Büchi reaction) with an oxetane structure, *i.e.* 1α,5-epoxy-5α-cholestan-3β-yl acetate (**7**)[5] in 36.5 % yield. Treatment of the oxetane derivative **7** with hydroiodic acid in glacial acetic acid at 5 ºC resulted in the opening of the four-membered ether ring and the formation of cholest-5-en-1α,3β-diol 3-acetate (**8**) in high yield (78.0 %).[5] The epoxy derivative **9** was prepared by *m*-chloroperbenzoic acid (MCPBA) oxidation of **8** (in 83.5 % yield).[6] This product under conditions of catalytic hydrogenation (performed over PtO_2 in acetic acid solution) gave 5α-cholestan-1α,3β,5-triol 3-acetate (**10**)[7] (35.7 %). Jones oxidation of the triol-monoacetate **10** in acetone solution at –5 ºC afforded the 5-hydroxy-1-oxo-5α-cholestan-3β-yl acetate (**11**) in 78.6 % yield.

Oxidations of alcohol **11** were performed with hypoiodite-forming reagents and LTA (thermal) under conditions similar to those previously applied to compounds **1**, **2** and **5**.[1–4]

The HgO/I_2 version of the hypoiodite reaction of **11** performed with an excess of oxidant in CCl_4 solution by irradiation with a 15 W-lamp at 220 V at room temperature for

90 min in the presence of air gave, besides starting material **11** (20 %), an unresolvable complex mixture from which not one product with a defined structure could be isolated. The same results were obtained when the reaction was performed under O_2. However, when the above irradiation was performed under Ar, the resulting mixture of reaction products, after separation by column chromatography on silica gel, gave the 1,5-dioxo-5,10-secocholest-10(19)-en-3β-yl acetate (**12**) (38 %), the starting compound **11** (27 %) and the cyclization product **13** (28 %) (Scheme 4).

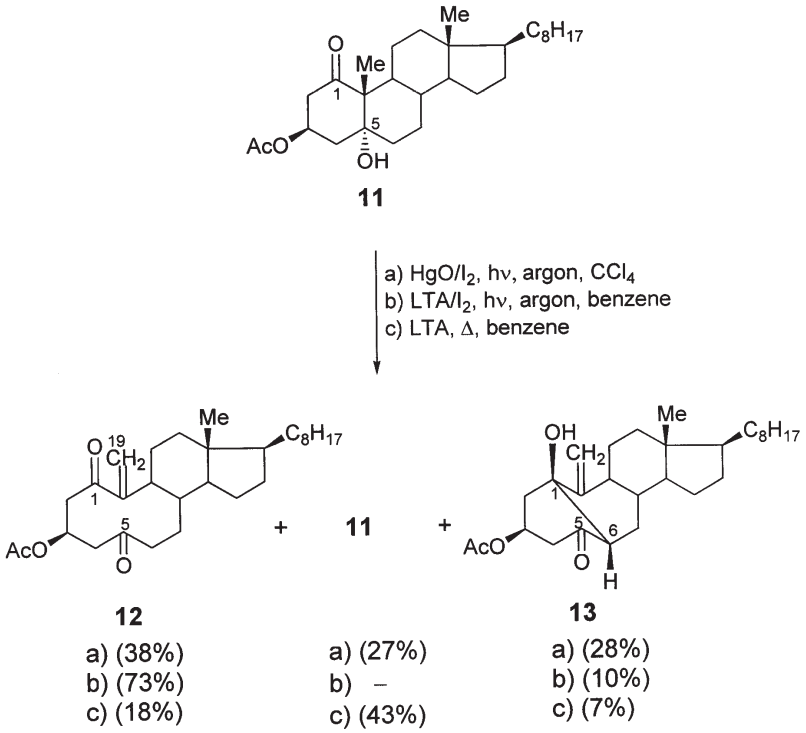

Scheme 4.

The structure of the product **12** was deduced from its analytical and spectral data (IR, ^{1}H-NMR, ^{13}C-NMR, MS). In the IR spectrum, the absorption of the 1-oxo group migrates from 1716 to 1670 cm^{-1}, indicating an α,β-unsaturated carbonyl, and the absorption for the original 5α-hydroxyl group was missing and instead a new absorption at 1701 cm^{-1} for the 5-oxo group appeared. In the ^{13}C-NMR spectrum, a new singlet appeared at 207.7 ppm for C(5). The presence of the exocyclic methylidene group CH_2=C(10) was evident from the IR spectrum (absorptions at 3100 and 1620 cm^{-1}) and confirmed by ^{1}H- and ^{13}C-NMR data. Instead of the signal for the Me(19) group, the ^{1}H-NMR spectrum showed a pair of singlets at 5.83 and 6.15 ppm, and the ^{13}C-NMR spectrum showed a triplet at 124.6 ppm for C(19) and a singlet at 155.0 ppm for C(10). Also, in the ^{13}C-NMR spectrum, a singlet at 199.4 ppm for C(1) in the 1,5-diketone **12** was situated upfield when compared to the resonance at 209.4 ppm for C(1) in compound **11**, indicating the influence of the exocyclic methylidene group in the α-position.

Compound **13** is a secondary reaction product, formed by intramolecular 1,6-cyclization of the 1,5-diketone **12**. This was confirmed by prolonged stirring (24 hours) of compound **12** with SiO_2 in toluene solution which afforded, besides the starting material, only one product, *i.e.* compound **13** (Scheme 5).

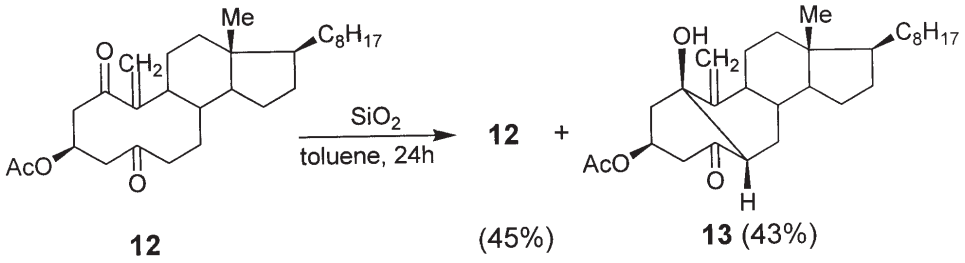

Scheme 5.

The structure of **13** was deduced from its analytical and spectral data (IR, ^{1}H-NMR, ^{13}C-NMR, MS). In the IR spectrum, the absorption of the 1-oxo group was replaced by a new absorption at 3483 cm^{-1} of the 1-hydroxy group. The IR band at 1643 cm^{-1} indicates that the exocyclic methylidene group still existed, which was confirmed by ^{1}H- and ^{13}C-NMR data. Its ^{1}H-NMR spectrum contained a pair of singlets at 4.86 and 5.00 ppm of the CH_2=C(10) group. Also, the ^{13}C-NMR spectrum contained the following characteristic signals: a triplet at 105.4 ppm of the C(19), a singlet at 74.0 ppm of the C(1) and a doublet at 56.0 ppm of the C(6). The *cis*-1β,6β-stereochemistry for the cyclization product **13** was deduced from its ^{1}H-NMR spectral characteristics. The signal for the H_β–C(6) (due to the deshielding influence by the 5-carbonyl group), was shifted downfield and appeared at 2.88 ppm as a *fine doublet of doublets*, indicating a dihedral angle of about 60º (J = 5.5 Hz) between the H_β–C(6) and H_β–C(7) and 180º (J = 13.5 Hz) between the H_β–C(6) and H_2C(7), and the "W" arrangement of the H_β–C(6)–C(5)–C(4)–H_β (J = 1.8 Hz), which is present only in the 1β,6β-isomer.

The LTA version of the hypoiodite reaction[8] of **11** was carried out with a large excess of oxidant in benzene solution by irradiation with a 15 W-lamp at 220 V at room temperature for 30 min, *i.e.*, until **11** had been completely consumed. The resulting mixture was separated by column chromatography (silica gel), affording the previously described compound **12** in a very good yield of 73 % and the cyclization product **13** in a 10 % yield (Scheme 4).

The thermal LTA oxidation of **11** was carried out with an excess of oxidant in the presence of $CaCO_3$ in boiling benzene for 48 h (practically, the reaction mixture was not changed after 4 h). After separation by chromatography on silica gel, the reaction mixture gave 1,5-dioxo-5,10-secocholest-10(19)-en-3β-yl acetate (**12**) (18 %), the starting compound **11** (43 %) and the cyclization product **13** (7 %) (Scheme 4).

From the above results it follows that the described oxidations of 5-hydroxy-1-oxo-5α-cholestan-3β-yl acetate (**11**) proceed (exclusively with HgO/I_2 and LTA/I_2 under Ar) as

expected *via* the C(10)-centered radical **C** (Scheme 6) which is formed according to the generally accepted mechanism,[8,9] *i.e.*, the homolysis of the O–I bond in the primarily formed species **A** is followed by fragmentation of the C(5)–C(10) bond in the thus obtained alkoxy radical **B**. The radical **C** is then stabilized by elimination of a H-atom from the Me(19) to give the 10-methylidene seco ketone **12**.

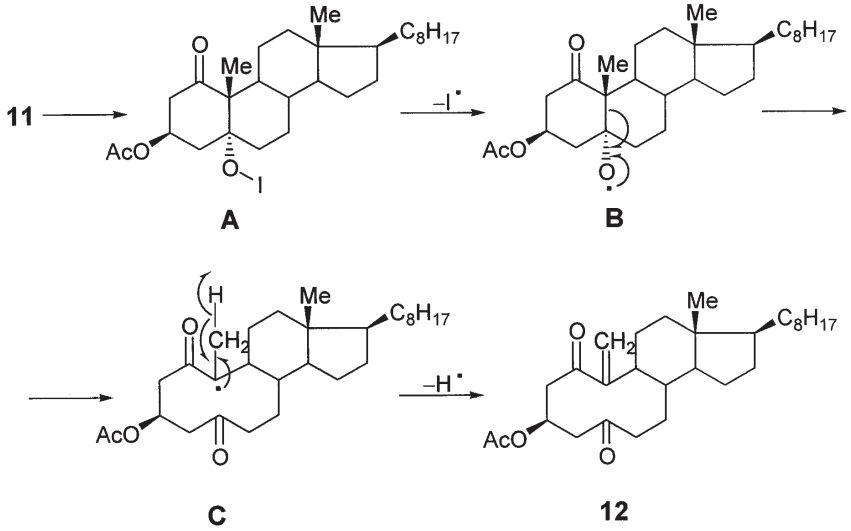

Scheme 6.

The formation of the cyclization product **13** may be explained by an acid-catalyzed intramolecular aldol reaction in compound **12** during the chromatography on SiO_2 (Scheme 7).

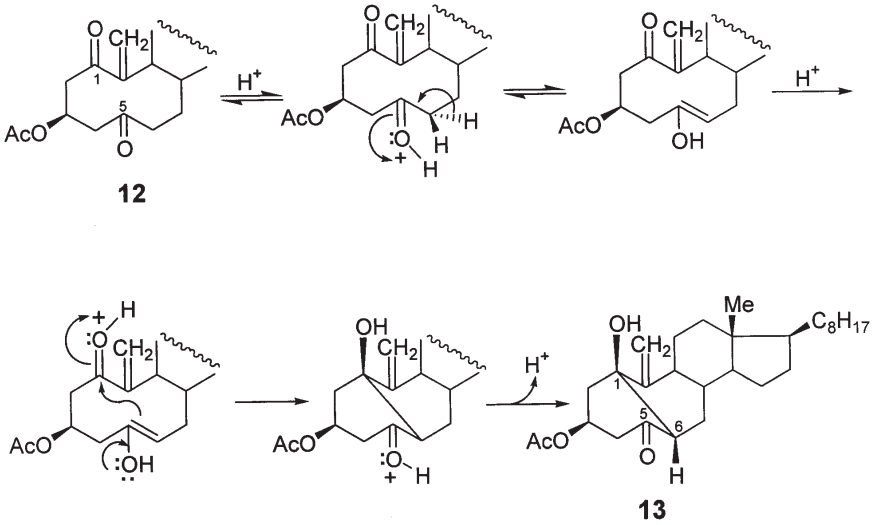

Scheme 7.

EXPERIMENTAL

General.

Prep. column chromatography: silica gel Merck 0.063–0.200 mm. TLC: control of reaction and separation of products on silica gel 60 F_{254} (Merck) with benzene/EtOAc 9:1, 8:2 and 7:3, detection with 50 % aq. H_2SO_4 soln. Mps.uncorrected. IR spectra: Perkin-Elmer-337 spectrophotometer; ν in cm^{-1}. NMR spectra: Varian Gemini 200 (^1H at 200 MHz, ^{13}C at 50 MHz); $CDCl_3$ soln. at r.t., TMS as internal standard; chemical shifts in ppm as δ values. *J* in Hz. Mass spectra: Finnigan-MAT 8230.

*1α 5-Epoxy-5α-cholestan-3β-yl acetate (**7**)*[5]

A stirred solution of (*E*)-5-oxo-5,10-secocholest-1(10)-en-3β-yl acetate (**6**) (2 g) in acetone (200 ml) was irradiated with a high pressure mercury lamp TQ 150 Z2 (Hanau) at room temperature for 6 h, evaporated to dryness and the oily residue (2.16 g) chromatographed on silica gel (100 g). Elution with toluene-EtOAc (98:2) gave the unchanged (*E*)-secoketone **6** (0.36 g, 18 %). Further elution with the same eluent gave 1α,5-epoxy-5α-cholestan-3β-yl acetate (**7**) (0.73 g, 36.5 %) as a white solid, m.p. 101–102 ºC (from acetone). $[\alpha]_D$ = +20±2 (*c* = 1.0). IR (CH_2Cl_2): 1732, 1238, 1025. ^1H-NMR: 0.68 (*s*, 3H, CH_3(18)), 0.85 (*s*, 3H, CH_3(19)), 0.88 (*d*, 6H, CH_3(26), CH_3(27)), 0.92 (*d*, 3H, CH_3(21)), 2.07 (*s*, 3H, AcO), 2.41 (*dd*, *J* = 9.8, 14.8, 1H, H_α–C(4)), 2.71 (*m*, 1H, H_α–C(2)), 3.99 (*d*, *J* = 5.8, 1H, H–C(1)), 5.24 (*m*, 1H, H–C(3)). ^{13}C-NMR: 170.7 (*s*, O*C*OCH$_3$), 88.6 (*s*, C(5)), 83.2 (*d*, C(1)), 66.7 (*d*, C(3)), 56.1 (2*d*, C(14), C(17)), 47.0 (*d*, C(9)), 45.4 (*s*, C(10)), 42.4 (*s*, C(13)), 39.8 (*t*, C(12)), 39.5 (*t*, C(24)), 38.6 (*t*, C(4)), 36.1 (*t*, C(22)), 35.8 (*d*, C(20)), 34.1 (*d*, C(8)), 31.5 (*t*, C(2)), 31.0 (*t*, C(6)), 28.1 (*t*, C(16)), 28.0 (*d*, C(25)), 27.8 (*t*, C(7)), 24.4 (*t*, C(15)), 23.8 (*t*, C(23)), 23.1 (*t*, C(11)), 22.8 (*q*, C(27)), 22.5 (*q*, C(26)), 21.3 (*q*, OCO*C*H$_3$), 18.7 (*q*, C(21)), 11.8 (*q*, C(18)), 11.7 (*q*, C(19)). MS: *m*/*z* = 444 (M^+). Anal. calcd. for $C_{29}H_{48}O_3$ (444.696): C 78.33, H 10.88; found: C 78.18, H 10.87.

*Cholest-5-en-1α,3β-diol 3-acetate (**8**)*[5]

The oxetane derivative **7** (2.30 g) was dissolved in glacial AcOH (47 ml) and cooled to 5 ºC. To this semi-solid solution, a cooled solution of hydroiodic acid (0.98 ml 57 % HI) in glacial AcOH (30.5 ml) was added portionwise. The resulting mixture was left at 5 ºC for 30 min, diluted with H_2O and extracted with Et_2O. The ethereal extract was washed with H_2O, saturated aq. $NaHCO_3$ and H_2O, dried over Na_2SO_4 and evaporated to dryness, leaving a crystalline solid (2.4 g) which was chromatographed on SiO_2 (100 g). Elution with toluene-EtOAc (95:5) gave cholest-5-en-1α,3β-diol 3-acetate (**8**) (1.80 g, 78 %), m.p. 166–168 ºC (from acetone). $[\alpha]_D$ = – 41 (*c* = 0.7). IR (KBr): 3450, 3020, 1730, 1275, 1040. ^1H-NMR: 0.68 (*s*, 3H, CH_3(18)), 0.86 (*d*, 6H, CH_3(26), CH_3(27)), 0.91, (*d*, 3H, CH_3(21)), 1.04 (*s*, 3H, CH_3(19)), 2.03 (*s*, 3H, AcO), 3.86 (*brs*, 1H, H–C(1)), 5.03 (*heptet*, 1H, H–C(3)), 5.61 (*bd*, *J* = 5.2, 1H, H–C(6)). ^{13}C-NMR: 170.6 (*s*, O*C*OCH$_3$), 136.2 (*s*, C(5)), 126.5 (*d*, C(6)), 72.5 (*d*, C(1)), 69.5 (*d*, C(3)), 56.5 (*d*, C(17)), 56.0 (*d*, C(14)), 42.2 (*s*, C(13)), 41.7 (*s*, C(10)), 41.4 (*d*, C(9)), 39.4 (2*t*, C(12), C(24)), 37.2 (*t*, C(2)), 36.1 (*t*, C(22)), 35.7 (*d*, C(20)), 34.4 (*t*, C(4)), 31.7 (*d*, C(8)), 31.7 (*t*, C(7)), 28.1 (*t*, C(16)), 28.0 (*d*, C(25)), 24.3 (*t*, C(15)), 23.8 (*t*, C(23)), 22.8 (*q*, C(27)), 22.5 (*q*, C(26)), 21.3 (*q*, OCO*C*H$_3$), 20.1 (*t*, C(11)), 19.3 (*q*, C(21)), 18.7 (*q*, C(19)), 11.8 (*q*, C(18)). MS: *m*/*z* = 384 (M^+ – 60, 99 %). Anal. calcd. for $C_{29}H_{48}O_3$ (444.696): C 78.33, H 10.88; found: C 78.31, H 10.69.

*5,6α-Epoxy-5α-cholestan-1α,3β-diol 3-acetate (**9**)*[6]

A solution of **8** (1.00 g) in CH_2Cl_2 (25 ml) was treated with 85 % *m*-chloroperbenzoic acid (500 mg in 25 ml CH_2Cl_2) at room temperature for 1 h. After the usual work–up, the obtained residue (0.980 g, 96.4 %) was recrystallized from acetone to give 5,6α-epoxy-5α-cholestan-1α,3β-diol 3-acetate (**9**) (0.865 g, 83.5 %), m.p. 156 ºC. $[\alpha]_D$ = –11.0 (*c* = 1.09). IR (KBr): 3450, 3030, 1730, 1710, 1275, 1042. ^1H-NMR: 0.62 (*s*, 3H, CH_3(18)), 0.86 (*d*, 6H, CH_3(26), CH_3(27)), 0.89 (*d*, 3H, CH_3(21)), 1.10 (*s*, 3H, CH_3(19)), 2.02 (*s*, 3H, AcO), 2.82 (*d*, *J* = 4.8, 1H, H–C(6)), 3.90 (*brs*, 1H, H–C(1)), 5.30 (*heptet*, 1H, H–C(3)). ^{13}C-NMR: 170.1 (*s*, O*C*OCH$_3$), 72.8 (*d*, C(3)), 67.6 (*d*, C(1)), 64.0 (*s*, C(5)), 56.7 (*d*, C(17)), 56.5 (*d*, C(6)), 55.8 (*d*, C(14)), 42.3 (2*s*, C(10), C(13)), 39.4 (*t*, C(24)), 39.0 (*t*, C(12)), 36.6 (*d*, C(9)), 36.1 (*d*, C(20)), 35.7 (*t*, C(4)), 35.6 (*t*, C(2)),

34.7 (*t*, C(22)), 29.8 (*d*, C(8)), 28.6 (*t*, C(16)), 28.0 (*d*, C(25)), 27.9 (*t*, C(7)), 24.1 (*t*, C(15), 23.8 (*t*, C(23)), 22.8 (*q*, C(27)), 22.5 (*q*, C(26)), 21.2 (*q*, OCO*C*H$_3$), 19.7 (*t*, C(11)), 18.6 (*q*, C(21)), 16.5 (*q*, C(19)), 11.8 (*q*, C(18)). Anal. calcd. for $C_{29}H_{48}O_4$ (460.699): C 75.61, H 10.50; found: C 74.43, H 10.68. CI-MS: *m*/*z* = 461 ($M^+ + 1$).

*5α-Cholestan-1α,3β,5-triol 3-acetate (**10**)*[7]

A solution of **9** (1.8 g) in AcOH–EtOH (10:1, 110 ml) was hydrogenated over PtO_2 (180 mg) in a Parr Hydrogenator at room temperature and 3 atm pressure, for 13 h. After removal of the catalyst and solvent, the residue was chromatographed on SiO_2 (120 g). Elution with toluene–EtOAc (95:5) afforded the unchanged starting compound **9** (0.86 g, 44.0 %). Elution with toluene–EtOAc (90:10) gave 5α-cholestan-1α,3β,5-triol 3-acetate (**10**) (0.70 g, 35.7 %), m.p. 178–179 ºC (from acetone). IR (KBr): 3368, 1737, 1467, 1374, 1247. ^{1}H-NMR: 0.66 (*s*, 3H, CH_3(18)), 0.85 (*d*, 6H, CH_3(26), CH_3(27)), 0.92 (*d*, 3H, CH_3(21)), 0.94 (*s*, 3H, CH_3(19)), 2.03 (*s*, 3H, AcO), 2.99 (*s*, 1H, OH–C(5)), 3.82 (*m*, 2H, H–C(1) and OH–C(1)), 5.41 (*heptet*, 1H, H–C(3)). ^{13}C-NMR: 170.8 (*s*, O*C*OCH$_3$), 77.3 (*s*, C(5)), 74.0 (*d*, C(3)), 67.8 (*d*, C(1)), 56.2 (*d*, C(17)), 56.0 (*d*, C(14)), 42.7 (*s*, C(13)), 41.4 (*s*, C(10)), 40.1 (*d*, C(9)), 39.7 (*t*, C(12)), 39.4 (*t*, C(24)), 36.1 (*t*, C(4)), 35.8 (*d*, C(20)), 35.1 (*t*, C(22)), 34.7 (*t*, C(6)), 34.6 (*d*, C(8)), 29.6 (*t*, C(2)), 28.2 (*t*, C(16)), 28.0 (*d*, C(25)), 25.6 (*t*, C(7)), 24.1 (*t*, C(15)), 23.9 (*t*, C(23)), 22.8 (*q*, C(27)), 22.5 (*q*, C(26)), 21.4 (*q*, OCO*C*H$_3$), 20.7 (*t*, C(11)), 18.6 (*q*, C(21)), 16.6 (*q*, C(19)), 12.1 (*q*, C(18)). CI-MS: *m*/*z* = 445 (463–18), 385 (463–60–18).

*5-Hydroxy-1-oxo-5α-cholestan-3β-yl acetate (**11**)*

To a cooled (–5 ºC) solution of **10** (1.26 g) in acetone (165 ml), a slight excess of Killiani's chromic acid solution was added with constant stirring. After 20 min ice-cold H_2O was added, the precipitate was filtered off, washed thoroughly with H_2O and air-dried to give a residue (1.2 g, 95.7 %), which was chromatographed on SiO_2 (40 g). Elution with toluene–EtOAc (95:5) afforded 5-hydroxy-1-oxo-5α-cholestan-3β-yl acetate (**11**) which was recrystallized from acetone (0.98 g, 78.6 %), m.p. 138.5–140 ºC. IR (KBr): 3494, 3454, 1716, 1377, 1245, 1032. ^{1}H-NMR: 0.66 (*s*, 3H, CH_3(18)), 0.85 (*d*, 6H, CH_3(26), CH_3(27)), 0.88 (*d*, 3H, CH_3(21)), 1.28 (*s*, 3H, CH_3(19)), 2.04 (*s*, 3H, AcO), 2.62 (*dd*, *J* = 6.8, 13.4, 1H, H_α–C(4)), 2.81 (*dd*, *J* = 10.8, 12.8, 1H, H_β–C(2)), 5.30 (*m*, H–C(3)). ^{13}C-NMR: 209.4 (*s*, C(1)), 170.2 (*s*, O*C*OCH$_3$), 76.0 (*s*, C(5)), 69.2 (*d*, C(3)), 56.2 (*d*, C(17)), 55.8 (*d*, C(14)), 53.8 (*s*, C(10)), 43.1 (*t*, C(2)), 42.7 (*s*, C(13)), 41.0 (*d*, C(9)), 39.8 (*t*, C(12)), 39.4 (*t*, C(24)), 39.2 (*t*, C(4)), 36.1 (*d*, C(22)), 35.8 (*t*, C(20)), 34.9 (*d*, C(8)), 33.6 (*t*, C(6)), 28.0 (*t*, C(16)), 27.9 (*d*, C(25)), 24.9 (*t*, C(7)), 24.0 (*t*, C(15)), 23.9 (*t*, C(23)), 22.8 (*t*, C(11)), 22.8 (*q*, C(27)), 22.5 (*q*, C(26)), 21.2 (*q*, OCO*C*H$_3$), 18.5 (*q*, C(21)), 16.4 (*q*, C(19)), 12.3 (*q*, C(18)). MS: *m*/*z* = 460 (M^+), 443 (460–17), 401 (460–59), 383 (460–60–17).

*Oxidation of 5-hydroxy-1-oxo-5α-cholestan-3β-yl acetate (**11**)*

(i) Hypoiodite mercuric oxide/iodine oxidation. A stirred suspension of **11** (100 mg, 0.217 mmol), yellow HgO (325 mg, 1.5 mmol) and I_2 (437 mg, 1.7 mmol) in CCl_4 (30 ml) was irradiated with a 15 W (220 V) fluorescent lamp for 90 min without heating. All the time argon was introduced through the reaction mixture. The solid was removed by filtration, washed with Et_2O, and filtrate washed successively with water, 10 % aq. $Na_2S_2O_3$, saturated $NaHCO_3$ and water, dried over Na_2SO_4 and evaporated to dryness. The resulting mixture (111 mg) was chromatographed on silica gel (10 g). Elution with toluene-EtOAc (99:1, 98:2, 97:3) afforded a complex mixture (11 mg) which was not further investigated. Toluene–EtOAc (96:4) eluted 1,5-dioxo-5,10-secocholest-10(19)-en-3β-yl acetate **12** which was recrystallized from acetone/methanol (38 mg, 38 %), m.p. 157–158 ºC. IR (KBr): 1735, 1701, 1672, 1620, 1251, 1032. ^{1}H-NMR: 0.74 (*s*, 3H, CH_3(18)), 0.86 (*d*, 6H, CH_3(26), CH_3(27)), 0.90 (*d*, 3H, CH_3(21)), 2.05 (*s*, 3H, AcO), 2.44 (*m*, 2H, H_2–C(6)), 2.65 (*dd*, *J* = 3.5, 15.7, 1H, H–C(4)), 2.93 (*d*, *J* = 11.4, 1H, H–C(4)), 3.00 (*ABq*, *J* = 3.6, 2H, H_2C(2)), 5.60 (*m*, H–C(3)), 5.83 and 6.15 (2*s*, 2H, H_2C(19)). ^{13}C-NMR: 207.7 (*s*, C(5)), 199.4 (*s*, C(1)), 169.8 (*s*, O*C*OCH$_3$), 155.0 (*s*, C(10)), 124.6 (*t*, C(19)), 68.8 (*d*, C(3)), 56.1 (*d*, C(17)), 54.2 (*d*, C(14)), 46.5 (*t*, C(4)), 44.5 (*d*, C(9)), 43.1 (*t*, C(2)), 42.5 (*s*, C(13)), 41.8 (*t*, C(12)), 39.7 (*t*, C(24)), 39.5 (*t*, C(6)), 38.3 (*d*, C(8)), 36.0 (*t*, C(22)), 35.7 (*t*, C(20)), 33.4 (*t*, C(7)), 28.0 (*d*, C(25)), 27.8 (*t*, C(16)), 26.8 (*t*, C(15)), 24.9 (*t*, C(11)), 23.8 (*t*, C(23)), 22.8 (*q*, C(27)), 22.5 (*q*, C(26)), 21.1 (*q*, OCO*C*H$_3$), 18.6 (*q*, C(21)), 11.8 (*q*, C(18)), CI-MS: *m*/*z* = 459 ($M^+ + 1$).

Further elution with the same eluent afforded the starting compound **11** (27 mg, 27 %).

Further elution with toluene–EtOAc (95:5) gave compound **13** (28 mg, 28 %). Oil. IR (KBr): 3483, 1732, 1708, 1643, 1269, 1028. ^{1}H-NMR: 0.67 (*s*, 3H, CH_3(18)), 0.85 (*d*, 6H, CH_3(26), CH_3(27)), 0.92 (*d*, 3H, CH_3(21)), 2.08 (*s*, 3H, AcO), 2.20–2.64 (*m*, 4H, H_2C(2), H_2C(4)), 2.88 (*fdd*, *J* = 1.8, 5.5, 13.5, 1H, H_β–C(6)), 4.86 and 5.00 (2*fs*, *J* = 1.6, 2H, H_2–C(19)), 5.38 (*heptet*, 1H, H–C(3)). ^{13}C-NMR: 206.2 (*s*, C(5)), 170.2 (*s*, O*C*OCH$_3$), 154.3 (*s*, C(10)), 105.4 (*t*, C(19)), 74.0 (*s*, C(1)), 69.2 (*d*, C(3)), 56.7 (*d*, C(17)), 56.0 (2*d*, C(6), C(14)), 46.5 (*t*, C(4)), 42.8 (*s*, C(13)), 42.3 (*d*, C(9)), 41.1 (*d*, C(8)), 40.4 (*t*, C(2)), 39.4 (*t*, C(12)), 39.3 (*t*, C(24)), 36.1 (*t*, C(22)), 35.8 (*d*, C(20)), 29.7 (*t*, C(7)), 28.2 (*t*, C(16)), 28.0 (*d*, C(25)), 25.3 (*t*, C(15)), 24.8 (*t*, C(11)), 23.8 (*t*, C(23)), 22.8 (*q*, C(27)), 22.5 (*q*, C(26)), 21.2 (*q*, OCO*C*H$_3$), 18.6 (*q*, C(21)), 12.0 (*q*, C(18)).

(ii) Hypoiodite lead tetraacetate/iodine oxidation. A stirred suspension of LTA (450 mg, 0.91 mmol), I_2 (94 mg, 0.37 mmol) and **11** (100 mg, 0.217 mmol), in dry benzene was irradiated with a 15 W (220 V) fluorescent lamp at room temperature for 30 min. All the time argon was introduced through the reaction mixture. The solid was removed by filtration, washed with Et_2O and filtrate washed successively with water, 10 % aq. $Na_2S_2O_3$, saturated $NaHCO_3$ and water, dried over Na_2SO_4 and evaporated to dryness. The resulting mixture (141 mg) was chromatographed on silica gel (10 g). Elution with toluene–EtOAc (99:1, 98:2, 97:3) afforded a complex mixture (17 mg) which was not further investigated. Toluene–EtOAc (96:4) eluted 1,5-dioxo-5,10-secocholest-10(19)-en-3β-yl acetate **12** which was recrystallized from acetone/methanol (73 mg, 73 %), m.p. 157–158 ºC.

Further elution with toluene–EtOAc (95:5) gave compound **13** (10 mg, 10 %).

(iii) Thermal lead tetraacetate oxidation. A suspension of **11** (100 mg, 0.217 mmol), LTA (450 mg, 0.900 mmol) and anh. $CaCO_3$ (95 mg, 0.960 mmol) in anh. benzene (15 ml) was heated under reflux with stirring for 48 h, after which time the starch-iodine test became negative. The cooled mixture was diluted with Et_2O, washed with water, sat. aq. $NaHCO_3$ and water, dried over Na_2SO_4 and evaporated to dryness. The resulting mixture (116 mg) was chromatographed on silica gel (20 g). Elution with toluene–EtOAc (99:1, 98:2, 97:3) afforded a complex mixture (15 mg, 15 %) which was not further investigated. Toluene–EtOAc (96:4) eluted the 1,5-dioxo compound **12** (18 mg, 18 %).

Further elution with same eluent afforded the starting compound **11** (43 mg, 43 %).

Elution with toluene–EtOAc (95:5) gave the cyclic compound **13** (7 mg, 7 %).

*Cyclization of 1,5-dioxo-5,10-secocholest-10(19)-en-3β-yl acetate **12** on SiO_2*

1,5-Diketone **12** (40 mg) was stirred with SiO_2 (Merck, 0.063–0.20 mm) in toluene (5 ml) for 24 h at room temperature. After removal of the SiO_2 and solvent the residue was chromatographed on SiO_2 (4 g). Elution with toluene–EtOAc (96:4) gave unchanged starting material **12** (18 mg, 45 %).

Further elution with toluene–EtOAc (95:5) afforded compound **13** (17.2 mg, 43 %).

Acknowledgement: The authors acknowledge financial support by the Ministry of Science, Technology and Development of Serbia. (Part of the project "Synthesis and chemical transformations of steroidal and modified steroidal molecules" - Project No. 1702).

ИЗВОД

ОКСИДАТИВНЕ ФРАГМЕНТАЦИЈЕ 5-ХИДРОКСИ-1-ОКСО-5α-ХОЛЕСТАН-3β-ИЛ-АЦЕТАТА

НАТАЛИЈА М. КРСТИЋ[а], МИРА С. БЈЕЛАКОВИЋ[а], ЉУБИНКА Б. ЛОРЕНЦ[а,б] и ВЛАДИМИР Д. ПАВЛОВИЋ[а,б]

[а]Центар за хемију, ИХТМ, п. пр. 473, 11001 Београд и [б]Хемијски факултет, Универзитет у Београду, Студентски трг 12-16, п. пр. 158, 11001 Београд

Синтетизован је 5-хидрокси-1-оксо-5α-холестан-3β-ил-ацетат (**11**) у 5 фаза полазећи од (*E*)-3β-ацетокси-5,10-секо-1(10)-холестен-5-она (**6**). Дејством олово-тетраацетата (LTA) (под термичким или хипојодитним условима), или меркури-оксид/јодног реагенса (HgO/I_2) на 1-оксо-5-хидрокси дериват **11**, врши се оксидативна β-фрагментација његове C(5)–C(10) везе, при чему се добија 1,5-диоксо-5,10-секохолест-10(19)-ен-3β-ил-ацетат (**12**), у различитим приносима у зависности од употребљеног реагенса. Такође, дискутована је стереохемија 1β,6β-циклизационог производа **13**, насталог интрамолекулском циклизацијом 1,5-диоксо-5,10-секо једињења **12** на силика гелу.

(Примљено 22. маја 2003)

REFERENCES

1. M. Lj. Mihailović, Lj. Lorenc, M. Gašić, M. Rogić, A. Melera, M. Stefanović, *Tetrahedron* **22** (1966) 2345
2. M. Akhtar, S. March, *J. Chem. Soc. (C)* (1966) 937
3. M. Lj. Mihailović, Lj. Lorenc, J. Foršek, V. Pavlović, M. Dabović, J. Kalvoda, *J. Serb. Chem. Soc.* **54** (1989) 645
4. M. Lj. Mihailović, M. M. Dabović, V. D. Pavlović, N. M. Krstić, Lj. B. Lorenc, *J. Serb. Chem. Soc.* **62** (1997) 719
5. M. Lj. Mihailović, Lj. Lorenc, V. Pavlović, J. Kalvoda, *Tetrahedron* **33** (1977) 441
6. M. Dabović, M. Bjelaković, V. Andrejević, Lj. Lorenc, M. Lj. Mihailović, *Tetrahedron* **50** (1994) 1833
7. Pl. A. Plattner, H. Heuser, A. B. Kulkarni, *Helv. Chim. Acta* **32** (1941) 267
8. J. Kalvoda, K. Heusler, *Synthesis* (1971) 525
9. K. Heusler, J. Kalvoda, *Angew. Chem. Int. Ed. Engl.* **3** (1964) 525
10. M. Lj. Mihailović, Ž. Čeković, *Synthesis* (1970) 209.

J.Serb.Chem.Soc. 68(11)795–804(2003)
JSCS – 3099

UDC 547.455.5+547.473:542.913:541.25
Original scientific paper

A formal synthesis of (+)-muricatacin from D-xylose

VELIMIR POPSAVIN[a*#], SANJA GRABEŽ[a#], IVANA KRSTIĆ[a#], MIRJANA POPSAVIN[a#] and DEJAN DJOKOVIĆ[b#]

[a]*Department of Chemistry, Faculty of Science, University of Novi Sad, Trg D. Obradovića 3, 21000 Novi Sad and* [b]*Faculty of Chemistry, University of Belgrade, Studentski trg 16, P. O. Box 158, 11001 Belgrade, Serbia and Montenegro*

(Received 9 June 2003)

Abstract: A multistep route towards the aldehydo-lactone **19**, the final chiral precursor in a new stereospecific synthesis of (+)-muricatacin, has been developed starting from D-xylose. The key step of the synthesis involves an *E*-selective Wittig olefination of the lactol **6** with methoxycarbonylmethylidene triphenylphosphorane, followed by successive catalytic reduction and γ-lactonisation processes. Subsequent selective functional groups interconversions furnished the key six-carbon intermediate **19**, which can be converted into the (+)-muricatacin *via* a three-step sequence already described in the chemical literature.

Keywords: muricatacin, Wittig reaction, γ-lactone, stereospecific synthesis, D-xylose.

INTRODUCTION

Muricatacin (5-hydroxyheptadecan-4-olide) is an acetogenin related γ-lactone which has attracted considerable attention since its recent isolation from the seeds of *Anona muricata*[1] owing to its cytotoxic activity against certain human tumour cells. Remarkably, the natural muricatacin is a mixture of (+)-(4*S*,5*S*)-5-hydroxyheptadecan-4-olide (**1**, Scheme 1) and its (–)-(4*R*,5*R*)-entantiomer, with the latter being predominant (ee of *ca.* 25 %). Both (+)- and (–)-muricatacin have shown the same antitumour activity.[1,2] The biological activity of muricatacin and other related compounds has stimulated a significant interest in the synthesis of this type of 5-hydroxyalkylbutan-4-olides. Many syntheses of (+)- and (–)-muricatacin and congeners from various non-carbohydrate precursors have been reported,[3] as well as a number of carbohydrate based approaches to the (–)-muricatacin.[4] However, only two syntheses of (+)-muricatacin (**1**) from carbohydrate precursors have been described so far. A stereoselective approach from L-glyceraldehyde,[5] as well as a stereospecific synthesis of (+)-**1** based on chirality transfer from D-glucose.[6] Herein an alternative route to the final chiral precursor in a new stereospecific synthesis of (+)-muricatacin (**1**) from D-xylose is reported.[7]

* Author for correspondence. Fax +381-21-454-065; e-mail address: popsavin@ih.ns.ac.yu
# Serbian Chemical Society active member.

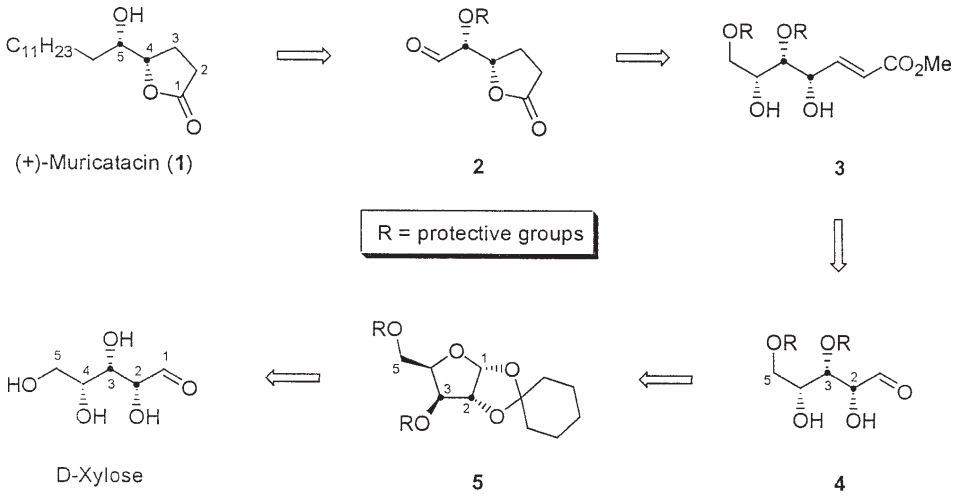

Scheme 1. Retrosynthetic analysis of (+)-muricatacin (**1**).

RESULTS AND DISCUSSION

The retrosynthetic analysis of (+)-muricatacin (**1**) outlined in Scheme 1 shows that this molecule might be available from an advanced intermediate of type **2** *via* a sequential Wittig elongation/catalytic hydrogenation manoeuvre followed by deprotection. Further disconnection of **2** shows that it can be derived from the enoate **3** by a number of selective transformations that involve successive catalytic hydrogenation, γ-lactonisation, 7-*O*-deprotection and an oxidative 6,7-glycol-cleavage process. Compound **3** can be further traced retrosynthetically to the 3,5-di-*O*-protected D-xylose derivative **4** *via* an *E*-selective Wittig transformation. Compounds of type **4** are readily available from D-xylofuranose derivatives of type **5** after hydrolytic removal of the 1,2-*O*-cyclohexylidene protective group. Accordingly, the 3,5-di-*O*-benzyl-D-xylose (**6**, Scheme 2), earlier prepared in our laboratory starting from D-xylose,[8] was chosen as a suitable starting compound in this work.

The crucial problem for elaboration of the 5-hydroxy-γ-lactone moiety in target (+)-**1** was the two-carbon homologation of **6** by the Wittig reaction with methoxycarbonylmethylidene triphenylphosphorane. The *E*-selectivity of the process is essential, because it is well known that some related *Z*-unsaturated esters may undergo a sequential lactonisation/Michael ring closure process.[9] Indeed, the preliminary experiments carried out with the lactol **6** confirmed that, depending on reaction conditions, the expected *E*-unsaturated derivative **8** was accompanied with variable amounts of the bicyclic lactone **7**, while the corresponding *Z*-stereoisomer could not be detected in the reaction mixtures. A reasonable chemoselectivity (**8**:**7** = 6:1) was achieved when the reaction was carried out in *N*,*N*-dimethylformamide at 65 ºC, whereupon the desired product **8** was isolated in 74 % yield.

Catalytic hydrogenation of **8** over PtO_2 in ethanol yielded the expected saturated ester **9**, which on exposure to 2:1 trifluoroacetic acid – water gave the γ-lactone **10** in an almost quantitative yield. Alternatively, catalytic reduction of **8** over the Adams catalyst in glacial

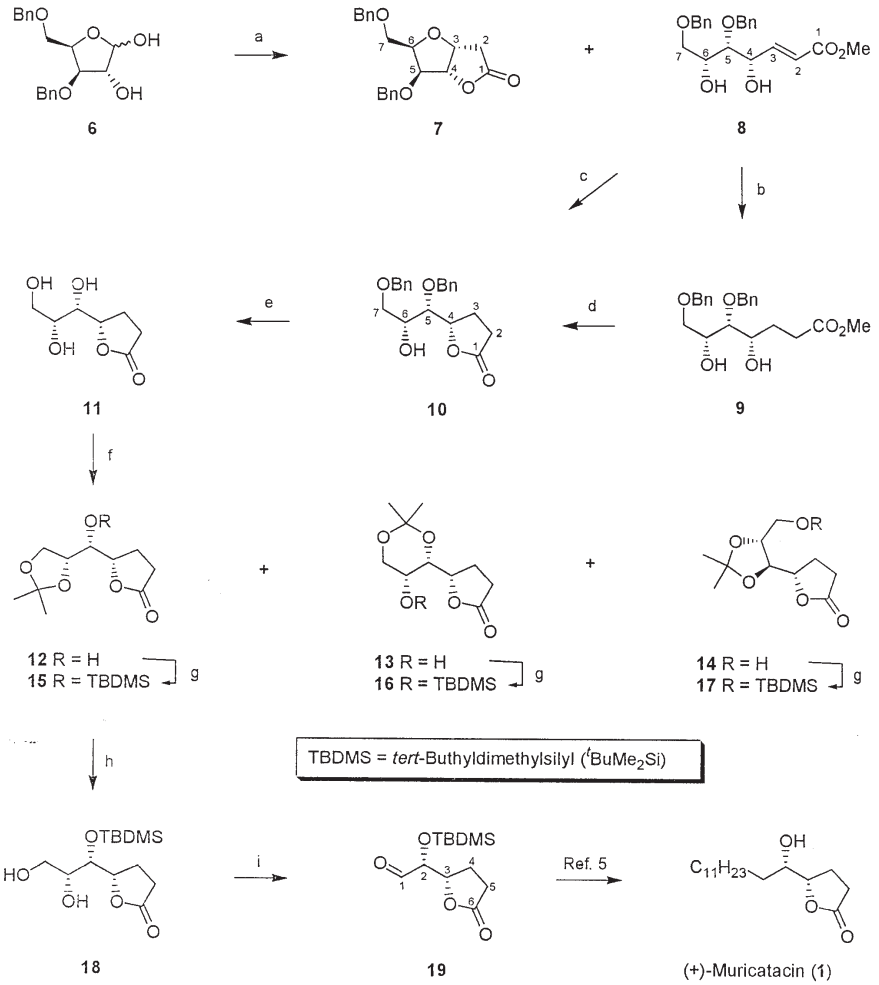

Scheme 2. (a) Ph_3P:$CHCO_2Me$, DMF, 60–70 ºC, 24 h; (b) H_2, PtO_2, EtOH, r.t. 24 h; (c) H_2, PtO_2, AcOH, r.t. 51 h; (d) 2:1 TFA–H_2O, r.t. 3 h; (e) H_2, 5 % Pd/C, r.t. 20 h; (f) $Me_2C(OMe)_2$, TsOH, DMF, r.t. 3.5 h; (g) $^tBuMe_2SiCl$, imidazole, DMF, r.t. 24 h; (h) 7:3 AcOH–H_2O, 50 ºC, 3 h; (i) 0.65 M aq. $NaIO_4$, silica gel, CH_2Cl_2, r.t. 0.5 h.

acetic acid gave directly the lactone **10** in 48 % yield. Obviously, the two-step sequence (**8**→**9**→**10**) represents a more convenient route toward the intermediate **10** since it provided a considerably higher overall yield (61 % from **8**). Catalytic debenzylation of **10** over 10 % Pd/C in ethanol furnished in 91 % yield the corresponding triol **11**, which was subsequently treated with 2,2-dimethoxypropane in the presence of catalytic amounts of *p*-toluenesulphonic acid to afford a mixture of isopropylidene derivatives **12**, **13** and **14** in an approximate ratio of 3:2:1, respectively. The desired product **12** was isolated in pure form by flash column chromatography (31.5 %) along with small amount of its regioisomer **13** (5 %). The structures of **12** and **13** were easily distinguished by comparison of

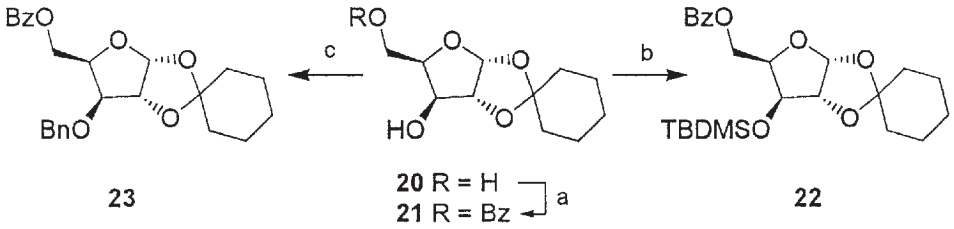

Scheme 3. (a) BzCl, Py, CH_2Cl_2, –22 ºC, 69 h, then r.t. 24 h; (b) $^tBuMe_2SiCl$, imidazole, DMF, r.t. 24 h; (c) BnBr, NaH, DMF, 0 ºC→r.t. then 2.5 h at r.t.

the ^{13}C-NMR data related to the resonance of both methyl groups from their isopropylidene functionalities (compound **12**: δ_{Me} 25.22 and 26.56 ppm; compound **13**: δ_{Me} 18.24 and 29.25 ppm). The small difference between the chemical shifts ($\Delta\delta_{Me}$ 1.34 ppm) along with the down-field position of the quaternary carbon signal in the spectrum of **12** (δ_C 109.36) clearly indicated that molecule **12** contains a 1,3-dioxolane five-membered ring.[10] Conversely, the large difference between the methyl carbon signals ($\Delta\delta_{Me}$ 11.01 ppm), as well as the high-field position of the quaternary carbon signal in the spectrum of **13** (δ_C 99.30) definitely confirmed the presence of a six-membered isopropylidene function in the molecule.[10] Since the regioisomer **14** could not be obtained free of **12** and **13**, it was therefore indirectly characterized after its conversion to the corresponding 7-*O*-silyl ether **17**. Namely, silylation of the mixture **12**, **13** and **14** with *tert*-butyldimethylsilyl chloride followed by chromatographic purification enabled the isolation of pure **17**, while the isomeric silylated products **15** and **16** could not be separated by column chromatography as they had the same mobility in different solvent systems. Reaction of pure **12** with *tert*-butyldimethylsilyl chloride and imidazole in DMF gave the corresponding silyl ether **15** (81 %), which was subsequently hydrolysed with 70 % aqueous acetic acid (50 ºC) to the expected diol **18**. Oxidative fission of the diol **18** was achieved by treatment with $NaIO_4$–impregnated wet silica in dichloromethane, whereupon the known[5] aldehyde **19** was obtained with the absolute configuration of all stereocentres corresponding to (+)-muricatacin. The ^{1}H and ^{13}C-NMR spectral data (Table I), as well as the optical rotation of the thus obtained **19** were in good agreement with the reported data.[5] Since the aldehyde **19** was earlier converted to (+)-muricatacin (**1**) in three synthetic steps,[5] the preparation of **19** formally represents a new stereospecific synthesis of (+)-**1** from D-xylose.

In the final stage of this study, the synthesis of several fully protected D-xylose derivatives of type **5** (Scheme 1) was achieved. Namely, the aim of this part of the work was to prepare the 1,2-*O*-cyclohexylidene derivatives bearing different protective groups at C-3 and C-5, in order to avoid the low-selectivity acetonation step in the presented route (**11**→**12**). Thus, 1,2-*O*-cyclohexylidene-α-D-xylofuranose[11] (**20**, Scheme 3) was selectively benzoylated to afford a high yield of the corresponding 5-*O*-benzoyl derivative **21** (84 %). Compound **21** was earlier described in the chemical literature[12] as an oil, $[\alpha]_D$ + 12.1º. However, our sample was a crystalline solid (m.p. 101.5–102 ºC) that showed a rather different value of optical rotation {$[\alpha]_D$ – 3.19º (*c* 1.0 in $CHCl_3$) }. In spite of this

disagreement, all spectral data of the thus obtained product were fully consistent with structure **21**. Further treatment of **21** with *tert*-butyldimethylsilyl chloride under standard reaction conditions furnished the corresponding 3-*O*-silyl ether **22** in 77 % yield. Finally, reaction of **21** with benzyl bromide in DMF, in the presence of sodium hydride as a base, gave the expected 3-*O*-benzyl derivative **23** in 64 % yield. According to the retrosynthetic analysis (Scheme 1), the synthesized compounds **22** and **23** also represent possible intermediates in a modified approach to (+)-muricatacin (**1**), hoping that the presence of different protective groups at C-3 and C-5 would provide a better chemoselectivity of the alternative synthetic routes, which are currently under study in our laboratory.

TABLE I. NMR spectral data for aldehyde **19** (in $CDCl_3$)

	Chemical shift (δ) and *J* (Hz)								
	H-1	H-2	H-3	H-4a	H-4b	2×H-5	$SiMe_2$	$SiCMe_3$	
This work	9.66	4.01	4.85	2.17	2.36	2.55	0.11	0.93	
Ref. 5	9.67	4.04	4.88	2.19	2.37	2.57	0.12	0.95	
	$J_{1,2}$	$J_{2,3}$	$J_{3,4a}$	$J_{3,4b}$					
This work	1.2	2.6	5.3	8.0					
Ref. 5	1.3	2.6	5.4	8.1					
	C-1	C-2	C-3	C-4	C-5	C-6	$SiMe_2$	$SiCMe_3$	$SiCMe_3$
This work	202.1	79.3	79.7	23.3	27.8	176.5	–5.1 and –4.6	18.0	25.6
Ref. 5	201.9	79.2	79.6	23.2	27.7	176.5	–5.2 and –4.7	18.0	25.5

In conclusion, a stereospecific route toward the aldehydo-lactone **19**, the known[5] chiral precursor of (+)-muricatacin, has been developed that may enable the preparation of the target **1** in 14 steps starting from D-xylose. The most recent synthesis of **1** has been accomplished in 15 synthetic steps starting from D-glucose.[6] Although this new synthesis of **19** consists of more synthetic steps than the earlier preparation from L-glyceraldehyde,[5] it uses conventional reagents and a less expensive starting material.

EXPERIMENTAL

General methods

Melting points were determined on a Büchi SMP 20 apparatus and were not corrected. Optical rotations were measured on a Polamat A (Carl-Zeiss, Jena) automatic polarimeter at room temperature. IR spectra were recorded with a Specord 75IR spectrophotometer and the band positions are given in cm^{-1}. NMR spectra were recorded on a Bruker AC 250 E instrument and the chemical shifts are expressed in ppm downfield from Me_4Si. Chemical ionisation mass spectra were recorded on Finnigan-MAT 8230 spectrometer with isobutane as the reagent gas. FAB mass spectra were taken on a VG AutoSpec instrument. TLC was performed on DC Alufolien Kieselgel 60 F_{254} (E. Merck). Flash column chromatography was performed using ICN silica 32-63. Column chromatography was carried out using Kieselgel 60 (under 0.063 mm; E. Merck). All organic extracts were dried with anhydrous Na_2SO_4. Organic solutions were concentrated in a rotary evaporator under reduced pressure at a bath temperature below 30 ºC.

*3,6-Anhydro-5,7-di-*O*-benzyl-2-deoxy-D-*ido*-heptono-1,4-lactone (**7**) and methyl (*E*)-5,7-di-*O*-benzyl-2,3-di-deoxy-D-*xylo*-hept-2-enonate (**8**)*

A solution of **6** (0.1078 g, 0.33 mmol) and methoxycarbonylmethylidene triphenylphosphorane (0.1395 g, 0.42 mmol) in dry DMF (40 mL) was stirred at 60–70 ºC for 24 h. The solvent was evaporated and the residue was chromatographed on a column of flash silica (Et_2O) to separate the reaction products from the Ph_3PO. Repeated chromatographic purification on a silica gel column (20 g, 3:7 hexane–Et_2O) gave pure lactone **7** (0.0139 g, 12 %). Crystallization from MeOH afforded an analytical sample of **7**, m.p. 90 ºC; $[\alpha]_D$ +8.60º (*c* 1.19 in $CHCl_3$); R_F 0.62 (4:1 hexane–Et_2O); ^{1}H-NMR ($CDCl_3$): δ 2.71 (*m*, 2H, $J_{2a,3}$ = 4,4, $J_{2b,3}$ = 2.9 Hz, H-2), 3.73 (*d*, 2H, $J_{6,7}$ = 5.5 Hz, 2×H-7), 4.22 (*dd*, 1H, $J_{4,5}$ = 0.6, $J_{5,6}$ = 4.1 Hz, H-5), 4.31 (*m*, 1H, H-6), 4.59 and 4.64 (2 partially overlapped 2×*d*, 4H, J_{gem} = 11.9 Hz, 2×C*H*$_2$Ph), 4.93 (*dd*, 1H, $J_{3,4}$ = 4.8 Hz, H-4), 4.96 (*m*, 1H, H-3), 7.26–7.42 (*m*, 10 H, 2×Ph); ^{13}C-NMR ($CDCl_3$): δ 36.05 (C-2), 68.19 (C-7), 72.79 and 73.65 (2×*C*H$_2$Ph), 76.95 (C-3), 79.73 (C-6), 81.62 (C-5), 85.55 (C-4), 127.84, 127.87, 128.23, 128.52, 128.67, 137.26 and 138.01 (2×Ph), 175.46 (C=O); CI MS: *m*/*z* 355 (M^+ +H), 263 (M^+ –Bn). Anal. Found: C, 70.89; H, 6.39. Calcd. for $C_{21}H_{22}O_5$: C, 71.17; H, 6.26. Further eluting of the column gave pure **8** (0.0938 g, 74 %) as a colourless oil, $[\alpha]_D$ –188.88º (*c* 1.08 in $CHCl_3$); R_F 0.50 (4:1 hexane–Et_2O); IR (film): ν_{max} 3430 (OH), 1730 (C=O), 1670 (C=C), 1610 (Ph); ^{1}H-NMR ($CDCl_3$): δ 2.81 and 3.22 (2×*d*, 1H each, exchangeable with D_2O, *J* = 6.1 Hz, 2×OH), 3.52 (*dd*, 1H, $J_{6,7a}$ = 5.6, $J_{7a,7b}$ = 9.7 Hz, H-7a), 3.60 (*dd*, 1H, $J_{6,7b}$ = 5.7, H-7b), 3.62 (*t*, 1H, $J_{4,5}$ = $J_{5,6}$ = 4.1 Hz, H-5), 3.76 (*s*, 3H, OMe), 3.97 (*m*, 1H, H-6), 4.50 (*m*, 1H, $J_{3,4}$ = 4.3, $J_{2,4}$ = 2 Hz, H-4), 4.51 (*s*, 2H, C*H*$_2$Ph), 4.61 (2×*d*, 2H, J_{gem} = 11.3 Hz, C*H*$_2$Ph), 6.16 (*dd*, 1H, $J_{2,3}$ = 15.6 Hz, H-2), 7.03 (*dd*, 1H, H-3), 7.25–7.42 (*m*, 10 H, 2×Ph); ^{13}C-NMR ($CDCl_3$): δ 51.54 (OMe), 70.67 (C-4), 70.76 (C-6), 71.09 (C-7), 73.45 and 74.70 (2×*C*H$_2$Ph), 80.64 (C-5), 121.11 (C-2), 127.87, 128.06, 128.16, 128.43, 128.45, 137.32 and 137.39 (2×Ph), 147.48 (C-3), 166.67 (C=O); CI MS: *m*/*z* 387 (M^+ +H), 355 (M^+ – OMe).

*Methyl 5,7-di-*O*-benzyl-2,3-dideoxy-D-*xylo*-heptonate (**9**)*

A solution of **8** (1.9443 g, 5.28 mmol) in EtOH (40 mL) was hydrogenated over PtO_2 (0.1076 g) for 24 h at room temperature. The mixture was filtered and the catalyst washed with EtOH. The filtrate and washings were combined and evaporated. The syrupy residue (1.9282 g) was purified by flash chromatography (7:3 Et_2O–cyclohexane) to give pure **9** (1.2164 g, 62 %) as a colourless oil, $[\alpha]_D$ –23.37º (*c* 1.16 in $CHCl_3$); R_F 0.20 (7:3 Et_2O–cyclohexane); IR (film): ν_{max} 3430 (OH), 1740 (C=O), 1610 (Ph); ^{1}H-NMR ($CDCl_3$) δ 1.84 (pseudo *q*, 2H, $J_{2,3a}$ = $J_{2,3b}$ = 7.3, $J_{3,4}$ = 6.4 Hz, 2×H-3), 2.43 (*dd*, 1H, $J_{2a,2b}$ = 16.5 Hz, H-2a), 2.52 (*dd*, 1H, H-2b), 2.71 (*bs*, 2H, exchangeable with D_2O, 2×OH), 3.48 (*t*, 1H, $J_{4,5}$ = $J_{5,6}$ = 3.7 Hz, H-5), 3.56 (*dd*, 1H, $J_{7a,7b}$ = 9.6, $J_{6,7a}$ = 5.8 Hz, H-7a), 3.60 (*dd*, 1H, $J_{6,7b}$ = 5.8, H-7b), 3.67 (*s*, 3H, OMe), 3.75 (*m*, 1H, H-4), 3.99 (*m*, 1H, H-6), 4.54 and 4.76 (2×*s*, 2H, each, 2×PhC*H*$_2$), 7.32–7.80 (*m*, 10H, 2×Ph); ^{13}C-NMR ($CDCl_3$): δ 28.74 (C-3), 30.24 (C-2), 51.40 (OCH_3), 70.57 (C-6), 70.78 (C-7), 70.82 (C-4), 73.14 and 74.74 (2×Ph*C*H$_2$), 80.90 (C-5), 127.23, 127.33, 127.55, 127.68, 127.97, 128.08, 128.16, 128.22, 137.52 and 137.65 (2×Ph), 174.15 (C=O); CI MS: *m*/*z* 389 (M^+ +H), 357 (M^+ –OMe).

*5,7-Di-*O*-benzyl-2,3-dideoxy-D-*xylo*-heptono-1,4-lactone (**10**)*

(*A*) A solution of **8** (0.1059 g, 0.29 mmol) in glacial AcOH (3 mL) was hydrogenated over PtO_2 (0.0058 g) for 3 h at room temperature. The flow of hydrogen was terminated and stirring at room temperature was continued for an additional 48 h. The suspension was filtered through a Celite pad and the catalyst was washed with ethanol. The combined filtrate and washings were evaporated and traces of AcOH were removed by co-distillation with toluene. Silica gel column chromatography (10 g; 3:2 Et_2O–cyclohexane) of the residue afforded pure **10** (49.1 mg, 48 %) as a colourless syrup, R_F 0.29 (7:3 Et_2O–cyclohexane).

(*B*) A solution of **9** (1.3268 g; 3.42 mmol) in a mixture of 2:1 TFA–H_2O (30 mL) was stirred at room temperature for 3 h and then evaporated. Traces of acid and water were removed by co-distillation with toluene and the oily residue (1.2744 g) was purified by flash chromatography (49:1 CH_2Cl_2–MeOH) to afford pure **10** (1.1874 g; 98 %) as a colourless oil, $[\alpha]_D$ +31.7º (*c* 0.86 in CH_3OH), R_F 0.29 (7:3 Et_2O–cyclohexane). ^{1}H-NMR ($CDCl_3$): δ 1.98 and 2.35 (2×*m*, 2H, 2×H-3), 2.50 (*m*, 3H, 2×H-2 and OH), 3.52 (*dd*, 1H,

$J_{6,7a}$ = 5.8, $J_{7a,7b}$ = 9.5 Hz, H-7a), 3.58 (*m*, 2H, $J_{5,6}$ = 3.1 Hz, H-7b and H-5), 3.92 (*td*, 1H, H-6), 4.51 (*s*, 2H, PhCH_2), 4.65 and 4.82 (2×*d*, J_{gem} = 11.4 Hz, PhCH_2), 4.75 (*m*, 1H, H-4), 7.27–7.47 (*m*, 10H, 2×Ph); ^{13}C-NMR ($CDCl_3$): δ 24.65 (C-3), 28.33 (C-2), 69.72 (C-6), 70.82 (C-7), 73.45 and 74.46 (2×PhCH_2), 80.13 (C-5), 81.07 (C-4), 127.90, 127.99, 128.22, 128.43, 128.46 and 137.63 (2×Ph), 177.09 (C=O); CI MS: *m*/*z* 357 (M^+ + H); FAB MS: *m*/*z* 379 (M^+ + Na), 357 (M^+ + H).

2,3-Dideoxy-D-xylo-*heptono-1,4-lactone* ***(11)***

A solution of **10** (1.1874 g, 3.34 mmol) in EtOH (50 mL) was hydrogenated over 5 % Pd/C (0.9705 g) for 20 h at room temperature. The mixture was filtered and the catalyst washed with EtOH. The filtrate washings were combined and evaporated. The syrupy residue (0.6390 g) was purified by flash chromatography (5:1 CH_2Cl_2–MeOH) to give pure **11** (0.5360 g, 91 %) as a colourless oil, $[\alpha]_D$ +48.61º (*c* 0.98 in Me_2CO); R_F 0.18 (47:3 EtOAc–MeOH); ^{1}H-NMR (pyridine-d_6): δ 2.23 (*m*, 2H, $J_{3,4}$ = 7.1, $J_{2,3}$ = 8 Hz; 2×H-3), 2.38–2.73 (*m*, 2H, $J_{2a,2b}$ = 16.5 Hz, 2×H-2), 4.17 (*t*, 1H, $J_{4,5}$ = $J_{5,6}$ = 4.4 Hz, H-5), 4.20–4.36 (*m*, 3H, $J_{7a,7b}$ = 11.6, $J_{6,7a}$ = 4.6 Hz, 2×H-7 and H-6), 5.09 (*td*,1H, H-4), 5.20–7.00 (*bs*, 3H, exchangeable with D_2O, 3×OH); ^{13}C-NMR (pyridine-d_6): δ 24.72 (C-3), 31.06 (C-2), 64.22 (C-7), 72.11 (C-6), 74.45 (C-5), 81.77 (C-4), 177.90 (C=O); CI MS: *m*/*z* 177 (M^+ + H), 159 (M^+ – OH); FAB MS: *m*/*z* 199 (M^+ + Na), 177 (M^+ + H), 159 (M^+ – OH).

*2,3-Dideoxy-6,7-*O-*isopropylidene-D*-xylo-*heptono-1,4-lactone* ***(12)*** *and*
*2,3-dideoxy-5,7-*O-*isopropylidene-D*-xylo-*heptono-1,4-lactone* ***(13)***

To a solution of **11** (0.5111 g; 2.90 mmol) in dry DMF (5 mL) were added TsOH×H_2O (0.006 g; 0.03 mmol) and 2,2-dimethoxypropane (1.3 mL; 10.36 mmol). The mixture was stirred for 3.5 h at room temperature and then neutralized by stirring with Amberlite IRA-400 resin at room temperature for 30 min. The mixture was filtered and the resin was washed with dry MeOH. The combined organic solutions were evaporated to an oil (0.5726 g), which was purified by flash chromatography (47:3 toluene–MeOH). Pure **12** (0.1976 g; 31.5 %) was first isolated as a white solid. Recrystallization from CH_2Cl_2-cyclohexane gave an analytical sample **12** as colourless needles, m.p. 94 ºC; $[\alpha]_D$ +44.92º (*c* 1.25 in $CHCl_3$); R_F 0.69 (47:3 EtOAc–MeOH); ^{1}H-NMR ($CDCl_3$): δ 1.37 and 1.44 (2×*s*, 3H each, CMe_2), 2.20–2.39 (*m*, 2H, $J_{2a,3}$ = 8.6, $J_{2b,3a}$ = 7.2, $J_{2b,3b}$ = 9.2, $J_{3,4}$ = 7 Hz, 2×H-3), 2.47 (*dd*, 1H, $J_{2a,2b}$ = 17.4 Hz, H-2a), 2.54–2.77 (*m*, 2H, H-2b and OH), 3.58 (*m*, after treatment with D_2O *dd*, 1H, $J_{5,6}$ = 5.9, $J_{4,5}$ = 3.2 Hz, H-5), 3.82 (*dd*, 1H, $J_{7a,7b}$ = 8.3, $J_{6,7a}$ = 6.4 Hz, H-7a), 4.09 (*dd*, 1H, $J_{6,7b}$ = 6.6 Hz, H-7b), 4.27 (pseudo *q*, 1H, H-6), 4.49 (*td*, 1H, H-4); ^{13}C-NMR ($CDCl_3$): δ 23.95 (C-3), 25.22 and 26.56 (CMe_2) 28.10 (C-2), 65.79 (C-7), 73.56 (C-5), 75.57 (C-6), 79.56 (C-4), 109.86 (CMe_2), 177.17 (C=O); CI MS: *m*/*z* 217 (M^+ + H); FAB MS: *m*/*z* 455 ($2M^+$ + Na), 433 ($2M^+$ + H), 239 (M^+ + Na), 217 (M^+ + H). Anal Found: C, 56.11; H, 7.51. Calcd. for $C_{10}H_{16}O_5$: C, 55.85; H, 7.46. Further elution of the column gave first a mixture of regioisomers **12**, **13** and **14** (0.2605 g; 41 %), followed by small amount of pure **13** (0.0322 g, 5 %) as a colourless oil, R_F 0.28 (47:3 EtOAc–MeOH); ^{1}H-NMR ($CDCl_3$): δ 1.46 (*s*, 6H, CMe_2), 1.91 (*m*, 1H, H-3a), 2.39 (*m*, 1H, H-3b), 2.54 (*m*, 2H, 2×H-2), 2.95 (*bs*, 1H, exchangeable with D_2O, OH), 3.48 (*bs*, 1H, $J_{6,7a}$ = 1.9, $J_{6,7b}$ = 1.2, $J_{5,6}$ = 3 Hz, H-6), 3.82 (*dd*, 1H, $J_{7a,7b}$ = 12.5 Hz, H-7a), 3.86 (*bd*, 1H, $J_{4,5}$ = 8.9 Hz, H-5), 4.06 (*dd*, 1H, H-7b), 4.61 (*m*, 1H, H-4); ^{13}C-NMR ($CDCl_3$): δ 18.24 and 29.25 (CMe_2), 23.67 (C-3), 28.29 (C-2), 62.95 (C-6), 65.56 (C-7), 74.64 (C-5), 80.44 (C-4), 99.30 (CMe_2), 176.62 (C=O); CI MS: *m*/*z* 217 (M^+ + H).

*5-*O-*(*tert-*Butyldimethylsilyl)-2,3-dideoxy-6,7-*O-*isopropylidene-D*-xylo-*heptono-1,4-lactone* ***(15)***

A solution of **12** (0.1888 g; 0.87 mmol), *tert*-butyldimethylsilyl chloride (0.5157 g; 3.42 mmol) and imidazole (0.2512 g, 3.69 mmol) in dry DMF (13 mL) was stirred for 24 h at room temperature. The mixture was evaporated and the residue (0.7762 g) purified by flash column chromatography (49:1 toluene-MeOH). Pure **15** (0.2328 g; 81 %) was obtained as an oil which crystallized from hexane as colourless prisms, m.p. 76–77 ºC; $[\alpha]_D$ +49.76º (*c* 1.16 in $CHCl_3$); R_F 0.18 (CH_2Cl_2); ^{1}H-NMR ($CDCl_3$): δ 0.12 and 0.13 (2×*s*, 3H each, SiMe_2), 0.89 (*s*, 9H, SiCMe_3), 1.34 and 1.41 (2×*s*, 3H each, CMe_2), 2.10–2.69 (*m*, 4H, 2×H-2 and 2×H-3), 3.71 (*dd*, 1H, $J_{5,6}$ = 5.8, $J_{4,5}$ = 3.3 Hz, H-5), 3.80 (*t*, 1H, $J_{6,7a}$ = $J_{7a,7b}$ = 8 Hz, H-7a), 4.03 (*dd*, 1H,

$J_{6,7b}$ = 6.4 Hz, H-7b), 4.19 (*m*, 1H, H-6), 4.52 (*m*, 1H, $J_{3a,4}$ = 6.4, $J_{3b,4}$ = 7.6 Hz, H-4); ^{13}C-NMR ($CDCl_3$): δ –4.76 and –4.32 ($SiMe_2$), 18.18 (Si*C*Me_3), 23.81 (C-3), 25.31 and 26.37 (C*Me*$_2$), 25.78 (SiC*Me*$_3$), 28.02 (C-2), 65.56 (C-7), 74.90 (C-5), 76.55 (C-6), 79.91 (C-4), 109.27 (*C*Me_2), 177.05 (C=O); CI MS: *m*/*z* 331 (M^+ + H); FAB MS: *m*/*z* 353 (M^+ + Na), 331 (M^+ + H), 315 (M^+ – Me). Anal. Found: C, 58.31; H, 9.41. Calcd. for $C_{16}H_{30}O_5Si$: C, 58.15; H, 9.15.

6-O-*(*tert-*Butyldimethylsilyl)-2,3-dideoxy-5,7*-O-*isopropylidene-D*-xylo-*heptono-1,4-lactone (**16**)*

A solution of **13** (0.032 g; 0.15 mmol), *tert*-butyldimethylsilyl chloride (0.0720 g; 0.51 mmol) and imidazole (0.0482 g, 0.71 mmol) in dry DMF (1.5 mL) was stirred for 24 h at room temperature. The mixture was evaporated and the residue purified by flash column chromatography (49:1 CH_2Cl_2–MeOH). Pure **16** (0.0361 g; 79 %) was obtained as a colourless oil, $[\alpha]_D$ +0.19º (*c* 1.1 in $CHCl_3$); R_F 0.18 (CH_2Cl_2); ^{1}H-NMR ($CDCl_3$): δ 0.12 and 0.69 (2×*s*, 3 H each, Si*Me*$_2$), 0.91 (*s*, 9 H, SiC*Me*$_3$), 1.42 and 1.44 (2×*s*, 3 H each, CMe$_2$), 1.93 (*m*, 1 H, H-3a), 2.30 (*m*, 1 H, H-3b), 2.46–2.61 (*m*, 2H, 2×H-2), 3.64–3.83 (*m*, 3 H, $J_{4,5}$ = 8.2, $J_{5,6}$ = 1.8, $J_{7a,7b}$ = 12.5, $J_{6,7a}$ = 3 Hz, H-5, H-6 and H-7a), 3.95 (*dd*, 1 H, $J_{6,7b}$ = 2.7 Hz, H-7b), 4.66 (*m*, 1 H, $J_{3a,4}$ = 6.4, $J_{3b,4}$ = 8.9 Hz, H-4); ^{13}C-NMR ($CDCl_3$): δ –4.66 and –3.84 ($SiMe_2$), 18.09 (Si*C*Me_3), 23.52 (C-3), 19.61 and 28.14 (C*Me*$_2$), 25.64 (SiC*Me*$_3$), 28.41 (C-2), 64.50 (C-7), 64.72 (C-6), 74.81 (C-5), 80.34 (C-4), 98.96 (*C*Me_2), 176.54 (C=O).

7-O-*(*tert-*Butyldimethylsilyl)-2,3-dideoxy-5,6*-O-*isopropylidene-D*-xylo-*heptono-1,4-lactone (**17**)*

A solution of a mixture containing **12**, **13** and **14** (0.1504 g; 0.70 mmol), *tert*-butyldimethylsilyl chloride (0.4068 g; 2.70 mmol) and imidazole (0.2067 g, 3.04 mmol) in dry DMF (2.5 mL) was stirred for 24 h at room temperature. The mixture was evaporated and the residue (0.5216 g) purified by flash column chromatography (97:3 toluene–MeOH). Pure **17** (0.0630 g; 27 %) was obtained as a colourless oil, $[\alpha]_D$ +23.07º (*c* 0.7 in $CHCl_3$); R_F 0.52 (19:1 toluene–MeOH); ^{1}H-NMR ($CDCl_3$): δ 0.79 (*s*, 6 H, Si*Me*$_2$), 0.90 (*s*, 9 H, SiC*Me*$_3$), 1.38 and 1.39 (2×*s*, 3 H each, CMe$_2$), 2.20–2.81 (*m*, 4 H, 2×H-2 and 2×H-3), 3.70 (*dd*, 1 H, $J_{6,7a}$ = 6.5, $J_{7a,7b}$ = 10.5 Hz, H-7a), 3.88 (*dd*, 1 H, $J_{6,7b}$ = 3.9 Hz, H-7b), 3.97 (*dd*, 1 H, $J_{4,5}$ = 1.7, $J_{5,6}$ = 8 Hz, H-5), 4.15 (*ddd*, 1 H, H-6), 4.61 (*ddd*, 1 H, $J_{3a,4}$ = 6.1, $J_{3b,4}$ = 4.4 Hz, H-4); ^{13}C-NMR ($CDCl_3$): δ –5.46 ($SiMe_2$), 18.27 (Si*C*Me_3), 24.78 (C-3), 25.84 (SiC*Me*$_3$), 26.34 and 27.22 (C*Me*$_2$), 27.89 (C-2), 63.46 (C-7), 76.20 (C-6), 77.43 (C-4), 81.58 (C-5), 109.73 (*C*Me_2), 177.62 (C=O). Further elution of the column gave an inseparable mixture of the regioisomers **15** and **16** (0.1548 g; 67 %) as a colourless syrup, R_F 0.18 (CH_2Cl_2).

5-O-*(*tert-*Butyldimethylsilyl)-2-3-dideoxy-D*-xylo-*heptono-1,4-lactone (**18**)*

A solution of **15** (0.2828 g, 0.86 mmol) in 70 % aq. AcOH (5 mL) was stirred for 3 h at 50 ºC. The mixture was evaporated and the residual AcOH was removed by co-distillation with toluene. Flash column chromatography (93:7 CH_2Cl_2–cyclohexane) of the residue (0.2755 g) yielded pure **18** (0.2264 g, 91 %) as a white solid. Recrystallization from CH_2Cl_2–cyclohexane gave colourless crystals, m.p. 79–80 ºC; $[\alpha]_D$ +33.86º (*c* 0.5 in $CHCl_3$); R_F 0.39 (23:2 CH_2Cl_2–MeOH); ^{1}H-NMR ($CDCl_3$): δ 0.11 and 0.14 (2×*s*, 3 H each, Si*Me*$_2$), 0.89 (*s*, 9 H, SiC*Me*$_3$), 2.06 (*m*, 1 H, H-3a), 2.31 (*m*, 1 H, H-3b), 2.54 (*m*, 2 H, 2×H-2), 2.62 and 2.90 (2×*bs*, 2 H, exchangeable with D_2O, 2×OH), 3.54–3.72 (*m*, 3 H, H-6 and 2×H-7), 3.76 (*dd*, 1 H, $J_{4,5}$ = 4.8, $J_{5,6}$ = 2.9 Hz, H-5), 4.67 (*td*, 1 H, $J_{3,4}$ = 7.3 Hz, H-4); ^{13}C-NMR ($CDCl_3$): δ –4.64 and –4.49 ($SiMe_2$), 18.08 (Si*C*Me_3), 24.06 (C-3), 25.77 (SiC*Me*$_3$), 28.42 (C-2), 63.05 (C-7), 71.34 (C-6), 74.16 (C-5), 80.03 (C-4), 177.13 (C=O); CI MS: *m*/*z* 291 (M^+ + H), 273 (M^+ + H – OH). Anal. Found: C, 54.01; H, 9.21. Calcd. for $C_{13}H_{26}O_5Si$: C, 53.76; H, 9.02.

2-O-*(*tert-*Butyldimethylsilyl)-4,5-dideoxy-L*-threo-*hexurono-6,3-lactone (**19**)*

Partially protected lactone **18** (0.0458 g, 0.16 mmol) was dissolved in CH_2Cl_2 (1 mL) and treated with a 0.65 M aqueous $NaIO_4$ solution (0.5 ml) and chromatography grade silica gel (0.063 – 0.200 mm, 0.3 g). The resulting heterogeneous mixture was vigorously stirred for 0.5 h at room temperature then filtered and evaporated to afford chromatographically pure **19** as a white solid (0.0397 g, 97 %). Recrystallization from hexane gave colourless crystals, m.p. 71–72 ºC; $[\alpha]_D$ +101.28º (*c* 2.1 in $CHCl_3$); lit.[5] $[\alpha]_D$ +96.3 (*c* 1.2 in $CHCl_3$); R_F 0.80 (47:3 EtOAc–MeOH). ^{1}H and ^{13}C-NMR data are presented in Table I. FAB MS: *m*/*z* 259 (M^+ + H), 201 (M^+ – CMe_3).

5-O-*Benzoyl-1,2*-O-*cyclohexylidene*-α-*D*-*xylofuranose* ***(21)***

To a cold solution (–22 ºC) of **20** (4.6 g, 20 mmol) in dry CH_2Cl_2 (40 mL) and pyridine (5 mL) was added benzoyl chloride (2.5 mL, 21.54 mmol) previously cooled to –22 ºC. The mixture was left at –22 ºC for 69 h and then at room temperature for an additional 24 h. The reaction mixture was poured into 4 M aq. HCl (100 mL), the organic layer was washed with brine (3×100 mL), dried and evaporated to a yellow syrup. The residue was purified by flash chromatography (19:1 CH_2Cl_2–EtOAc) to give pure **21** (5.6254 g, 84 %) as a white solid. Recrystallization from hexane afforded colourless crystals, m.p. 101.5–102 ºC; $[\alpha]_D$ –3.19º (c 1.0 in $CHCl_3$); lit.[12] $[\alpha]_D$ +12.1º; R_F 0.32 (19:1 CH_2Cl_2–EtOAc); IR (KBr): ν_{max} 3460–3400 (OH), 1720 (C=O), 1610 (Ph); ^{1}H-NMR ($CDCl_3$): δ 1.32–1.77 (*m*, 10 H, C_6H_{10}), 3.53 (*bs*, 1H, exchangeable with D_2O, OH), 4.22 (*d*, 1 H, $J_{3,4}$ = 2.1 Hz, H-3), 4.39 (*m*, 1 H, $J_{4,5a}$ = 5.4, $J_{4,5b}$ = 8.8 Hz, H-4), 4.42 (*dd*, 1 H, $J_{5a,5b}$ = 13 Hz, H-5a), 4.58 (*d*, 1 H, $J_{1,2}$ = 3.6 Hz, H-2), 4.76 (*dd*, 1 H, H-5b), 5.97 (*d*, 1 H, H-1), 7.39–8.09 (*m*, 5 H, Ph); ^{13}C-NMR ($CDCl_3$); δ 23.47, 23.80, 24.78, 35.50 and 36.32 (5×CH_2 from C_6H_{10}), 61.56 (C-5), 74.45 (C-3), 78.40 (C-4), 84.53 (C-2), 104.28 (C-1), 112.44 (qC from C_6H_{10}), 128.37, 129.20, 129.78 and 133.40 (Ph), 167.20 (C=O); CI MS: *m*/*z* 335 (M^+ + H).

5-O-*Benzoyl-3*-O-tert-*butyldimethylsilyl-1,2*-O-*cyclohexylidene-a-D-xylofuranose* ***(22)***

A solution of **21** (0.40 g; 1.20 mmol), *tert*-butyldimethylsilyl chloride (0.3644 g; 2.42 mmol) and imidazole (0.2436 g, 3.6 mmol) in dry DMF (2 mL) was stirred for 23 h at room temperature. The mixture was evaporated and the residue (0.7762 g) purified by flash column chromatography (7:1 toluene–CH_2Cl_2). Pure **22** (0.4123 g; 77 %) was obtained as colourless crystals, m.p. 75–76 ºC; $[\alpha]_D$ –31.1º (*c* 0.99 in $CHCl_3$); R_F 0.67 (9:1 toluene–EtOAc); IR (KBr) ν_{max} 1730 (C=O), 1600 (Ph); ^{1}H-NMR ($CDCl_3$): δ 0.10 and 0.15 (2×*s*, 3 H each, Si*Me*$_2$), 0.91 (*s*, 9 H, SiC*Me*$_3$), 1.33–1.78 (*m*, 10 H, C_6H_{10}), 4.32 (*bs*, 1 H, $J_{3,4}$ = 2 Hz, H-3), 4.39 (*d*, 1 H, $J_{1,2}$ = 3.7 Hz, H-2), 4.43–4.57 (*m*, 3 H, H-4 and 2×H-5), 5.97 (*d*, 1 H, H-1), 7.38–8.11 (*m*, 5 H, Ph); ^{13}C-NMR ($CDCl_3$): δ –5.20 and –4.70 ($SiMe_2$), 17.97 (Si*C*Me$_3$), 23.56, 23.88, 24.86, 35.82 and 36.55 (5×CH_2 from C_6H_{10}), 25.61 (SiC*Me*$_3$), 62.69 (C-5), 75.75 (C-3), 78.72 (C-4), 85.00 (C-2), 104.75 (C-1), 112.58 (qC from C_6H_{10}), 128.29, 129.70, 129.77, 129.87 and 133.00 (Ph), 166.26 (C=O); CI MS: *m*/*z* 449 (M^+ + H).

5-O-*Benzoyl-3*-O-*benzyl-1,2*-O-*cyclohexylidene*-α-*D*-*xylofuranose* ***(23)***

To a cooled (0 ºC) and stirred solution of **21** (1.3482 g, 4 mmol) in dry DMF (20 mL) were added successively NaH (0.2633 g, 9.8 mmol) and BnBr (0.72 mL, 6 mmol). The mixture was stirred for 2.5 h at room temperature and then evaporated. The oily residue was partitioned between CH_2Cl_2 (50 mL) and 10 % aqueous NH_4Cl (45 mL). The organic layer was washed with water (2×45 mL), dried and evaporated to a yellow syrup. The residue was purified by flash column chromatography (CH_2Cl_2–light petroleum) to afford pure **23** (1.0841 g, 64 %) as a pale yellow oil, $[\alpha]_D$ –68.8º (*c* 1.02 in $CHCl_3$); R_F 0.76 (4:1 toluene–EtOAc); IR (film): ν_{max} 1720 (C=O), 1610 (Ph); ^{1}H-NMR ($CDCl_3$): δ 1.35–1.81 (*m*, 10 H, C_6H_{10}), 4.08 (*d*, 1 H, $J_{3,4}$ = 2.7 Hz, H-3), 4.50–4.78 (*m*, 6 H, J_{gem} = 12 Hz, Ph*C*H$_2$, H-2, H-4 and 2×H-5), 6.02 (*d*, 1 H, $J_{1,2}$ = 3.8 Hz, H-1), 7.23–8.07 (*m*, 10 H, Ph); ^{13}C-NMR ($CDCl_3$); δ 23.51, 23.80, 24.80, 35.64 and 36.35 (5×CH_2 from C_6H_{10}), 62.37 (C-5), 72.00 (Ph*C*H$_2$), 77.98 (C-4), 81.55 (C-2 and C-3), 104.81 (C-1), 112.49 (qC from C_6H_{10}), 127.63, 127.91, 128.23, 128.44, 129.68, 129.75, 132.97 and 137.11 (2×Ph), 166.18 (C=O); CI MS: *m*/*z* 425 (M^+ + H).

Acknowledgement: This work was supported by a research grant from the Ministry of Science, Technology and Development of the Republic of Serbia (Grant No. 1896). The authors are grateful to Mrs. Tanya Marinko-Covell (School of Chemistry, University of Leeds, UK) for recording the FAB mass spectra.

ИЗВОД

ФОРМАЛНА СИНТЕЗА (+)-МУРИКАТАЦИНА ИЗ D-КСИЛОЗЕ

ВЕЛИМИР ПОПСАВИН[a], САЊА ГРАБЕЖ[a], ИВАНА КРСТИЋ[a], МИРЈАНА ПОПСАВИН[a] и ДЕЈАН ЂОКОВИЋ[б]

[a]*Департман за хемију, Природно-математички факултет, Универзитет у Новом Саду, Трг Д. Обрадовића 3, 21000 Нови Сад и* [б]*Хемијски факултет, Универзитет у Београду, Студентски трг 16, 11001 Београд*

У раду је остварена вишефазна синтеза алдехидо-лактона **19**, финалног хиралног прекурсора у новој стереоспецифичној синтези (+)-мурикатацина, полазећи из D-ксилозе. Кључну етапу синтезе представља *E*-стереоселективна Wittig-ова реакција лактола **6**, са метоксикарбонилметилиден-трифенилфосфораном, праћена накнадном каталитичком редукцијом и γ-лактонизацијом. Низом селективних интерконверзија присутних функционалних група награђен је кључни шесто-угљенични интермедијер **19**, који се може превести у (+)-мурикатацин трофазном синтетичком секвенцом која је раније описана у литератури.

(Примљено 9. јуна 2003)

REFERENCES

1. M. J. Reiser, J. F. Kozlowski, K. V. Wood, J. L. McLaughlin, *Tetrahedron Lett.* **32** (1991) 1137
2. A. Cave, C. Chaboche, B. Figadère, J. C. Haramange, A. Laurens, J. F. Peyrat, M. Pichon, M. Szlosek, J. Cotte-Lafitte, A. M. Quero, *Eur. J. Med. Chem.* **32** (1997) 617
3. (a) S. Rangavan, S. C. Joseph, *Tetrahedron: Asymmetry* **14** (2003) 101; (b) M. Carda, S. Rodriguez, F. Gonzalez, E. Castillo, A. Villanueva, J. A. Marco, *Eur. J. Org. Chem.* (2002) 2649; (c) C. Baylon, G. Prestat, M.-P. Heck, C. Mioskowski, *Tetrahedron Lett.* **41** (2000) 3833; (d) E. A. Couladouros, A. P. Mihou, *Tetrahedron Lett.* **40** (1999) 4861; (e) G. Solladie, G. Hanquet, I. Izzo, R. Crumbie, *Tetrahedron Lett.* **40** (1999) 3071; (f) M. Szlosek, X. Franck, B. Figadère, A. Cavé, *J. Org. Chem.* **63** (1998) 5169; (g) S. -W. Chang, C. -Y. Hung, H. -H. Liu, B. J. Uang, *Tetrahedron: Asymmetry* **9** (1998) 521; (h) P. Quayle, S. Rahman, J. Herbert, *Tetrahedron Lett.* **36** (1995) 8087; (i) M. P. M. van Aar, L. Thijis, B. Zwanenburg, *Tetrahedron* **51** (1995) 11223; (j) C. Bonini, C. Federici, L. Rossi, G. Righi, *J. Org. Chem.* **60** (1995) 4803; (k) P. Somfai, *J. Chem. Soc. Perkin Trans. 1* (1995) 817; (l) J. A. Marshall, G. S. Welmaker, *J. Org. Chem.* **59** (1994) 4122; (m) H. Makabe, A. Tanaka, T. Oritani, *Bioscience*, *Biotechnol. Biochem.* **57** (1993) 1028; (n) M. Saiah, M. Bessodes, K. Antoniakis, *Tetrahedron Lett.* **34** (1993) 1597; (o) Z. M. Wang, X. L. Zhang, K. B. Sharpless, S. C. Sinha, A. Sinha-Bagchi, E. Keinan, *Tetrahedron Lett.* **33** (1992) 6407; (p) W. Tochtermann, G. Scholz, G. Bunte, C. Wolff, E. M. Peters, K. Peters, H. G. Von Schnering, *Liebigs Ann. Chem.* (1992) 1069; (q) J. A. Marshall, G. S. Welmaker, *Synlett* (1992) 537; (r) B. Figadère, J. C. Haramange, A. Laurens, A. Cavé, *Tetrahedron Lett.* **32** (1991) 7539; (s) G. Scholz, W. Tochtermann, *Tetrahedron Lett.* **32** (1991) 5535
4. (a) M. Chadrasekhar, K. L. Chandra, V. K. Singh, *Tetrahedron Lett.* **43** (2002) 2773; (b) M. Saniere, I. Charvet, Y. Le Merrer, J. -C. Depezay, *Tetrahedron* **51** (1995) 1653; (c) C. Gravier-Pelletier, M. Saniere, I. Charvet, Y. Le Merrer, J. -C. Depezay, *Tetrahedron Lett.* **35** (1994) 115; (d) S. K. Kang, H. S. Cho, H. S. Sim, B. K. Kim, *J. Carbohydr. Chem.* **11** (1992) 807
5. G. Rassu, L. Pinna, P. Spanu, F. Zanardi, L. Battistini, G. Casiraghi, *J. Org. Chem.* **62** (1997) 4513
6. S.-H. Yoon, H.-S. Moon, S.-K. Hwang, S. R. Choi, S. K. Kang, *Bioorg. Med. Chem.* **6** (1998) 1043
7. For a preliminary account of this work see: V. Popsavin, S. Grabež, M. Popsavin, J. Petrović, *Carbohydr. Lett.* **3** (2000) 411
8. V. Popsavin, S. Grabež, B. Stojanović, M. Popsavin, V. Pejanović, D. Miljković, *Carbohydr. Res.* **321** (1999) 110
9. K. R. Prakash, S. P. Rao, *Tetrahedron* **49** (1993) 1505
10. J. G. Buchanan, M. E. Chacón-Fuertes, A. R. Edgar, S. J. Moorhouse, D. I. Rawson, R. H. Wightman, *Tetrahedron Lett.* **21** (1980) 1793
11. M. Popsavin, V. Popsavin, N. Vukojević, D. Miljković, *Collect. Czech. Chem. Commun.* **59** (1994) 1884
12. W. Szeja, *Pol. J. Chem.* **54** (1980) 1323.

J.Serb.Chem.Soc. 68(11)805–809(2003)
JSCS – 3100

UDC 547.918+543.635.2:582.282.23:54.02
Preliminary communication

PRELIMINARY COMMUNICATION

A glucan from active dry baker's yeast (*Saccharomyces cerevisiae*): A chemical and enzymatic investigation of the structure

DRAGANA ZLATKOVIĆ[1], DRAGICA JAKOVLJEVIĆ[2*#], DJORDJE ZEKOVIĆ[3] and MIROSLAV M. VRVIĆ[2,4]

[1]Confectionery Industry "Štark", 11010 Belgrade, Kumodraška 249, [2]Department of Chemistry, Institute of Chemistry, Technology and Metallurgy, 11001 Belgrade, Njegoševa 12, P.O. Box 473, [3]"Alltech YU" Ltd., 21000 Novi Sad, Kralja Aleksandra 5, [4]Faculty of Chemistry, University of Belgrade, Studentski trg 16, P.O. Box 158, 11001 Belgrade, Serbia and Montenegro

(Received 14 April 2003)

Abstract: The structure of a polysaccharide consisting of D-glucose isolated from the cell-wall of active dry baker's yeast (*Saccharomyces cerevisiae*) was investigated by using methylation analysis, periodate oxidation, mass spectrometry, NMR spectroscopy, and enzymic hydrolysis, as a new approach in determination of structures. The main structural feature of the polysaccharide deduced on the basis of the obtained results is a linear chain of (1 → 3)-linked β-D-glucopyranoses, a part of which is substituted through the positions O-6. The side units or groups are either a single D-glucopyranose or (1 → 3)-β-oligoglucosides, linked to the main chaing through (1 → 6)-glucosidic linkages. The low optical rotation as well as the ^{13}C-NMR and FTIR spectra suggest that the glycosidic linkages are in the β-D-configuration.

Keywords: active dry baker's yeast, *Saccharomyces cerevisiae*, polysaccharides, glucan, structure, chemical and enzymatic methods.

Considerable information on the structure of polysaccharides isolated from the cell-walls of baker's yeast (*Saccharomyces cerevisiae*) have already been reported.[1–3] The difficulties of obtaining and analysing purified wall components are numerous, because of the insolubility of some of them. When insoluble polysaccharides are associated with other cell wall polymers, the isolation becomes more difficult. The choice of suspending medium for the cell-wall isolation procedure also needs careful consideration. One of the most difficult problems in the purification of yeast glucans is their separation from close association with other insoluble polysaccharides, such as chitin and mannans. In recent years glucans from the cell-walls of many microorganisms have attracted a great deal of attention in view of their antitumor activity, especially the β-D-glucans.[4,5] Also, it was recently

* Corresponding author. Phone/Fax: +381-11-636-061. E-mail: djakovlj@chem.bg.ac.yu
# Serbian Chemical Society active member.

reported that a polysaccharide from the cell wall of brewer's yeast promotes the absorption of dietary iron and that the yeast glucan is the main polysaccharide having this effect.[6] In this communication preliminary results are presented of the isolation and structure determination of the glucan obtained from the cell-wall of baker's yeast (*Saccharomyces cerevisiae*), an important raw material for glucan production. Besides chemical methods, enzymatic hydrolysis, as a new approach in structure investigation, was also applied.

The active dry baker's yeast (commercial product made by Fermentation Industry "Alltech-Fermin", Senta, Serbia and Montenegro) as the polysaccharide material of the yeast cell-walls, was treated successively with acetate buffer (pH 5), 0.75 M sodium hydroxide, hot water, and 0.5 M acetic acid. The residue obtained by repeated extraction with acetic acid was dialysed and lyophilized. Further purification was achieved by salivary amylase and by pullulanase. The in this way obtained glycan was insoluble in water, alkalis, and most common organic solvents, but soluble in dimethyl sulphoxide, being one of the best solvents for many polysaccharides.

The pure polysaccharide gave one component after total acid hydrolysis, identified as D-glucose by paper chromatography and gas-liquid chromatography (GLC) analysis of the derived alditol acetates.[7]

The polysaccharide showed $[\alpha]_D^{20}$ –87° (c = 0.1 in DMSO) and displayed a band at 890 cm^{-1} in its FTIR spectrum, which is a characteristic feature of polysaccharides having the β-configuration. In addition there were bands at 2920, 1370, 1250, 1155, 1075, and 1040 cm^{-1} which indicate β-(1 → 3)-linkages.[8] The ^{1}H-NMR spectrum (DMSO-d_6, 200 MHz) of the polysaccharide contained signals at δ (ppm) 4.57 and 4.81 consistent with anomeric protons due to (1→6)- and (1→3)-β-D-glucosidic linkages, respectively.[9] In the ^{13}C-NMR spectrum (DMSO-d_6, 50 MHz) of the polysaccharide, signals were found at δ (ppm): 103.26; 86.47; 76.58; 73.05 and 68.68. Based on literature data,[10,11] these signals are assigned to carbon atoms of the 3-mono-O-substituted β-D-glucopyranosyl residue. The signal at 61.09 ppm corresponds to the C-6 of the non-reducing residue of the side groups and may also be assigned to 3,6-di-O-substituted units at branch point of the main chain, due to overlapping of the signals.

Additional evidence for the structure of this polysaccharide was provided by enzyme digestion by the (1→3)-β-D-glucanase of *Helix pomatia*. After incubation for 48 h, paper chromatography revealed two components, corresponding to glucotriose and gentiobiose.

The results of periodate oxidation[12] were in agreement with the above data. The polysaccharide consumed 1.30 mol of periodate and released 0.62 mol of formic acid per hexosyl residue. The Smith degradation of the polysaccharide,[13] *i.e.* borohydride reduction and hydrolysis of the periodate oxidized polysaccharide, afforded a mixture of two main components: glucose and glycerol, the first being the major component, as concluded on the basis of GLC of the alditol acetate derivatives (column DB-5, argon, 30 mL/min, FID).[7] The small amount of glycerol (≈ 10%) suggested either (1→6)-linkages or a slightly branched polymer of both. The D-glucose found in the hydrolysate of the periodate oxidized and reduced polysaccharide confirmed (1→3)-linkages and branching points.

Methylation analysis substantiated the above results. The methylation was performed by the Hakomori procedure,[14,15] *i.e.*, by treatment of the polysaccharide with methyl iodide and methylsulfinyl carbanion in dimethyl sulfoxide. The per-*O*-methylated product (no hydroxyl absorption in the FTIR spectrum), $[\alpha]_D^{20}$ +5.8° (*c* = 0.15 in chloroform) on acid hydrolysis afforded a mixture of three components which by their chromatographic mobilities (see Table I) corresponded to 2,3,4,6-tetra-*O*-methyl-glucose, 2,4,6-tri-*O*-methyl-glucose, and 2,4-di-*O*-methyl glucose. Part of the hydrolysate was reduced, acetylated, and analyzed by GLC and GLC-MS (capillary column Supelco PTE-5, mass spectrometer "Finnigan Mat" model 8230).[16] The components were identified by their retention times and typical MS breakdown patterns obtained on electron impact. A summary of the results obtained by methylation analysis is shown in Table I.

TABLE I. Summary of the results of the methylation analysis of active dry baker's yeast (*Saccharomyces cerevisiae*) glucan

Cleavage product	Paper chromatography		Relative mole ratio[c]	Fragment ions (*m*/*z*)	Mode of linkage
	R_{Glc}[a]	R_{Glc}[b]			
2,3,4,6-Tetra-*O*-methyl-D-glucose	1.00	0.78	1	45; 89; 117; 161; 205	Glcp-(1→
2,4,6-Tri-*O*-methyl-D-glucose	0.76	0.48	8	45; 117; 161; 201; 233	→3)-Glcp-(1→
2,4-Di-*O*-methyl-D-glucose	n.i.[d]	0.20	1	43; 87; 117; 129; 189; 233	→3, →6)-Glcp-(1→

[a] Butan-1-ol:ethanol:water = 4:1:5 (v/v); [b] Butan-2-one, saturated with water; [c] Based on the peak area by GLC; [d] Not identified.

The presence of 2,4,6-tri-*O*-methyl-glucose as the major component proves that D-glucose in the pyranoid form is incorporated into the main chain by (1→3)-linkages, a known linkage mode in many glucans from microorganisms and plants. The 2,4-di-*O*-methyl sugar, identified on the basis of combined evidence obtained by paper chromatography and GLC, as well as by GLC-MS analysis, indicates branching points, as represented by structures (1)-(3). 2,3,4,6-Tetra-*O*-methyl-D-glucose arises from nonreducing end units. The presence of small quantities of 2,4-di-*O*-methyl, and 2,3,4,6, tetra-*O*-methyl-D-glucose indicates that this glucan is slightly branched.

→3)-β-D-Glcp-(1→	Glcp	→3)-β-D-Glcp-(1→
	6	6
	↓	↓
	1	1
	→3)-β-D-Glcp-(1→3)-	→3)-β-D-Glcp-(1→3)-
(1)	(2)	(3)

On the basis of these first results, a structure having a main chain composed principally of (1→3)-linked D-glucopyranoses (structure 1) may be proposed for the

homopolysaccharide. The main chain is 6-*O*-substituted with single D-glucopyranoses (structure 2) or (1→3)- β-oligoglucosides linked to the main chain through (1→6)-glucosidic linkages (structure 3).

Concerning the relationship between the structure of the investigated glucan of *Saccharomyces cerevisiae* with those of other yeasts, it is evident that the linear part of this polymer has a structure known in many yeasts glucans. A difference exists in the mode of branching, the content of side groups or chains, and in the configuration of the glycosidic linkages in the basic chain (α-D- and β-D-types).

Acknowledgments: The authors are grateful to the Ministry of Science, Technology and Development of the Republic of Serbia for financial support.

ИЗВОД

ГЛУКАН ИЗ СУВОГ АКТИВНОГ ПЕКАРСКОГ КВАСЦА (*SACCHAROMYCES CEREVISIAE*): ХЕМИЈСКО И ЕНЗИМСКО ИЗУЧАВАЊЕ СТРУКТУРЕ

ДРАГАНА ЗЛАТКОВИЋ[1], ДРАГИЦА ЈАКОВЉЕВИЋ[2], ЂОРЂЕ ЗЕКОВИЋ[3] и МИРОСЛАВ М. ВРВИЋ[2,4]

[1]Кондиторска индустрија "Штарк", 11010 Београд, Кумодрашка 249, [2]Центар за хемију, Институт за хемију, технологију и металургију, 11001 Београд, Његошева 12, п. пр. 473, [3]"Alltech YU" д.о.о., 21000 Нови Сад, Краља Александра 5 и [4]Хемијски факултет, Универзитет у Београду, Студентски трг 16, п. пр. 158, 11001 Београд, Србија и Црна Гора

Испитивана је структура хомополисахарида изолованог из сувог активног пекарског квасца (*Saccharomyces cerevisiae*), методом метиловања, перјодатном оксидацијом, масеном спектрометријом, NMR спектроскопијом и ензимском хидролизом, као новим приступом у изучавању структуре полисахарида. Добијени резултати указују да полисахарид, који се састоји из D-глукозе, има (1→3)-D-глукополимерни низ као основни, а да су D-глукопиранозни остаци везани за основни низ преко положаја O-6 и то или као појединачне бочне јединице или као део олигомерних бочних група које чине (1→3)-D-глукопиранозил остаци. Конфигурација гликозидних веза је β-D-типа.

REFERENCES

1. J. S. D. Bacon, V. C. Farmer, D. Jones, I. F. Taylor, *Biochem. J.* **114** (1969) 557
2. C. H. Ha, K. H. Lim, Y. T. Kim, S. T. Lim, C. W. Kim, H. I. Chang, *Appl. Microbiol. Biotechnol.* **58** (2002) 370
3. G. J. P. Dijkgraaf, H. Li, H. Bussey, in *Biopolymers*, A. Steinbüchel Ed., Vol. 6, Wiley-VCH, Weinheim, 2002, p. 179
4. N. N. Miura, N. Ohno, Y. Adachi, T. Yadomae, *Chem. Pharm. Bull.* **44** (1996) 2137
5. V. Vervicka, B. P. Thornton, T. J. Wieman, G. D. Ross, *J. Immunol.* **159** (1997) 599
6. T. T. Mai, K. Igarashi, R. Hirunama, S. Takasaki, M. Yasue, S. Enomoto, S. Kimura, N. V. Chuyen, *Biosci. Biotechnol. Biochem.* **66** (2002) 1744
7. J. H. Sloneker, in *Methods in Carbohydrate Chemistry*, R. L. Whistler, J. BeMiller Eds., Vol 6, Academic Press, New York, 1972, p. 20
8. A. J. Mitchell, G. Scurfield, *Aust, J. Biol. Sci.* **23** (1970) 345
9. T. Usui, N. Yamaoka, K. Matsuda, K. Tuzimara, H. Sugiyama, S. Seto, *Argric. Biol. Chem.* **39** (1975) 1071
10. S. Jamas, Y. C. J. Chem, C. H. von der Osten, A. J. Sinskey, C. K. Rha, *Carbohydr. Polym.* **13** (1990) 207

11. N. Ohno, M. Uchiyama, A. Tsuzuki, K. Tokunaka, N. N. Miura, Y. Adachy, M. W. Aizava, H. Tamura, S. Tanaka, T. Yadomae, *Carb. Res.* **316** (1999) 161
12. W. Hay, B. A. Lewis, F. Smith, in *Methods in Carbohydrate Chemistry*, R. L. Whistler, Ed., Vol. 5, Academic Press, New York, 1965, p. 296
13. J. Goldstien, G. W. Hay, B. A. Lewis, F. Smith, *ibid*, p. 357
14. S. Hakomori, *J. Biochem. (Tokyo)* **55** (1964) 205
15. P. A. Sandford, H. E. Conrad, *Biochemistry* **5** (1966) 1508
16. P. F. Jansson, L. Kennc, H. Liedgren, B. Lindberg, J. Lonngren, *Chem. Commun. Univ. Stockholm* (1976) 1.

J.Serb.Chem.Soc. 68(11)811–818(2003)
JSCS – 3101

UDC 577.175.72:576.314:66.067+541–148
Original scientific paper

Membrane-associated insulin-like growth factor (IGF) binding structures in placental cells

ROMANA MASNIKOSA, J. ANNA NIKOLIĆ and OLGICA NEDIĆ#

INEP – Institute for the Application of Nuclear Energy, Banatska 31 B, 11080 Zemun-Belgrade, Serbia and Montenegro

(Received 21 February, revised 20 June 2003)

Abstract: The biological activities of IGF-I and –II are mediated mainly by the type 1 IGF receptor (IGF 1R) and controlled by their interaction with soluble proteins, the IGF binding proteins (IGFBPs). Although there is a growing body of evidence that some IGFBPs may be cell surface-bound, published data concerning cell association of IGFBP-1 are scarce and none of them concern placental cells. The cell membranes used in this study were isolated from term human placentae. Detergent-solubilized membranes were shown to contain two types of IGF binding structures that were separated by gel filtration on a Sephadex G-100 column. Proteins in the first peak were eluted at V_0 (M_r > 100 kD) and they bound IGF-I with greater specificity and affinity than IGF-II and insulin. Most likely, they represented the IGF 1R. Small proteins ($M_r \approx$ 45 kD) were eluted with the membrane proteins in the second maximum. They were able to bind IGF-I and IGF-II, but not insulin. The identity of these proteins was shown to be IGFBP-1 on the basis of their reaction with specific anti-IGFBP-1 antibodies. To the best of our knowledge, the existence of IGFBP-1 associated with human placental cell membranes has not been reported in the literature before. Colocalisation of IGFBP-1 with IGF 1R in cell membranes could provide efficient modulation of IGF 1R receptor-ligand interactions.

Keywords: IGF-I, IGF-II, IGF 1R, IGFBP-1, placental cell membranes, gel filtration.

INTRODUCTION

The insulin-like growth factors, IGF-I and IGF-II, are polypeptides with structural homology to proinsulin, affecting growth, differentiation, and various metabolic processes in an endocrine and autocrine/paracrine fashion. The signalling of both IGFs is mediated by the type 1 IGF receptor (IGR 1R), a heterotetrameric glycoprotein composed of two ligand-binding α-subunits and two transmembrane β-subunits (M_r 350 kD). It shares structural and functional homology with the well-characterized insulin receptor.[1] The IGF 1R binds IGF-I with high affinity, IGF-II with several fold lower affinity and insulin with more than 100-fold lower affinity.[2] IGF-II also binds to a type 2 IGF receptor (IGF 2R), a single-chain membrane-spanning glycoprotein (M_r 300 kD), which is selective for IGF-II and has no affinity for insulin. Its role in IGF-II signal transduction is still a matter of debate.[3]

Serbian Chemical Society active member.

Finally, the actions of the IGFs are modulated by a superfamily of six IGF-binding proteins (IGFBPs), IGFBP-1 through IGFBP-6, and a growing number of related proteins (IGFBP-rPs) whose physiological relevance has yet to be established. IGFBPs bind the IGFs with equal or even greater affinities than do the IGF receptors, and therefore are placed in a critical regulatory position between IGFs and their cell surface receptors. While some IGFBPs have been shown to inhibit IGF actions by preventing them from gaining access to the IGF receptors, others potentiate IGF actions by facilitating the ligand-receptor interaction.[4] Recent studies indicated that some IGFBPs have their own receptors that mediate IGF-independent actions. IGFBP-1 and IGFBP-2 contain intergrin recognition sequences, Arg-Gly-Asp (RGD), which is the minimum requirement for interaction with integrins on the cell surface. IGFBP-3 was shown to possess its own receptor and binds to heparin.[5]

The aim of this work was to investigate the membrane-associated IGF binding structures in human placental cell membranes.

EXPERIMENTAL

Materials

Sephadex G-100 was obtained from Pharmacia Biotech AB, Sweden. Human IGF-I and IGF-II were from ICN Biomedicals, USA. Porcine insulin was from Novo Research Institute, Denmark. Na^{125}I was supplied by Polatom, Poland. Goat anti-hIGFBP-1 antiserum was obtained from Diagnostic Systems Laboratories Inc., USA. All other employed chemicals were purchased from Sigma Chemicals, USA.

Tracer

IGF-I, IGF-II and insulin were iodinated by the chloramine T method.[6] The specific activities of the ^{125}I-labelled peptides were approximately 100 μCi/μg.

Preparation of placental membranes

Placental membranes were prepared by a modification of the procedure given by Perdue *et al.*[7] Term human placenta was collected immediately after delivery, placed in ice-cold 50 mM phosphate buffered saline (pH 7.5) and washed extensively with the same buffer. The placenta was dissected free from large vessels, amniotic and chorionic membranes. The remaining tissue was minced and homogenized in a polytron homogenizer with 5 volumes of 50 mM HEPES buffer (pH 7.5) containing 250 mM sucrose, 1 mM EDTA and 2 mM phenylmethylsulphonyl fluoride. The homogenate was centrifuged at 600 × g for 15 min. The pellet was discarded and the supernatant centrifuged at 18 000 × g for 30 min. The supernatant obtained was further centrifuged at 100 000 × g for 60 min to yield a pellet designated as placental membranes. The crude membrane pellet was washed twice and finally resuspended in membrane buffer (50 mM HEPES, pH 7.5, containing 4 mM $MgCl_2$). Aliquots were stored frozen at – 80 ºC.

Solubilization of placental membranes

Membranes (20 mg of membrane proteins) were solubilized for 2 h at 4 ºC in 5 mL of 2 % Triton X-100 in membrane buffer. After centrifugation at 100 000 × g for 90 min, the insoluble pellet was discarded and the clarified extract (solubilizate) was divided into aliquots and stored frozen at –80 ºC until use.

The membrane protein concentration was determined by the method of Lowry,[8] and in Triton solubilizates by the method of Bradford.[9]

Gel filtration

Solubilized membrane proteins (1 mg) were incubated with 0.5 pmol ^{125}I-IGF-I (500 000 cpm) in the presence or absence of unlabelled ligands (65 pmol IGF-I, or 65 pmol IGF-II or 170 nmol insulin) at 4 ºC

overnight and chromatographed in 50 mM sodium phosphate buffer containing 100 mM NaCl and 0.1 % Triton X-100 (pH 7.5) on a Sephadex G-100 column (1.8 × 60 cm). The flow rate was 20 mL/h. 1 mL fractions were collected and their radioactivity (cpm) measured in a γ-counter (APEX Auto Gamma Counter, Micromedic Systems Inc.). The same experiments were performed with ^{125}I-IGF-II and ^{125}I-insulin as tracers. The column was calibrated using Blue Dextran 2000, egg albumin (EA, 45 kD) and IGF-I (7.5 kD).

Gel filtration was also used for the separation of the IGF binding structures. The solubilizate (4 mg of membrane proteins) was chromatographed without tracer and the proteins eluting between fractions 36 and 46 were collected and designated "peak 1 preparation", while those eluting between fractions 52 and 72 were designated "peak 2 preparation". The proteins present in peaks 1 and 2 were concentrated 2-5-fold and stored at 4 ºC. The proteins from the peak 1 preparation were used in competitive ligand binding assays, while the proteins from the peak 2 preparation were used in immunoaffinity interactions. The proteins from the peak 2 preparation (0.5 mL) were incubated with 0.5 pmol ^{125}I-IGF-I (or ^{125}I-IGF-II) in the presence or absence of goat anti-IGFBP-1 antiserum at 4 ºC overnight and analysed by gel filtration on the Sephadex G-100 column as described.

Competitive ligand binding assays

100 μg of membrane proteins (from placental membranes or solubilizate) or 0.1 mL of proteins from the peak 1 preparation were incubated with 17 fmol ^{125}I-IGF-I or –II (≈ 20 000 cpm) and increasing concentrations of unlabelled ligands (IGF-I, -II or insulin) in a final volume of 0.5 mL of membrane buffer containing 2 mg/mL BSA, at 4 ºC overnight. Triton X-100 at a final concentration of 0.04 % was present in all binding assays. Following incubation, 1.5 mL of 20 % (w/v) polyethylene glycol 6000 (PEG) was added. The tubes were vortex-mixed vigorously, left at 4 ºC for 20 min, then centrifuged (3000 × g, for 40 min) and the supernatants were discarded. Precipitated radioactivity was measured in the γ-counter. Nonspecific binding (NSB) was determined by incubating ^{125}I-IGF with binding buffer without membrane proteins. The specific binding was calculated as the difference between the total binding and the NSB.[10] The data were expressed as IC_{50} (concentration of the competing ligand that inhibited labelled ligand-specific binding by 50 %) and analysed by the method of Scatchard.[11]

RESULTS

Detergent solubilized IGF-I binding structures from placental cell membranes were resolved into two components on a Sephadex G-100 column (Fig. 1a). The first peak, designated peak 1, appeared at an elution volume (V_e) of 41 mL which was equivalent to the void volume of the column, V_o. The second peak, designated peak 2, eluted at V_e of 62 mL, which is the V_e of egg albumin, indicating that proteins in this peak had a molecular weight of approximately 45 kD. Proteins in the second maximum bound approximately three times more ^{125}I-IGF-I than proteins in the first peak. The third radioactive maximum in the elution profile ($V_e \approx 99$ mL) represented unbound ^{125}I-IGF-I. (Fig. 1a)

The ^{125}I-IGF-I binding to the proteins present in peaks 1 and 2 was specific, as both peaks disappeared upon gel filtration in the presence of 65 pmol of unlabelled IGF-I. IGF-II was an equally potent inhibitor of the ^{125}I-IGF-I binding (results not shown), while insulin at a 2000-fold greater concentration could displace only about 30 % of the radioactivity initially bound in peak 1 (Fig. 1b). This pattern of crossreactivity is characteristic of placental IGF 1R and it suggested the presence of this receptor in peak 1.[12] Proteins in peak 2, however, bound more ^{125}I-IGF-I in the presence of insulin than in its absence (Fig. 1b). It is probable that insulin occupied a proportion of the IGF-I binding sites on IGF 1R, allowing ^{125}I-IGF-I to bind to a greater extent to proteins in peak 2.

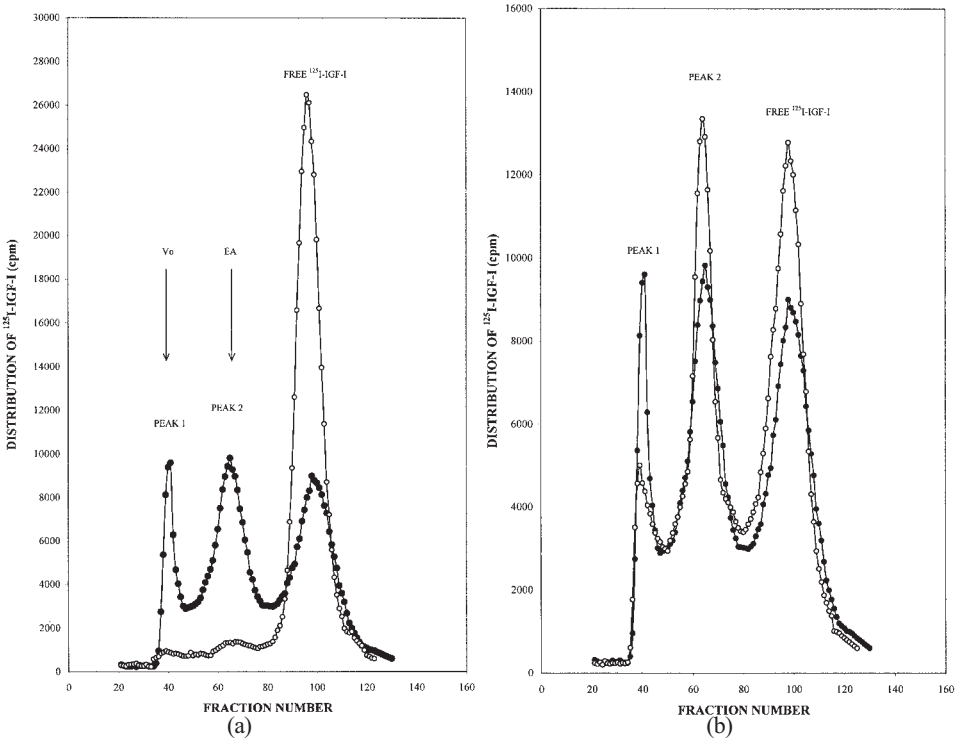

Fig. 1. Gel filtration of solubilized placental membrane proteins, preincubated with ^{125}I-IGF-I, without competing ligand (●) or in the presence of unlabelled competitor (○): a) IGF-I; b) insulin.

As decidua is the primary source of IGFBP-1 in pregnant women[13] and as IGFBP-1 is the predominant IGFBP in amniotic fluid,[14] the interaction between specific anti-IGFBP-1 antibodies and proteins in peak 2 was tested. Proteins in peak 2 were separated by gel filtration, equilibrated with ^{125}I-IGF-I in the presence or absence of anti-IGFBP-1 antibodies and, again, analysed by gel filtration. The elution profiles obtained are given in Fig. 2. In the presence of anti-IGFBP-1 antibodies the peak at a V_e of 62 mL disappeared from the elution profile and a new peak, expected to represent the ^{125}I-IGF-I/IGFBP-1/anti-IGFBP-1 antibody complex, appeared at V_o. The experiment was also performed with ^{125}I-IGF-II as a tracer and similar elution profiles were obtained, while ^{125}I-insulin did not interact at all (data not shown). These results strongly indicated the presence of IGFBP-1 in the placental membranes. The possibility that peak 2 reflected the presence of contaminating soluble IGFBP-1 was ruled out, since repeated washing of the membranes prior to solubilization did not alter the magnitude of the peak.

The displacement of ^{125}I-IGF-I from crude placental membranes, membrane solubilizates or proteins in peak 1, separated by gel filtration, by competitive binding assays with unlabelled IGF-I, IGF-II and insulin was examined and the IC_{50} values obtained are summarized in Table I. The pattern of crossreactivity was again characteristic of the IGF

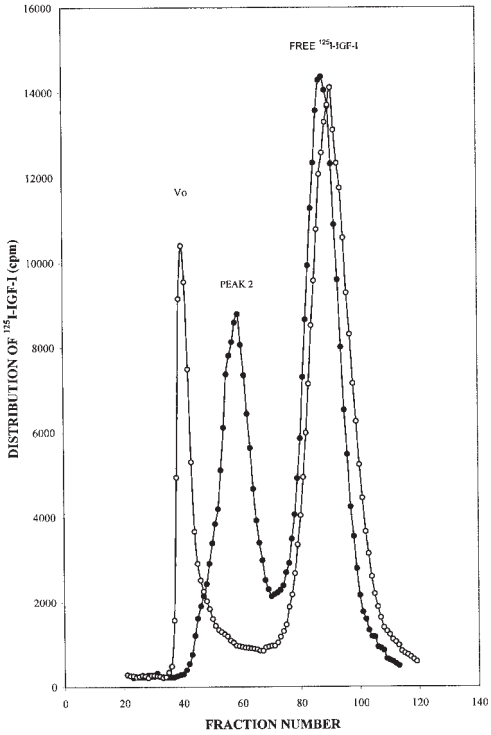

Fig. 2. Gel filtration of the proteins in peak 2, preincubated with ^{125}I-IGF-I in the absence (●) or in the presence of anti-IGFBP-1 antibodies (○).

1R: IGF-I > IGF-II >> insulin.[12] Moreover, each successive step in the IGF 1R separation (membrane solubilization and chromatographic separation of IGF 1R) caused the IC_{50} values for all unlabelled ligands to decrease.

TABLE I. Binding of ^{125}I-IGF-I to crude placental membranes, solubilized membranes and proteins in peak 1 separated by gel filtration in competition with the unlabelled ligands: IGF-I, IGF-II and insulin

	IC_{50} (nM)		
	IGF-I	IGF-II	INSULIN
Crude membranes	0.4	0.8	1000
Solubilizates	0.1	0.6	72
Peak 1 proteins	0.05	0.3	8.3

The IC_{50} values obtained could be attributed to the interaction of ligands with the IGF 1R, because IGFBP-1/^{125}I-IGF-I complexes were not precipitated by PEG (results not shown). Scatchard analysis of the IGF-I binding to solubilized membrane proteins resulted in a curvilinear plot, providing evidence that both high affinity and low affinity binding sites existed (Fig. 3). The dissociation constant (K_d) that characterized high affinity interaction was estimated to be 0.08 nM, and the binding capacity (R_o) was approximately 0.05 pmol/mg membrane protein. The slope of the curve representing the low affinity binding system was very flat on the Scatchard plot and could not be clearly distinguished

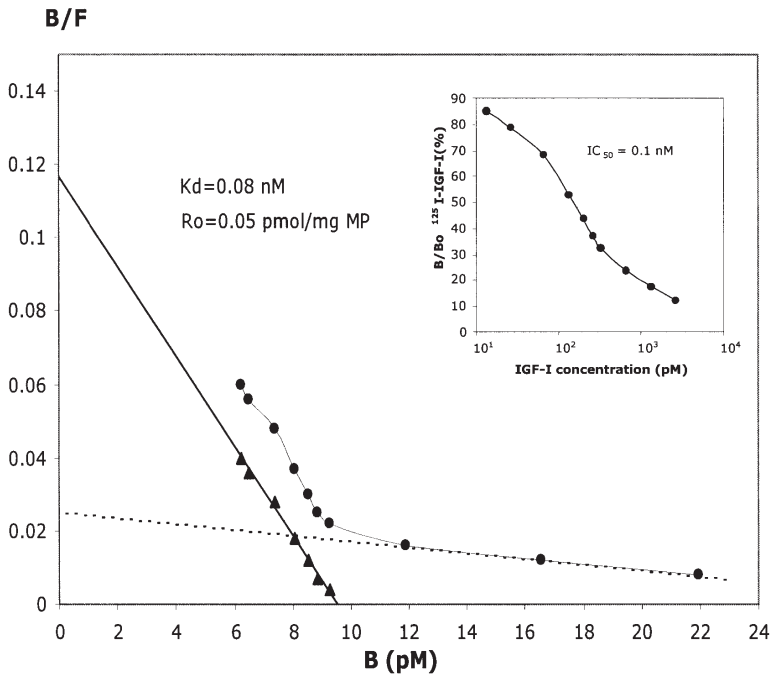

Fig. 3. Scatchard plot of IGF-I binding to placental membrane solubilizates. The ordinate represents the ratio of bound to free IGF-I (B/F). The contribution of the low affinity binding sites was extrapolated (– – –) and subtracted from the total binding (●) to yield the line representing the high affinity binding system (▲). The displacement of ^{125}I-IGF-I bound to membrane solubilizate by increasing concentrations of IGF-I is inserted as a curve (●).

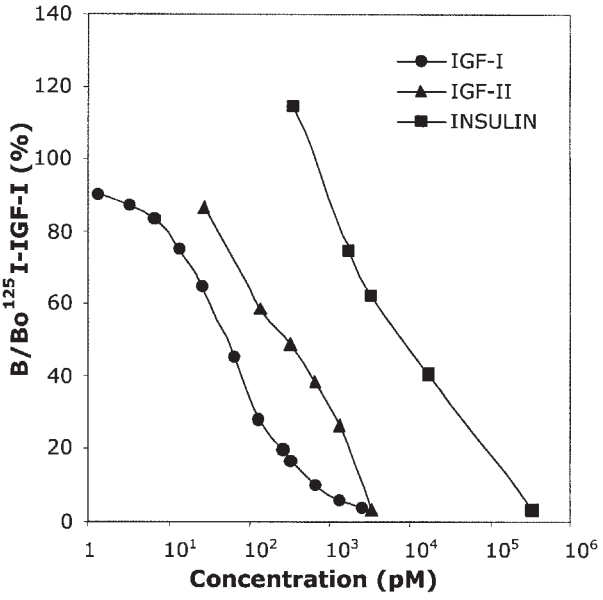

Fig. 4. Inhibition of ^{125}I-IGF-I binding to proteins of peak 1 by increasing concentrations of IGF-I (●), IGF-II (▲) and insulin (■). Data are expressed as the percentage of maximal specific binding in the absence of unlabelled ligand. Each point represents the mean of two independent determinations.

from nonspecific binding. In binding studies using ^{125}I-IGF-I and proteins in peak 1 (IGF 1R), insulin in low doses caused enhancement of ^{125}I-IGF-I binding to IGF 1R compared to the degree of binding in the absence of this competitor, demonstrating that the affinity of IGF 1R is influenced by interaction with other proteins (Fig. 4).

DISCUSSION

Two IGF-I binding species were detected in human placental cell membranes and solubilizates and separated by gel filtration. The first IGF-I binding structure bound IGF-I with high affinity (IC_{50} = 0.05). The specific interaction could be inhibited by IGF-II and insulin in a pattern characteristic of placental IGF 1R.[12] The second site of ^{125}I-IGF-I (and ^{125}I-IGF-II) binding was shown to be IGFBP-1. Widely recognised as soluble proteins, IGFBPs have been recently shown to associate with cell surfaces and components of the extracellular matrix.[5] Specific binding of IGFBP-1 to the $\alpha 5\beta 1$ integrin (fibronectin receptor) in Chinese hamster ovary cells has been demonstrated.[15] In this study evidence is provided that IGFBP-1 is associated with human placental cell membranes. However, it is premature to speculate about the nature of this association.

It has recently been postulated that IGFBP-1 is a key regulator of IGF-I activity within the local environment of the placenta.[16] IGFBP-1 is synthesised in decidual cells, while the highest levels occur in amniotic fluid.[13,14] Therefore, it is reasonable to speculate that decidual IGFBP-1 is transported through the trophoblast cells of the placenta to the amniotic fluid. The mechanism of transport is still unknown.

It has been noted in this study that IGF-1, IGF-II and insulin bind with higher affinity to solubilized receptors compared to crude membranes and that the proteins in peak 1 (presumed to be IGF 1R) exhibited an even greater difference in their binding properties when separated from IGFBP-1 by gel filtration. One possible explanation of this phenomenon would be a conformational change in the receptor structure, due to the artificial experimental milieu, which resulted in a high-affinity state of the IGF 1R.[17] It should be noted that the insulin receptor does not exhibit a comparable change in properties following solubilization.[18]

Data from our laboratory support an alternative hypothesis, that a competitive binder, IGFBP-1, positioned in the proximity of IGF 1R, in the placental cell membranes, regulates the affinity of IGF 1R for its ligands. The concept of an affinity regulator, whose activity might be modulated by physiological circumstances, although attractive, needs further investigation.

Acknowledgements: This work was supported by the Ministry of Science, Technology and Development of Serbia, project 1504: Glycobiological aspects of physiological and pathophysiological processes.

ИЗВОД

ВЕЗУЈУЋЕ СТРУКТУРЕ ЗА ИНСУЛИНУ СЛИЧНЕ ФАКТОРЕ РАСТА (IGF) У МЕМБРАНАМА ПЛАЦЕНТАЛНИХ ЋЕЛИЈА

РОМАНА МАСНИКОСА, Ц. АНА НИКОЛИЋ и ОЛГИЦА НЕДИЋ

ИНЕП – Институт за примену нуклеарне енергије, Банатска 31 Б, 11080, Београд-Земун

IGF-I и IGF-II постижу своје биолошке ефекте првенствено путем везивања за тип 1 IGF рецептора (IGF 1R), а у интеракцији између ових пептида и рецептора посредују специфични растворни протеини, IGF везујући протеини (IGFBPs). У литератури је све више података о везивању појединих IGFBP за ћелијске површине, мада је мало радова који се односе на везивање IGFBP-1 за ћелије. Ћелијске мембране, које су коришћене у овом раду, изоловане су из ткива терминске хумане плаценте. Након солубилизације мембрана, гел-филтрацијом на Sephadex-у G-100 раздвојене су две врсте протеина које везују IGF молекуле. Протеини у првом максимуму, елуирани у нултој запремини колоне (V_o), везивали су IGF-I са већом специфичношћу и афинитетом у поређењу са IGF-II и инсулином и највероватније представљају IGF 1R. У оквиру мембранских протеина елуираних у другом максимуму детектовани су мањи протеини ($M_r \approx 45$ kD), који су везивали IGF-I и IGF-II, али не и инсулин. На основу њихове реактивности са анти-IGFBP-1 антителима, утврђено је да се ради о IGFBP-1. Колико је нама познато, овај рад представља прву потврду присуства IGFBP-1 у мембранама плацентних ћелија. Присуство молекула IGFBP-1 у близини мембрански усидреног IGF 1R могло би обезбедити ефикасну модулацију интеракција између рецептора и одговарајућег лиганда.

(Примљено 21 фебруара, ревидирано 20 јуна 2003)

REFERENCES

1. D. LeRoith,. H. Werner, D. Beitner-Johnson, C. T. Roberts, *Endocr. Rev.* **16** (1995) 143
2. C. E. H. Stewart, P. Rotwein, *Physiol. Rev.* **76** (1996) 1005
3. S. Kornfeld, *Annu. Rev. Biochem.* **61** (1992) 307
4. J. L Martin, R. C. Baxter, in *The IGF System*, Humana Press, New Jersey, 1999, p. 227
5. O. Youngman, R. G. Rosenfeld, in *The IGF System*, Humana Press, New Jersey, 1999, p. 257
6. J. A. Nikolić, M. Ratković, O. Nedić, *J. Serb. Chem. Soc.* **61** (1996) 1149
7. J. F. Perdue, J. K. Chan, C. Thibault, P. Radaj, B. Mills, W. H. Daughaday, *J. Biol. Chem.* **258** (1983) 7800
8. O. H. Lowry, N. J. Rosebrough, A. L. Farr, R. J. Randall, *J. Biol. Chem.* **193** (1951) 265
9. M. M. Bradford, *Anal. Biochem.* **72** (1976) 248
10. W. H. Daughaday, I. K. Mariz, B. Trivedi, *J. Clin. Endocrinol. Metab.* **53** (1981) 282
11. G. Scatchard, *Ann. N. Y. Acad. Sci.* **51** (1949) 660
12. A. E. Bennett, R. L. Hintz, *Horm. Metab. Res.* **18** (1986) 49
13. E. M. Rutanen, M. Seppälä, *Int. J. Gynaecol. Obstet.* **39** (1992) 3
14. G. Póvoa, G. Enberg, H. Jörnvall, K. Hall, *Eur. J. Biochem.* **144** (1984) 199
15. J. I. Jones, A. Gockerman, W. H. Busby, G. Wright, D. R. Clemmons, *Proc. Natl. Acad. Sci. USA* **90** (1993) 10553
16. J. M. Gibson, J. D. Aplin, A. White, M. Westwood, *Mol. Hum. Reprod.* **7** (2001) 79
17. E. L. Germain-Lee, M. Janicot, R. Lammers, A. Ullrich, S. J. Casella, *Biochem. J.* **281** (1992) 413
18. K. Siddle, M. A. Soos, in *The IGF System*, Human Press, New Jersey, 1999, p. 207.

*J.Serb.Chem.Soc. 6*8(11)819–824(2003) UDC 542.943+664.164:541.183+679.91+547.458.2
JSCS – 3102 *Original scientific paper*

Immobilization of periodate oxidized invertase by adsorption on sepiolite

RADIVOJE M. PRODANOVIĆ[1#], MILOŠ B. SIMIĆ[2] and ZORAN M. VUJČIĆ[1#]

[1]*Faculty of Chemistry, University of Belgrade, Studentski trg 16, 11001 Belgrade and* [2]*Center for New Technologies, CNT, Studentski trg 16, 11001 Belgrade, Serbia and Montenegro*

(Received 17 September 2002, revised 4 June 2003)

Abstract: Periodate oxidized invertase was immobilized by adsorption on sepiolite. The obtained immobilized enzyme was more resistant to washing out by concentrated salt solution, and had an eight times higher half-life at 60 ºC than adsorbed native invertase. In packed bed reactor 50 % conversion of 500 g/dm^3 sucrose at 40 ºC and a flow rate of 1 bv/h was achieved. The specific productivity of the immobilized invertase was 0.187 kg/dm^3/h.

Keywords: invertase, periodate oxidation, sepiolite, immobilization, sucrose.

INTRODUCTION

Invert sugar from sucrose can be produced by acid hydrolysis or by using the enzyme invertase (E.C.3.2.1.26.). The enzymatic process has advantages over acid hydrolysis because neither color nor byproducts are obtained.

Inorganic materials have high storage, mechanical, thermal and microbial stability, and enable the possiblity of regeneration by pyrolysis which make them suitable for use as supports for enzyme immobilization. Invertase has previously been immobilized on inorganic supports by linking it covalently to modified silica gel[1] and activated clay[2] and by adsorption on tuff,[3] magnetite,[4] and sepiolite.[5]

Adsorption of enzymes on inorganic supports is a simple and cheap method of immobilization, but leakage of the enzyme from the support can occur. Covalent immobilization of enzymes on inorganic supports or crosslinking of the adsorbed enzyme by glutaraldehyde,[6] results in no leakage of the enzyme from the support, but the enzyme is partly inactivated, due to reaction of amino groups in the active site. Immobilization of invertase *via* its carbohydrate moiety by periodate oxidation does not affect the protein part of the enzyme molecule and hence there is no inactivation of the enzyme.[7–9]

A new procedure for the preparation of stabilized immobilized invertase by adsorption of previously periodate oxidized enzyme was developed. Further, the immobilized enzyme was characterized for use in the hydrolysis of concentrated sucrose solutions.

Serbian Chemical Society active member.

EXPERIMENTAL

Sepiolite

Sepiolite was taken from several locations near Obrenovac (Serbia) and prepared by a previously described method.[5] Then the sepiolite was milled with a pestle and mortar. The milled sepiolite was rinsed with distilled water and the smaller particles were removed by fractional sedimentation. The particle diameters were between 0.1 mm and 0.5 mm.

Enzyme

Invertase was obtained from bakers yeast by purification using DEAE chromatography and gel filtration chromatography on Sephadex G-200.[9] The activity of the lyophilized enzyme was 250 IU/mg of solid.

Enzyme activity

The activity was determined in a 5 ml reactor at 1000 rpm in 50 mmol/dm^3 acetate buffer pH 4.7 in 100 g/dm^3 sucrose at 25 ºC. One unit of enzyme activity was the amount of enzyme which catalyzes the hydrolysis of 1 μmol of sucrose per minute under the test conditions. The reducing sugars formed were determined using dinitrosalicylic acid reagent.[10]

Periodate oxidation

Invertase was oxidized by incubating 2.0 mg/cm^3 of enzyme with 2 mmol/dm^3 sodium metaperiodate in acetate buffer pH 5.0 in the dark at 4 ºC for 6 h. The unreacted $NaIO_4$ was then removed with 10 mmol/dm^3 ethylene glycol for 30 min. The oxidized invertase was then dialyzed against 50 mmol/dm^3 acetate buffer pH 5.0 for 18 h.

Immobilization

0.1 g of sepiolite was incubated with 2 cm^3 invertase (5, 50 and 500 IU/cm^3) in 50 mM sodium acetate buffer pH 5.0 for two days at 4 ºC. Then the sepiolite was rinsed twice with 2 cm^3 0.1 M sodium acetate buffer pH 5.0 for 10 min.

Packed bed reactor

The experiments were carried out in a 10 cm^3 water-jacketed glass column (the diameter : height ratio was 1:3) at 40 ºC. The substrate solution was brought to 40 ºC before entering the column, and then pumped through the bed by means of a peristaltic pump. After steady state had been attained, the ratio of conversion was evaluated at the outlet of the column by determining the reducing sugars.

RESULTS AND DISCUSSION

The specific activity of immobilized enzyme increased with increasing amount of added enzyme, Fig. 1.

A specific activity of 130 IU/g for adsorbed native invertase and 180 IU/g for adsorbed periodate oxidized invertase was obtained when 10000 IU of enzyme was added per 1 g of sepiolite.

To determine leakage of the enzyme from the support 0.1 g of immobilized enzyme was rinsed with 10 cm^3 1 M NaCl in 50 mM sodium acetate buffer pH 5.0 for 4 days at 4 ºC, Table I.

After rinsing with 1 M NaCl, only 14.2 % of the initial activity of adsorbed native invertase was retained, while adsorbed periodate oxidized invertase retained 91.6 % of its initial activity. This could be explained by the formation of oligomers of enzyme molecules of the periodate oxidized invertase on the surface of the sepiolite. This is possible be-

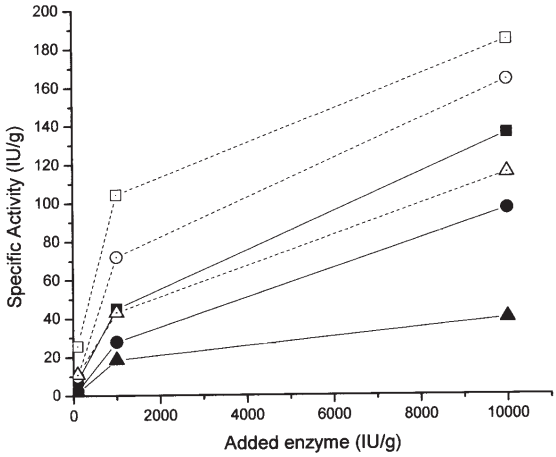

Fig. 1. Dependence of the specific activity of immobilized native (—) and periodate oxidized (···) invertase on the amount of added enzyme for three different charges of sepiolite 1 (□), 2 (○), 3 (Δ).

cause periodate oxidized invertase has aldehyde and amino groups in the same eznyme molecule so that they could react and form oligomers.[11] Such cross-linked enzyme molecules on the surface of a support are difficult to wash out because of the chelate effect, which has been reported in the literature for invertase adsorbed on alumina and further cross-linked with glutaraldehyde.[6]

TABLE I. Retention of the activity of immobilized enzyme after rinsing with 1 M NaCl at pH 5.0 and 4 ºC for 4 days

Enzyme	Relative activity before rinsing/%	Relative activity after rinsing/%
Native invertase	100	14.2
Periodate oxidized invertase	100	91.6

Such conclusions are further confirmed by the thermostability of the immobilized enzyme, Fig. 2.

The half life at 60 ºC for the adsorbed periodate oxidized enzyme was 8 times higher than that for native adsorbed invertase (16.6 min compared to 2.0 min). This further con-

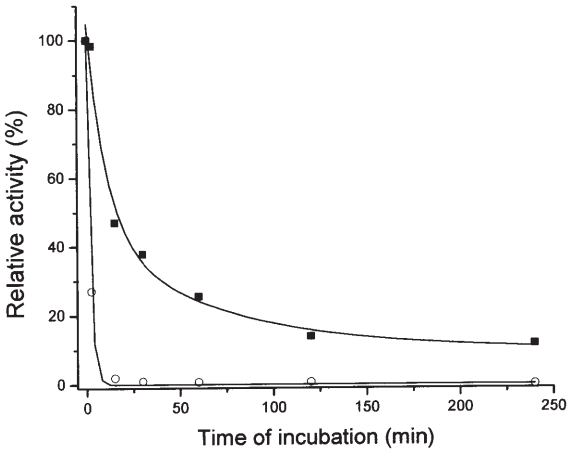

Fig. 2. Dependence of the relative activity of immobilized invertase on time of incubation at 60 ºC in 50 mM sodium acetate buffer pH 4.7. Adsorbed periodate oxidized invertase (■) and adsorbed native invertase (○).

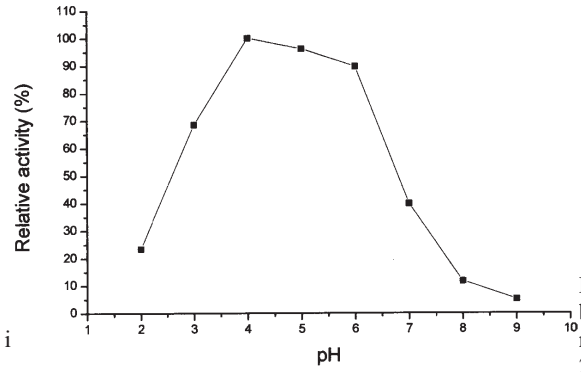

i

Fig. 3. Dependence of the activity of immobilized periodate oxidized invertase on pH, n 50 mM sodium citrate phosphate buffer at 25 ºC.

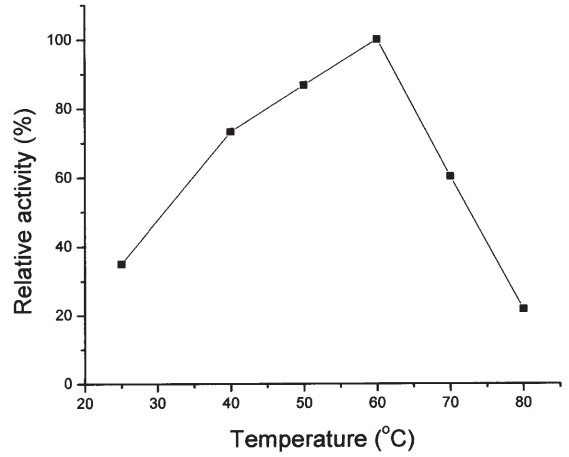

Fig. 4. Dependence of the activity of immobilized periodate oxidized invertase on temperature in 50 mM sodium acetate buffer pH 4.7 and 100 g/dm^3 sucrose.

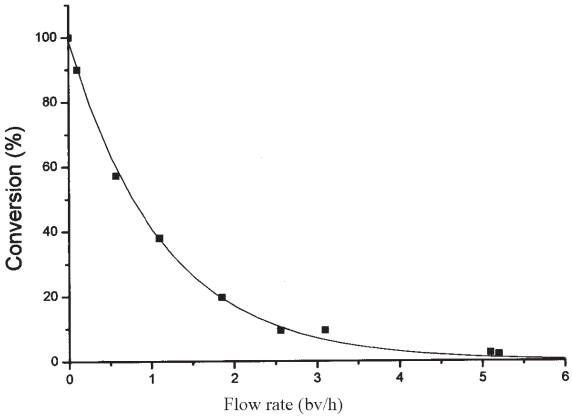

Fig. 5. Dependence of the degree of sucrose conversion on flow rate for 2 cm^3 of immobilized periodate oxidized invertase in a thermostated packed bed reactor in 50 mM sodium acetate buffer pH 4.7 and 500 g/dm^3 of sucrose at 40 ºC.

firmed that periodate oxidized invertase was stabilized by cross-linking on the surface of the sepiolite.

The immobilized periodate oxidized invertase had a pH optimum between 4 and 6, Fig. 3.

The temperature optimum of immobilized invertase was 60 ºC, Fig. 4.

In a thermostated packed bed reactor at 40 ºC and 500 g/dm^3 of sucrose in 50 mM sodium acetate buffer pH 4.7, 90 % conversion of sucrose was obtained at a flow rate of 0.1 bv/h (bed volume per hour), and 50 % at a flow rate of 1 bv/h, Fig. 5.

The specific productivity of immobilized invertase for 90 % degree of conversion was 0.045 kg hydrolyzed sucrose per 1 dm^3 of immobilized invertase per 1 hour. For a degree of conversion of 50 %, the specific productivity was 0.188 kg/dm^3/h. The productivity was two times higher than previously reported in the literature for adsorbed native invertase on sepiolite.[5]

CONCLUSIONS

A new procedure for immobilizing invertase on sepiolite by oxidizing it with periodate before adsorption has been developed. The obtained immobilized invertase was more tightly bound to the sepiolite, and more stable against temperature than adsorbed native invertase. The specific productivity of the immobilized invertase was two times higher than that previously reported in the literature.

Acknowledgement: This research was supported by grant number 1586 from the Ministry of Science, Technology and Development of the Republic of Serbia.

ИЗВОД

ИМОБИЛИЗАЦИЈА ПЕРЈОДАТНО ОКСИДОВАНЕ ИНВЕРТАЗЕ АДСОРПЦИЈОМ НА СЕПИОЛИТУ

РАДИВОЈЕ М. ПРОДАНОВИЋ[1], МИЛОШ Б. СИМИЋ[2] и ЗОРАН М. ВУЈЧИЋ[1]

[1]*Хемијски факултет, Универзитет у Београду, Студентски трг 16, 11001 Београд и* [2]*Центар за нове технологије, ЦТМ, Студентски трг 16, 11001 Београд*

Перјодатно оксидована инвертаза је имобилизована адсорпцијом на сепиолиту. Добијени имобилизовани ензим је био резистентнији на испирање концентрованим растворима соли и имао је осам пута већи полуживот на 60 ºC од адсорбоване нативне инвертазе. У проточном цевастом реактору добили смо 50 % конверзију раствора сахарозе концентрације 500 g/dm^3 на 40 ºC и при протоку од 1 bv/h. Специфична продуктивност имобилизоване инвертазе је била 0,187 kg/dm^3/h.

(Примљено 17. септембра 2002, ревидирано 4. јула 2003)

REFERENCES

1. N. N. Samoshina, N. I. Shustrova, I. D. Stalnaya, L. A. Nakhapetyan, *Prikladn. Biohim. Mikrobil.* **16B** (1980) 915
2. J. Lopez-Santin, C. Sola, J. M. Paris, G. Caminal, *J. Chem. Technol. Biotechnol.* **33B** (1983) 101
3. P. Parascandola, V. Scardi, O. Tartaglione, *Appl. Microbiol. Biotechnol.* **26** (1987) 507

4. B. S. Kubal, K. Sankaran, S. F. D'Souza, *J. Microb. Biotechnol.* **4** (1989) 98
5. M. Kawase, Y. Yoshida, H. Yonekawa, *U. S. P.* (1992) 143847
6. Z. Xiaohua, Z. Jiyan, R. Shaoguang, *Shipin Kexue (Beijing)* **169** (1994) 8
7. P. Monsan, D. Combes, I. Alemzadeh, *Biotechnol. Bioeng.* **26** (1984) 658
8. M. Marek, O. Valentova, J. Kas, *Biotechnol. Bioeng.* **26** (1984) 1223
9. R. Prodanović, S. Jovanović, Z. Vujčić, *Biotechnol. Lett.* **23** (2001) 1171
10. G. L. Miller, *Anal. Chem.* **31** (1959) 426
11. R. Prodanović, S. Jovanović, Z. Vujčić, *Acta. Per. Technol.* **32** (2001) 151.

J.Serb.Chem.Soc. 68(11)825–831(2003)
JSCS – 3103

UDC 547–304.9:543.544.3:66–948.3
Original scientific paper

Gas chromatographic retention indices for N-substituted amino *s*-triazines on capillary columns. Part V. Temperature dependence of the retention index

DUŠAN Ž. MIJIN,* # DUŠAN G. ANTONOVIĆ# and BRATISLAV Ž. JOVANOVIĆ#

Department of Organic Chemistry, Faculty of Technology and Metallurgy, University of Belgrade, P. O. Box 3503, 11120 Belgrade, Serbia and Montenegro

(Received 9 June 2003)

Abstract: The temperature dependence of the retention index was studied for N-substituted amino *s*-triazines on DB-1, DB-5 and DB-WAX capillary columns within the temperature range 190–230 ºC. Two linear equations with the column temperature and its reciprocal as variables were studied. The first one shows a slightly better precision for 2,4-bis(alkylamino)-6-chloro-*s*-triazines and 2-alkylamino-4,6-dichloro-*s*-triazines, while the second one shows a better precision for 2,4-bis(cycloalkylamino)-6-chloro-*s*-triazines.

Keywords: retention indices, *s*-triazines, temperature dependence.

INTRODUCTION

The Kovats retention index I is a useful analytical tool for the identification of a compound in gas chromatography. Since these indices are not sensitive to the gas chromatographic conditions, they can be reproduced in various laboratories.

The temperature dependence of the retention data, especially of Kovats indices, has been debated for a long time.[1] The linear equations for the dependence of the retention index on column temperature t, ºC or $1/T$, K^{-1}:

$$I = a + bt \tag{1}$$

$$I = A + B/T \tag{2}$$

are valid for more or less extended temperature ranges and a variety of solutes and stationary phases. As $b = \mathrm{d}I/\mathrm{d}T$, Equation (1) corresponds (as 10 $\mathrm{d}I/\mathrm{d}T$) to the initially introduced Kovats retention index increments per 10 ºC obtained by finite differences, δI/10 ºC.

The comparative evaluation of Eqs. (1) and (2) has been considered in some papers only graphically with the conclusion that the second equation is less linear than the first one

* Author to whom correspondence should be addresed: e-mail: kavur@elab.tmf.bg.ac.yu
# Serbian Chemical Society active member.

for larger temperature ranges, while some authors indicated only the δI/10 ºC of 10 dI/dT value. A comparative, detailed evaluation of Eqs. (1) and (2) was studied for perfumery compounds by Tudor.[2,3]

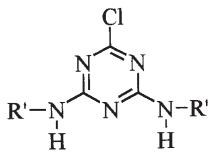

(I)

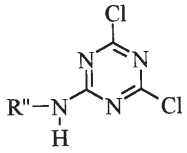

(II)

where R' is:
1-methylethyl (1),
1-methylpropyl (2),
1,2-dimethylpropyl (3),
1,2,2-trimethylpropyl (4),
1-methylbutyl (5),
1,3-dimethylbutyl (6),
1,3,3-trimethylbutyl (7),
1,1-dimethylpropyl (8),
1,1-dimethylbutyl (9),
1,1,3-trimethylbutyl (10),
1,1,3,3-tetramethylbutyl (11),

cyclopropyl (18),
cyclobutyl (19),
cyclopentyl (20),
cyclohexyl (21),
cycloheptyl (22),
cyclooctyl (23),
cyclononyl (24),
cyclodecyl (25),
cycloundecyl (26),
cyclododecyl (27).

and R" is:
1-methylbutyl (12),
1,3-dimethylbutyl (13),
1,1-dimethylpropyl (14),
1,1-dimethylbutyl (15),
1,1,3-trimethylbutyl (16),
1,1,3,3-tetramethylbutyl (17)

Fig. 1. Structural formulae of the 2,4-bis(alkylamino)-6-chloro-*s*-triazines (I), 2-alkylamino-4,6-dichloro-*s*-triazines (II) and 2,4-bis(cycloalkylamino)-6-chloro-*s*-triazines (I).

As part of our study[4–7] of chemical structure-retention index relationships, a study of the temperature dependence of the retention indices for a series of 27 N-substituted amino derivatives of *s*-triazines, 11 compounds of the general formula 2,4-bis(RNH)-6-Cl-*s*-triazine (di-N-substituted alkylamino derivatives of *s*-triazines), 6 compounds of the general formula 2-RNH-4,6-Cl_2-*s*-triazine (mono-N-substituted alkylamino derivatives of *s*-triazines) and 10 compounds of the general formula 2,4-bis(RNH)-6-Cl-*s*-triazine (di-N-substituted cycloalkylamino derivatives of *s*-triazines) (Fig. 1) on capillary columns of different polarity (DB-1, DB-5 and DB-WAX) is reported here.

EXPERIMENTAL

The GC analyses were performed on a Varian 3400 gas chromatograph equipped with a flame ionization detector and an all-glass split-splitless sample injector (1071 capillary injector). Data handling was provided by a Varian 4720 data system.

The capillary columns used were as follows: DB-1, obtained from J & W Scientific, Folsom, CA, USA, dimensions 30 m × 0.256 mm, film thickness 0.25 μm, theoretical plates/meter 4554 for tridecane, coating efficiency 100.3 for tridecane; DB-5, obtained from J & W Scientific, Folsom, CA, USA, dimensions 60 m ×

0.321 mm, film thickness 0.25 μm, theoretical plates/meter 3409 for tridecane, coating efficiency 94.5 for tridecane; DB-WAX, obtained from J & W Scientific, Folsom, CA, USA, dimensions 30 m × 0.234 mm, film thickness 0.25 μm, theoretical plates/meter 3260 for methyl undecanoate, coating efficiency 90.2 for undecanoate.

All columns were operated under isothermal conditions (190, 210 and 230 ºC). The carrier gas was nitrogen, the carrier gas flow 1 ml/min, injector temperature 250 ºC, split ratio 1:60, detector temperature 300 ºC, attenuation 1 and range 10^{-10} amps /mV.

The N-substituted amino *s*-triazines were synthesized from the corresponding amines using the general procedure of Thurston.[8] The purity of all products was controlled by GC, IR and NMR.

The hydrocarbons used in this study as standards were obtained from Fluka (Switzerland).

RESULTS AND DISCUSSION

Table I lists the parameters (*a*,*b*) of Eq. (1) and statistical data (*r*; correlation coefficient; *s*, standard error) for 2,4-bis(alkylamino)-6-chloro-*s*-triazines and 2-alkylamino-4,6-dichloro-*s*-triazines on the capillary columns DB-1 and DB-5. Table II gives the parameters (*A*, *B*) of Eq. (2) and statistical data (*R*, correlation coefficient; *S*, standard error) for 2,4-bis(alkylamino)-6-chloro-*s*-triazines and 2-alkylamino-4,6-dichloro-*s*-triazines on the same columns.

TABLE I. The parameters *a*,*b*; correlation coefficient *r* and standard error *s* for the linear regressions for Eq. (1) on capillary columns DB-1 and DB-5 in the temperature range 190–230 ºC (number of experimental points = 3) for 2,4-bis(alkylamino)-6-chloro-*s*-triazines and 2-alkylamino-4,6-dichloro-*s*-triazines

Column	DB-1					DB-5				
Comp. No	*eI* 190 ºC	*b*	*a*	*r*	*s*	*eI* 190 ºC	*b*	*a*	*r*	*s*
1	1753.88	0.5957	1650.45	0.9972	1.25	1763.13	0.5957	1650.45	0.9972	1.26
2	1918.11	0.6650	1789.94	0.9730	4.45	1929.42	0.6652	1801.20	0.9732	4.44
3	2032.28	0.7212	1894.02	0.9894	2.98	2055.34	0.7217	1916.99	0.9896	2.96
4	2122.01	0.6175	2003.21	0.9794	3.60	2146.94	0.6185	2027.95	0.9794	3.60
5	2001.81	0.9735	1816.86	0.9999	0.15	2066.83	0.9740	1881.80	0.9999	0.08
6	2123.87	0.6970	1991.72	0.9991	0.81	2188.26	0.6980	2055.97	0.9991	0.82
7	2235.62	0.9012	2064.88	0.9988	1.22	2251.95	0.9013	2081.20	0.9988	1.22
8	1959.48	0.7702	1814.79	0.9829	4.07	2002.28	0.7710	1857.45	0.9829	4.07
9	2111.91	0.7772	1965.66	0.9875	3.49	2125.36	0.1800	1898.00	0.9955	3.20
10	2205.28	0.7417	2065.88	0.9841	3.77	2258.03	0.7420	2118.58	0.9843	3.75
11	2344.28	0.7400	2205.03	0.9877	3.30	2390.01	0.7400	2250.76	0.9876	3.32
12	1643.16	0.6900	1510.84	0.9902	2.74	1668.31	0.6912	1535.85	0.9903	2.73
13	1702.15	0.7232	1563.15	0.9825	3.87	1731.01	0.7237	1591.91	0.9825	3.87
14	1617.49	0.5047	1520.85	0.9922	1.79	1647.65	0.5055	1550.87	0.9922	1.78
15	1724.43	0.5167	1625.88	0.9982	0.87	1757.99	0.5175	1659.30	0.9989	0.85
16	1814.45	0.4607	1726.56	0.9979	0.84	1843.66	0.4615	1755.62	0.9978	0.84
17	1906.55	0.4772	1815.46	0.9972	1.00	1936.94	0.4770	1845.70	0.9972	1.00

TABLE II. The parameters *A*,*B*; correlation coefficient *R* and standard error *S* for the linear regressions for Eq. (2) on capillary columns DB-1 and DB-5 in the temperature range 190–230 ºC (number of experimental points = 3) for 2,4-bis(alkylamino)-6-chloro-*s*-triazines and 2-alkylamino-4,6-dichloro-*s*-triazines

Column	DB-1					DB-5				
Comp. No	*eI* 190 ºC	*–B*	*A*	*R*	*S*	*eI* 190 ºC	*–B*	*A*	*R*	*S*
1	1753.88	138823	2053.95	0.9987	0.85	1763.13	138999	2063.58	0.9987	0.86
2	1918.11	154002	2248.70	0.9672	4.90	1929.42	154062	2260.15	0.9674	4.89
3	2032.28	167392	2392.34	0.9857	3.47	2055.34	167512	2415.66	0.9858	3.45
4	2122.01	143108	2429.42	0.9743	4.02	2146.94	143341	2454.85	0.9743	4.02
5	2001.81	226819	2491.34	0.9998	0.50	2066.83	226863	2556.43	0.9998	0.56
6	2123.87	162550	2474.97	0.9998	0.34	2188.26	162727	2539.74	0.9998	0.35
7	2235.62	210142	2689.58	0.9997	0.61	2251.95	210155	2705.94	0.9997	0.62
8	1959.48	180193	2349.92	0.9871	3.55	2002.28	180368	2393.10	0.9870	3.55
9	2111.91	181711	2505.41	0.9910	2.97	2125.36	276171	2720.80	0.9929	4.01
10	2205.28	173497	2581.16	0.9881	3.27	2258.03	173552	2634.02	0.9882	3.25
11	2344.28	172997	2518.90	0.9912	2.80	2391.01	173001	2764.64	0.9911	2.82
12	1643.16	160278	1987.96	0.9866	3.21	1668.31	160455	2013.50	0.9868	3.19
13	1702.15	167683	2062.49	0.9778	4.36	1731.01	167800	2091.60	0.9778	4.36
14	1617.49	117204	1869.71	0.9889	2.13	1647.65	117380	1900.25	0.9890	2.13
15	1724.43	120179	1983.43	0.9965	1.22	1757.99	120357	2017.38	0.9966	1.20
16	1814.45	107143	2045.33	0.9961	1.15	1843.66	107317	2074.91	0.9960	1.16
17	1906.55	110954	2145.59	0.9951	1.33	1936.94	111070	2176.23	0.9951	1.33

Table III lists the parameters of Eq. (1) and statistical data for 2,4-bis(cycloalkylamino)-6-chloro-*s*-triazines on the capillary columns DB-1, DB-5 and DB-WAX. Table IV gives the parameters of Eq. (2) and statistical data for 2,4-bis(cycloalkylamino)-6-chloro-*s*-triazines on the same capillary columns.

All experimental points were recorded in the temperature range 190–230 ºC (at 190, 210 and 230 ºC).

A rather good linear temperature dependence of the retention index is noticed for all used columns. Eq. (1), which is mostly used in the literature, shows a slightly better precision in comparison to Eq. (2) when 2,4-bis(alkylamino)-6-chloro-*s*-triazines and 2-alkylamino-4,6-dichloro-*s*-triazines are considered, whereas Eq. (2) gives slightly better results than Eq. (1) for 2,4-bis(cycloalkylamino)-6-chloro-*s*-triazines.

The standard error for some 2,4-bis(alkylamino)-6-chloro-*s*-triazines and 2-alkylamino-4,6-dichloro-*s*-triazines is around 1.00 or less. In most cases the standard error is higher indicating a hyperbolic curve. The *s*-triazines in this work were studied over a narrow temperature range of 40 ºC with only three experimental points. The hyperbolic temperature dependence of the retention index can be applied only for compounds having more experimental points.[9]

TABLE III. The parameters *a*, *b*; correlation coefficient *r* and standard error *s* for the linear regressions for Eq. (1) on capillary columns DB-1, DB-5 and DB-WAX in the temperature range 190–230 ºC (number of experimental points = 3) for 2,4-bis(cycloalkylamino)-6-chloro-*s*-triazines.

Column	DB-1					DB-5					DB-WAX				
Comp. No.	*eI* 190ºC	*b*	*a*	*r*	*s*	*eI* 190 ºC	*b*	*a*	*r*	*s*	*eI* 190 ºC	*b*	*a*	*r*	*s*
18	2048.58	0.5540	1936.56	0.9801	3.17	2086.66	0.5967	1974.45	0.9865	2.88	2137.93	0.5947	2026.06	0.9864	2.79
19	2146.08	0.5300	2046.82	0.9732	3.53	2192.25	0.5475	2089.49	0.9804	3.11	2243.45	0.5472	2140.73	0.9805	3.09
20	2245.29	0.5585	2140.42	0.9818	3.05	2291.48	0.5757	2183.40	0.9808	3.23	2342.60	0.5787	2233.95	0.9811	3.22
21	2345.05	0.5645	2239.41	0.9705	3.96	2391.99	0.5525	2288.64	0.9687	4.00	2443.11	0.5545	2339.38	0.9698	4.00
22	2439.67	0.5602	2334.58	0.9786	3.32	2484.55	0.6100	2369.79	0.9871	2.79	2535.73	0.6112	2420.71	0.9876	2.74
23	2545.82	0.4672	2458.51	0.9646	3.61	2592.24	0.4807	2501.96	0.9818	2.62	2643.48	0.4800	2553.32	0.9827	2.55
24	2643.75	0.6225	2527.06	0.9763	3.89	2688.93	0.6447	2568.23	0.9748	4.42	2740.13	0.6442	2619.50	0.9723	4.37
25	2744.88	0.5560	2640.21	0.9887	2.37	2790.12	0.5912	2678.63	0.9923	2.07	2841.32	0.5912	2729.81	0.9926	2.03
26	2847.33	0.5160	2750.29	0.9860	2.46	2893.51	0.5145	2796.53	0.9915	1.91	2944.77	0.5127	2848.10	0.9919	1.84
27	2947.38	0.4800	2857.91	0.9544	4.24	2992.06	0.5270	2893.89	0.9518	4.80	3043.27	0.5267	2945.12	0.9526	4.75

TABLE IV. The parameters *A*, *B*; correlation coefficient *R* and standard error *S* for the linear regressions for Eq. (2) on capillary columns DB-1, DB-5 and DB-WAX in the temperature range 190–230 ºC (number of experimental points = 3) for 2,4-bis(cycloalkylamino)-6-chloro-*s*-triazines.

Column	DB-1					DB-5					DB-WAX				
Comp. No.	*eI* 190ºC	*–B*	*A*	*R*	*S*	*eI* 190 ºC	*–B*	*A*	*R*	*S*	*eI* 190 ºC	*–B*	*A*	*R*	*S*
18	2048.58	129709	2321.73	0.9846	2.79	2086.66	139551	2388.94	0.9894	2.48	2137.93	139068	2439.13	0.9901	2.39
19	2146.08	124133	2415.34	0.9785	3.17	2192.25	128125	2649.96	0.9848	2.73	2243.45	128065	2521.02	0.9849	2.73
20	2245.29	130676	2528.48	0.9860	2.67	2291.48	134730	2583.49	0.9851	2.84	2342.60	135425	2636.17	0.9855	2.83
21	2345.05	132252	2631.99	0.9761	3.57	2391.99	129465	2672.94	0.9744	3.62	2443.11	129931	2725.06	0.9745	3.62
22	2439.67	131137	2723.96	0.9832	2.94	2484.55	142619	2793.41	0.9906	2.37	2535.73	142901	2845.18	0.9911	2.33
23	2545.82	109534	2783.61	0.9706	3.30	2592.24	112484	2836.00	0.9861	2.29	2643.48	112295	2886.81	0.9868	2.23
24	2643.75	145747	2959.80	0.9812	3.47	2688.93	151033	3016.58	0.9772	3.98	2740.13	150907	3067.50	0.9777	3.93
25	2744.88	129960	3026.26	0.9921	2.00	2790.12	138111	3088.98	0.9950	1.68	2841.32	138103	3140.14	0.9953	1.64
26	2847.33	120662	3108.68	0.9897	2.12	2893.51	120203	3153.65	0.9943	1.56	2944.77	119784	3203.98	0.9947	1.50
27	2947.38	112628	3192.09	0.9613	3.92	2992.06	123683	3260.85	0.9588	4.44	3043.27	123616	3311.89	0.9596	4.40

CONCLUSION

The linear temperature dependence of retention index for *s*-triazines was established on capillary columns of different polarity. A good linearity of the retention index versus column temperature was found in the investigated temperature range.

Acknowledgment: The authors are grateful to the Ministry of Science, Technology and Development of Serbia for financial support (Project 1694).

ИЗВОД

ГАСНОХРОМАТОГРАФСКИ РЕТЕНЦИОНИ ИНДЕКСИ N-СУПСТИТУИСАНИХ АМИНО ДЕРИВАТА *s*-ТРИАЗИНА НА КАПИЛАРНИМ КОЛОНАМА. ДЕО V. УТИЦАЈ ТЕМПЕРАТУРЕ НА РЕТЕНЦИОНИ ИНДЕКС

ДУШАН Ж. МИЈИН, ДУШАН Г. АНТОНОВИЋ и БРАТИСЛАВ Ж. ЈОВАНОВИЋ

Катедра за органску хемију, Технолошко-металуршки факултет, Универзитет у Београду, Карнегијева 4, 11120 Београд

У раду је приказана линеарна заивсност ретенционог индекса од температуре коришћењем линеарних зависности ретенционог индекса у функцији температуре колоне t, °C или $1/T$, K^{-1} за *s*-триазине на капиларним колонама DB-1, DB-5 и DB-WAX у температурном интервалу 190–230 °C.

(Примљено 9. јуна 2003)

REFERENCES

1. K. Heberger, M. Gorgenyi, T. Kowalska, *J. Chromatography A* **973** (2002) 135
2. E. Tudor, *J. Chromatography A* **779** (1997) 287
3. E. Tudor, *Rev. Roumain. Chim.* **43** (1998) 587
4. D. G. Antonović, G. A. Bončić, *J. Serb. Chem. Soc.* **59** (1994) 993
5. D. G. Antonović, G. A. Bončić, *J. Serb. Chem. Soc.* **60** (1995) 669
6. O. S. Rajković, D. G. Antonović, B. Ž. Jovanović, G. A. Bončić, *J. Serb. Chem. Soc.* **59** (1996) 993
7. D. Ž. Mijin, D. G. Antonović, G. A. Bončić, B. Ž. Jovanović, O. S. Rajković, *J. Serb. Chem. Soc.* **68** (2003) 557
8. J. T. Thurston, J. R. Dudley, D. W. Kaisler, J. Hechenbleinker, F. C. Shafner, D. Holm-Hansen, *J. Am. Chem. Soc.* **73** (1951) 2983
9. E. Tudor, *J. Chromatography A* **848** (1999) 215.

J.Serb.Chem.Soc. 68 (11)833–841(2003)
JSCS – 3104

UDC 541.183:549.08:504.55.054
Original scientific paper

Adsorption of inorganic anionic contaminants on surfactant modified minerals

ALEKSANDRA VUJAKOVIĆ, ALEKSANDRA DAKOVIĆ, JOVAN LEMIĆ, ANA RADOSAVLJEVIĆ-MIHAJLOVIĆ and MAGDALENA TOMAŠEVIĆ-ČANOVIĆ*

Institute for the Technology of Nuclear and Other Mineral Raw Materials, P. O. Box 390, Franshe d Epere 86, 11001 Belgrade, Serbia and Montenegro (e-mail: m.tomasevic@itnms.ac.yu)

(Received 20 March, revised 16 June 2003)

Abstract: Organo-mineral complexes were obtained by treatment of aluminosilicate minerals (zeolite, bentonite and diatomaceous earth) with a primary amine (oleylamine) and an alkyl ammonium salt (stearyldimethylbenzyl ammonium chloride). The modification of the zeolite surface was carried out in two steps. The first step was treatment of the zeolite with 2 M HCl. This acid treatment of the zeolite increased its affinity for neutral molecules such as surface-active amines. The second step of the modification was the adsorption of oleylamine on the acid treated zeolite. Four types of organo-mineral complexes were prepared and their anion adsorption properties were compared to those of organo-zeolite. The adsorption of sulphate, bichromate and dihydrogenphosphate anions on the organo-mineral complexes was investigated. The anion adsorption measurements showed that the most efficient adsorbent for anion water pollutants was the primary amine modified H^+-form zeolite.

Keywords: zeolite, bentonite, diatomaceous earth, oleylamine, adsorption, anions.

INTRODUCTION

Zeolites posses a negative net charge compensated by the presence of exchangeable cations at the aluminosilicate surfaces. A variety of cations can be adsorbed on zeolites by the cation exchange mechanism. Therefore, natural zeolites are known as efficient adsorbents for cation water pollutants. To increase the ability of zeolites to remove nonpolar and anion water pollutants, it is necessary to modify their surface. The permanent negative charge in the crystal structures of some minerals (zeolite, bentonite, illite, kaolinite *etc.*), make them suitable for surface modification by long chain organic cations – surfactants.[1–5] When the aqueous surfactant concentration is greater than the critical micelle concentration (CMC) and sufficient surfactant is present in the system, the sorbent surfactant molecules primarily form a bilayer on the external surface[6] of the zeolite. Three-dimensional framework of zeolites retains the high molecular weight surfactants primarily on their outer surfaces, whereby at sufficient loading the surfactant forms a bilayer. This bilayer forma-

* Author for correspondence.

tion results in a reversal of the charge on the external surface of the zeolite, providing sites where anions will be retained and cations repelled, while neutral species can partition into the hydrophobic core.

On the other hand, surfactant retention occurs in the interlayer space of bentonite and other layer silicates. These modified minerals provide a primarily hydrophobic environment for the retention of organic molecules of low polarity.[6]

The first aim of this study was to provide an efficient anion adsorbent based on zeolite modified by acid and amine treatment. For comparison of the efficiency of different modification of non-metallic minerals, it was considered to be of interest to examine the possibilities of various organo-mineral complexes based on zeolite, bentonite and diatomaceous earths to remove anion water pollutants.

EXPERIMENTAL

Materials

The purity of all the used chemicals was reagent-grade. Distilled water was used. The surface-active agents used for obtaining the organo-mineral complexes were oleylamine and stearyldimethylbenzyl-ammonium chloride (SDMBA), both supplied by Akzo-Chemie. Oleylamine is a primary, long chained fatty amine with the chemical formula: $C_{18}H_{35}NH_2$. Oleylamine is insoluble in water but readily soluble in polar and non-polar organic solvents. SDMBA is a quaternary ammonium salt with the chemical formula $[CH_3(CH_2)_{17}(CH_3)_2NC_6H_5]^+ Cl^-$. It is soluble in water and in organic solvents.

Synthesis of organo-zeolite adsorbents

Natural clinoptilolite from the deposit Zlatokop, Serbia was used as the starting material for the preparation of organo-zeolite adsorbents. The raw material was ground and wet-classified to < 0.063 mm. The purity degree of the clinoptilolite was higher than 90 %, with pyrite, quartz and feldspar as the major impurities. The chemical composition of the mineral (wt%) was: SiO_2, 68.90; Al_2O_3 13.40; Fe_2O_3 1.84; TiO_2 0.25; MnO 0.01; CaO 3.25; MgO 0.92; Na_2O 1.20; K_2O 1.00 and H_2O 9.25. This clinoptilolite is predominantly of the calcium type with a cation exchange capacity (CEC) of 1420 mmol M^+/kg, and an external cation exchange capacity (ECEC) of 190 mmol M^+/kg. The ECEC value refers to exchangeable cations at the external zeolite surface.[7,8] The zeolite was first treated with an aqueous 2 M HCl solution. The zeolite (5 %) was suspended in the acid solution. The suspension was stirred for 2 h at 60 ºC and 24 h at room temperature. The centrifuged zeolite sample was repeatedly washed until Cl^- free. The sample was dried at 105 ºC until constant mass (Sample HZ. The ECEC value of this zeolite was 187 mmolM^+/kg.[7]

The results of a detailed study of the structural property of the natural and acid treated zeolite are given elsewhere.[7,9]

The surface modified zeolite samples were prepared as follows:

Sample OHZ. Oleylamine was adsorbed onto the H^+-from zeolite (HZ). An alcoholic oleylamine solution (190 mmol/kg) was added to a 5 % aqueous zeolite suspension. The mixture was stirred in a turbo-mixer for 30 min at 10 000 rev. min^{-1}. The filteres organo-zeolite was repeatedly washed unitl it was amine free. The sample was dried at 80 ºC until constant mass (OHZ). The free, non-adsorbed, oeylamine was determined in the supernatant by titration with 0.1 M HCl (ASTM D2074-66).[10] The sample characterization has been described in a previous papers.[7,9,11]

Sample OZ. This organo-zeolite sample was prepared by the reaction of SDMBA with natural zeolite: An aqueous solution CDMBA (190 mmol/kg) was added to a 5 % zeolite suspension. The mixture was stirred in a turbo-mixer for 30 min at 10 000 rev. min^{-1}. The filtered organo-zeolite was repeatedly washed until it was amine free. The sample was dried at 80 ºC until constant mass. The free, non-adsorbed SDMBA was determined in the supernatant using a method for the determination of quaternary amines (AkzoChemie, WV/2.001-2).

Synthesis of organo-bentonite adsorbents

Bentonite from the deposit Petrovac, Montenegro, was used as the starting material for the preparation of organo-bentonite adsorbents. This bentonite ore consists of montmorillonite as the main componenet and impurities such as crystobalite and quartz. A montmorillonite concentrate with particle size (< 10 μm) was obtained by centrifugal classification. The chemical composition of the mineral (wt%) was: SiO_2 67.59; Al_2O_3 16.70; Fe_2O_3 2.83; TiO_2 0.30; CaO 1.62; MgO 4.06; Na_2O 0.52, K_2O 0.58 and H_2O 6.10. The predominant exchangeable cation was calcium with a CEC value of 780 mmol M^+/kg.[8] This purified bentonite was used in the further procedures. The modified bentonite samples were prepared as follows:

Sample OHB. Montmorillonite concentrate (< 10 μm) was firstly treated with an aqueous 1 M HCl solution. The 5 % montmorillonite was suspended in the acid solution, stirred for 24 h at room temperature. The montmorillonite sample was then centrifuged and repeatedly washed until it was Cl^- free. Sample was dried at 105 ºC until constant mass. The oleylamine was adsorbed on such a prepared H^+-form bentonite. An alcoholic oleylamine solution (780 mmol/kg) was added to a 5 % aqueous bentonite suspension. The mixture was stirred in a turbo-mixer for 30 min at 10 000 rev. min^{-1}. The filtered organo-bentonite was repeatedly washed until it was amine free. The sample was dried at 80 ºC until constant mass. The characterization of this complex has already been described.[12]

Sample OB. This organo-bentonite sample was prepared by the adsorption of SDMBA on montmorillonite. An aqueous SDMBA solution (780 mmol/kg) was added to a 5 % montmorillonite suspension. The mixture was stirred in a turbo-mixer for 30 min at 10 000 rev. min^{-1}. The filtered organo-bentonite was repeatedly washed until it was amine free. The sample was dried at 80 ºC until constant mass.

Sample ODE (diatomaceous earth adsorbent)

The diatomaceous earth, which is applied as a clarifying agent in the beer industry, was used in this experiment. This amorphous silicate contains large amounts of impurities such as clay, quartz, mica. The sample was ground and used without purification.

The organo-minearl complex was obtained by adding an alcoholic oleylamine solution (190 mmol/kg) to an aqueous 5 % suspension of diatomaceous earth. The mixture was stirred in a turbo-mixer for 30 min at 10 000 rev. min^{-1}. The filtered organo-mineral complex was repeatedly washed until it was amine free. The sample was dried at 80 ºC until constant mass.

Anion adsorption tests

The prepared organo-mineral complexes were tested on the adsorption of $Cr_2O_7^{2-}$ (1.4 mmol/dm^3), SO_4^{2-} (3.2 mmol/dm^3) and $H_2PO_4^-$ (3.2 mmol/dm^3) anions. The aqueous solution of the anions were mixed with a 5 % organo-mineral suspension for 5 h on a magnetic stirrer, at room temperature. The adsorption mixtures were left standing overnight, filtered, and the concentration of the anions in the supernatant determined. The amount of anion adsorbed on the organo-mineral complex was calculated from the difference between the anion concentration in solution before and after equilibration. The anion adsorption index was calculated as the ratio of the amount of adsorbed anion and the initial amount of anion. Adsorption isotherms of anions were performed on sample OHZ using the batch equilibrium technique.[7]

Characterization methods

The CEC and ECEC values were determined by the method of Ming and Dixon.[8]

The stability of organo-mineral complexes was estimated in the following manner:

When amine adsorption on a mineral was finished, the amine remaining in the supernatant combined with the wash solution was determined by known methods (oleylamine- ASTM D2074-66).[10] SDMBA AkzoChemie, WV/2.001-2). The percent of amine bound to the mineral surface was calculated from the difference between the added and remaining amount of amine, divided by the amount of amine added.

Bichromate was determined by atomic absorption spectroscopy, sulphate by a turbidimetric method using a spectrophotometer[13] and phosphate by the molybdo-vanadate method using a spectrophotometer.[14]

RESULTS AND DISCUSSION

A few facts must be considered when choosing a mineral that could be a potential base for the creation of anion adsorbents. Zeolites and bentonites are among the most widely used adsorbing minerals. It is known that minerals such as zeolites and bentonites possess a net negative charge owing to isomorphous substitutions in the crystal lattice. This negative charge is compensated by exchangeable cations present at the external and internal mineral surfaces. The first condition for anion adsorption is the neutralization or inversion of a negative charge. Neutralization can be achieved by adsorption of a surface-active amine. The large amine molecules can penetrate in-between the expandable bentonite layers, but in case of zeolite such adsorption can occur only at the external surfaces. So, the cation exchange capacity (CEC) is a relevant values for the adsorption of amines on bentonites, while the external cation exchange capacity (ECEC) is a value of major importance for the adsorption of amines on zeolites.[7,11] Therefore, the employed amines were adsorbed in amounts equivalent to the CEC value for bentonites and the ECEC values for zeolites. For bentonites, the ECEC value is equal to the CEC value. The results of amounts of SDMBA or oleylamine adsorbed on different forms of zeolite and bentonite are presented in Table I, together with the results of the quantification of amine bonding on a mineral surface.

TABLE I. Results of the adsorption of SDMBA or oleylamine on zeolites and bentonites

Samples	ECEC mmol/kg	Amine/(mmol/kg)				Amine bound/%
		SDMBA		Oleyamine		
		Added	Adsorbed	Added	Adsorbed	
OZ	190	190	133	–	–	70
OHZ	190	–	–	190	190	100
OB	1317	1317	1083	–	–	97
OHB	1317	–	–	1317	1222	93
ODE	–	–	–	–	–	< 4

It can be seen from Table I that a higher oleylamine adsorption was obtained by using acid pretreated zeolite OHZ (100 %). On natural Ca-zeolite, 50 % of oleylamine was adsorbed,[7] which can be explained by the presence of active acid sites at the mineral surface, as a result of the acid treatment of the zeolite.[7,9] Binding of quaternary (SDMBA) amine on a untreated natural zeolite was 70 %. If amounts of amine bound on these two organo-zeolites are compared, it is obvious that a far better product was obtained by oleylamine chemisorptions on H^+-zeolite (100 %), than when naturally zeolite with SDMBA (70 %) was used.

Natural (Ca-form) bentonite formed a stable product with the quaternary amine (OB) (binding 97 % of the amine), as was the case with the H^+-form and the primary amine (HB – 93 %).

The lowest amount of amine was bound on diatomaceous earth, as was to be expected. It cannot be claimed that the formation of an organo-mineral complex occurred in

this case. The diatomaceous earth, known as an adsorbent of colloid particles and not of polar organic species, was chosen in this experiment to prove that acid modification of the zeolite surface is a decisive factor for amine and anion adsorption.

As amount and kind of organic components in the organo-mineral complexes have a great influence on the ability of an organo-mineral to adsorb anions,[7] it was necessary to examine these points.

The comparative results of the anion adsorption tests on the organo-mineral complexes, all samples being prepared under the same conditions, are presented in Table II and Fig. 1. It can be seen that the most efficient anion adsorbent is OHZ, which removes all the bichromate and 95 % of the sulphate and dihydrogenphosphate from polluted water. The other organo-mineral complexes showed relatively high affinities for bichromate, which can be attributed to amine-bichromate interaction which was proven by preliminary tests. The affinity of the adsorbents for phosphate is not negligible, and may also be partially due to amine-phosphate interaction, according to preliminary studies. The adsorption of sulphate was weak on these adsorbents.

TABLE II. Adsorption of amions on the examined adsorbents (mmol/kg)

	SO_4^{2-}		$Cr_2O_7^{2-}$		PO_4^{3-}	
	Added	Adsorbed	Added	Adsorbed	Added	Adsorbed
OZ	82	1.5	158	126	98	19
OHZ	82	78	158	158	98	93
OB	82	8	158	77	98	18
OHB	82	2.5	158	12	98	40
ODE	82	3	158	48	98	8

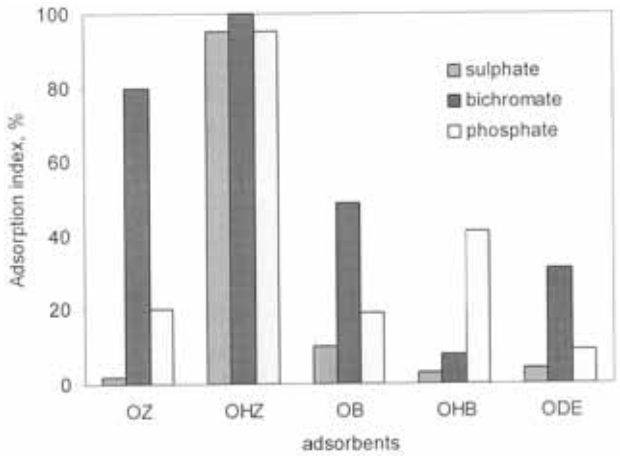

Fig. 1. Anion adsorption indexes for the organo-mineral complexes.

It can be seen, from the Table II and Fig. 1, that the most efficient anion adsorbent was sample OHZ – oleylamine adsorbent on the H^+-form zeolite. The adsorption isotherms for the three examined anions were obtained using the batch equilibrium technique (Table III, Figs. 2, 3 and 4).

TABLE III. The results of the adsorption of different amount of anions (SO_4^{2-}, $Cr_2O_7^{2-}$, PO_4^{3-}) on the OHZ-adsorbent

Anion	Added/(mmol/kg)	Adsorbed/(mmol/kg)	Equilibrium conc./(mmol/l)	% A
SO_4^{2-}	20	18.5	0.20	92.5
	40	37	0.30	92.5
	60	57	0.30	95.0
	80	75	0.47	93.7
	100	78	2.6	78
CrO_4^-	32	32	< 0.1	100
	64	63.5	< 0.1	99
	96	95	< 0.2	99
	128	126	0.3	98
	160	157	0.5	98
$H_2PO_4^-$	20	19.7	0.12	98.5
	40	39.5	0.12	98.7
	60	59	0.18	98.1
	80	77	0.30	96.2
	100	92.5	0.55	92.5

The results of SO_4^{2-} adsorption on OHZ are given in Fig. 2: sulphate adsorbed, mmol/kg depending of the added amount, mmol/kg (Fig. 2a) and as a function of equilibrium concentration, mmol/l (Fig. 2b).

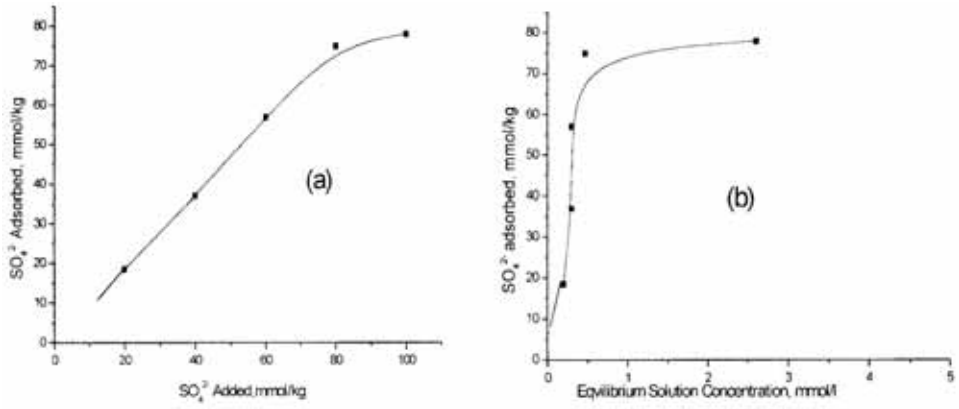

Fig. 2. Sulphate adsorbed on organozeolite – OHZ (as a function of the added amount (a) and the equilibrium concentration (b)).

As can be seen from Fig. 2, more than 90 % of sulphate anions were adsorbed up to 80 mmol/kg SO_4^{2-} and the equilibrium concentration was below 0.5 mmol/l. With the higher sulphate concentrations, the efficacy of adsorption decreased.

Efficient adsorption of $Cr_2O_7^{2-}$ ions, was obtained over the whole examined concentration range (Fig. 3). The equilibrium concentration was below 0.5 mmol/l and more than 98 % of the $Cr_2O_7^{2-}$ ions were adsorbed.

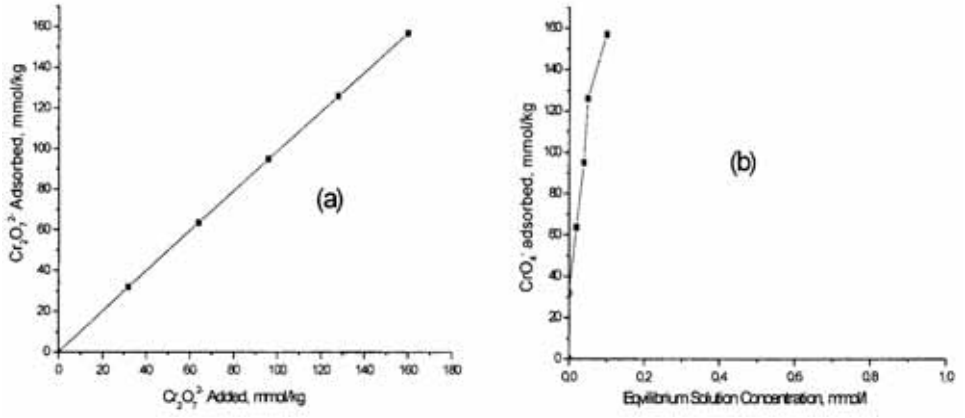

Fig. 3. Bichromate adsorbed on organo-zeolite – OHZ (as a function of the added amount (a) and the equilibrium concentration (b)).

Dihydrogenphosphate adsorption on this adsorbent was also high (Fig. 4).

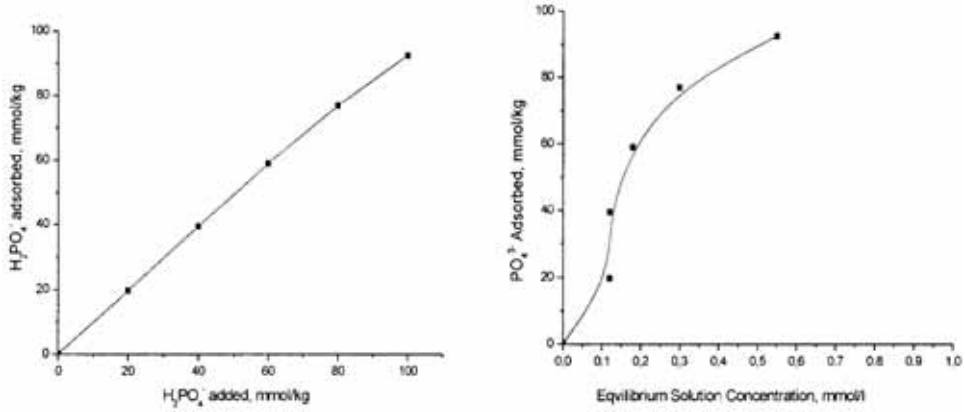

Fig. 4. Dihydrogenphosphate adsorbed on organo-zeolite – OHZ (as a function of the added amount (a) and the equilibrium concentration (b)).

The phenomena of anion adsorption on organo-mineral complexes are probably electrostatic in nature.[11,15] The hemimicelles of the organo-mineral complex attract and trap the anions on the mineral surface. The mechanism of anion adsorption, which is still not clearly

understood, is thought to be surface precipitation on the organo-zeolite.[11,12,15] However, the explanation for such a superior anion adsorption on OHZ lies in the acid surface modification, which resulted in the formation of the most stable organo-mineral complex.

CONCLUSION

The obtained results shows efficient anion adsorbents were prepared by appropriate modification of natural zeolite and bentonite. The organo-zeolite obtained by oleylamine modification of the H^+ form of zeolite is an effective adsorbent of SO_4^{2-}, $Cr_2O_7^{2-}$ and $H_2PO_4^-$ anions present in water. The protonated amine molecules at the external surface of the H^+ clinoptilolite act as much stronger anions adsorption sites than the quaternary ammonium salt cations on natural clinoptilolite.

Acknowledgement: This work is part of research activities of the project 1814. The authors would like to thank the Ministry of Science, Technology and Development of the Republic of Serbia for financial support of the project.

ИЗВОД

АДСОРПЦИЈА НЕОРГАНСКИХ АНЈОНСКИХ ЗАГАЂИВАЧА НА МОДИФИКОВАНИМ МИНЕРАЛИМА

АЛЕКСАНДРА ВУЈАКОВИЋ, АЛЕКСАНДРА ДАКОВИЋ, ЈОВАН ЛЕМИЋ, АНА РАДОСАВЉЕВИЋ-МИХАЈЛОВИЋ и МАГДАЛЕНА ТОМАШЕВИЋ-ЧАНОВИЋ

Институт за технологију нуклеарних и других минералних сировина, Франше д'Епереа 86, 11000 Београд

Органо минерални комплекси су добијени активацијом основних минерала (зеолита, бентонита и диатомијске земље) са примарним амином (олејламином) и алкил амонијум јоном (стеарил диметил бензил амонијум хлоридом). Ефикасан адсорбент анјона је припремљен модификацијом површине природног зеолита са примарним амином. Полазни зеолит је прво третиран са 2 M HCl, а затим је на H-форми зеолита извршена адсорпција олејламина. Направљена су још четири органо комплекса модификацијом бентонита и диатомијске земље са стеарил диметил бензил амонијум јоном и испитана је адсорпција анјона на њима. Експерименти адсорпције анјона су показали да се најефикаснији адсорбент за пречишћавање вода контаминираним анјонима добија двостепеним (киселинско / аминским) третирањем природног зеолита.

(Примљено 20. марта, ревидирано 16. јуна 2003)

REFERENCES

1. R. S. Bowman, Z. Li, S. J. Roy, T. Burt, T. L. Johnson, R. L. Johnson, in *Physical and Chemical Remediation of Contaminated Aquifers*, J. A. Smith and S. Burns, (Eds.), Kluwer Academic Publishers, 2001, p. 161
2. R. S. Bowman, E. J. Sullivan, Z. Li, in *Natural Zeolites for the Third Millennium*, C. Colella and F. A. Mumpton (Eds.), De Frede Editore, Naples, Italy, 2000, p. 287
3. Z. Li, R. S. Bowman, *Wat. Res.* **35** (2001) 16, 3771
4. Z. Li, D. Alessi, P. Zhang, R. S. Bowman, *J. Environ. Eng.* **128** (2002) 7, 583
5. M. Tomašević-Čanović, R. Petronijević, D. Nedeljković, A. Lađević, *Proc. I Regional Symposium "Chemistry and Environment"*, Vrnjačka Banja, 25–29 September 1995, Serbian Chemical Society and Montenegrin Chemical Society, 1995, p. 767

6. Z. Li, R. S. Bowman, *Environ. Sci. Technol.* **31** (1997) 2407
7. A. D. Vujaković, M. R. Tomašević-Čanović, A. S. Daković, V. T. Dondur, *Appl. Clay Sci.* **17** (2000) 265
8. D. W. Ming, J. B. Dixon, *Clays Clay Miner.* **35** (1987) 6, 463
9. A. S. Radosavljević-Mihajlović, A. S. Daković, M. R. Tomašević-Čanović, *J. Mining and Metallurgy* **38 A** (2002) 87
10. ASTM D2074-66, 1982. *Standard Test Method for Sulphate in Water*. Water and Environmental Technology, American Society for Testing and Materials, pp. 337–9
11. A. D. Vujaković, M. A. Đuričić, M. R. Tomašević-Čanović, *J. Therm. Anal. Cal.* **63** (2001)
12. A. D. Vujaković, M. R. Tomašević-Čanović, V. T. Dondur, *J. Serb. Chem.. Soc.* **7** (1997) 599
13. ASTM D516, 1982. *Standard Test Method for Sulphate in Water*. Water and Environmental Technology, American Society for Testing and Materials, pp. 660–1
14. ASTM D515, 1982. *Standard Test Method for Phosphorus in Water*. Water and Environmental Technology, American Society for Testing and Materials, pp. 595–6
15. G. M. Haggerty, R. S. Bowman, *Environ. Sci. Technol.* **28** (1994) 3, 452.

J.Serb.Chem.Soc. 68(11)843–847(2003)
JSCS – 3105

UDC 542.913:546.56+541.13+621.357
Original scientific paper

Synthesis of copper nanorods using electrochemical methods

XUEGENG YANG[a], SHENHAO CHEN[a,b*], SHIYONG ZHAO[a], DEGANG LI[a] and HOUYI MA[a]

[a]*Department of Chemistry, Chandong University, Jinan 250100, PR China and* [b]*State Key Laboratory for Corrosion and Protection of Metals, Shenyang 110015, PR China (e-mail: shchen@sdu.edu.cn.)*

(Received 28 March 2003)

Abstract: Copper nanorods were synthesized using controlled-current electrochemical methods. The surfactants in the electrolyte served as both a templates and stabilizers during the synthesis procedure. TEM images show that the products consist mainly of nanosized rod-like structures. The current density applied during the electrodeposition was found to have an effect on the shape and yield of the copper nanorods.

Keywords: copper nanorods, electrochemical, template, microemulsion.

INTRODUCTION

There is significant interest and ongoing research in the preparation and application of nanometer sized materials. The physical and chemical properties of these matenals are quite different from those of the bulk phase due to the high surface area to volume ratio. Their distinctive electronic, magnetic, and optical properties contribute attractive prospects in the design of new electronic and optical devices, information storage, gas sensors, *etc*.[1]

Metal nanoparticles are of interest due to their special properties in many aspects, such as catalysis,[2–4] template for assembly of nano-sized materials,[5] *etc*. Their properties and applications are strongly dependent on their shapes.[6,7] Of all the methodologies developed for the production of metal nanoparticles, on either a physical or chemical basis, the electrochemical method[8–10] offers an simple alternative means for high yield production of nanoparticles. Wang's group has synthesized gold nanorods *via* an an electrochemical method by introducing a shape-reducing co-surfactant into the electrolyte.[11,12] The surfactants they used were employed as both the supporting electrolyte and the stabilizer for the resulting cylindrical Au nanoparticles. The mechanisms of particle-growth when using the electrochemical technique and the mixed cationic surfactant system are not fully understood. Yet it is generally considered to be a template method with a dynamic micelle system serving as the template.[12] M. B. Mohamed *et al.* reported the effect of temperature on the gold nanorods produced by this electrochemical method.[13] They found that the mean aspect ratio of the nanorods in solution decreases with increasing temperature while the average width remains constant.

* Author to whom correspondence should be addressed. Fax: +86-531-8565167.

Micromulsions find application in enhanced oil recovery, as well as in the pharmaceuticals and cosmetic industries. Water-in-oil microemulsions have been extensively used as microreactors to prepare monodisperse nanosized particles, such as metal, metal borides and metal oxides.[14] Pileni *et al.* reported the synthesis of copper nanorods by using reverse micelles as templates.[15]

The previous electrochemical synthesis method using a surfactant as the template was limited to Au nanorods.[11–13] Recently, we extended the method to a more active metal, *i.e.*, copper. In this paper, attempts to prepare copper nanorods using a new experiment system are reported. TEM results show that the product consists of nanorods with a mean diameter of 30 nm and length of up to 1 μm. The effect of the current density applied in the experiment on the shape of the product is also reported in this communication.

EXPERIMENTAL

A two-electrode cell was used for the electrodeposition. A copper plate (1.2×1.2 cm^2) was used as the anode and a platinum plate (1.5×1.5 cm^2) as the cathode. Both the electrodes were immersed in an electrolyte consisting of a hydrophilic cationic surfactant, 0.08 mol dm^{-3} hexadecyltrimethylammonium bromide (C_{16}TABr), and a hydrophobic cationic co-surfactant, 0.01 mol dm^{-3} tetrabutylammonium bromide (TC_4ABr). The glass electrochemical cell was then placed in an ultrasonic cleaner.

Controlled-current electrolysis was used throughout the experiments at two different current densities: 0.14 mA cm^{-2} and 0.3 mA cm^{-2}. The typical electrolysis time was 30 minutes. The synthesis was performed under an ultrasonication at a controlled temperature, 38 ± 2 ºC. The surface of the copper electrode was polished with emery papers and ultrasonically cleaned first in ethanol and then in water before the experiment. Immediately before the electrolysis, 0.2 mL of acetone and 0.16 mL of cyclohexane were added into 10 mL of electrolyte solution. Acetone was used to loosen the micellar framework and cyclohexane was necessary for enhancing the formation of elongated rodlike C_{16}TABr micelle.[11] After several minutes of electrolysis, the white solution turned a light red color, which indicates the formation of colloidal copper nanostructures. During the synthesis procedure, the bulk copper anode was converted into copper nanorods, probably at the interfacial region of the surfactants in the electrolyte, which allows the production of the resulting cylindrical structure.

Transmission electron microscope (TEM) data were acquired on a Hitachi H-800 TEM operated at 100 kV acceleration voltage. Samples containing Cu nanorods were prepared by dip coating the colloidal solutions on formvar/carbon film Cu grids.

RESULTS AND DISCUSSION

Typical TEM morphologies of the products are shown in Figs. 1–3. It can be seen that the products mainly consist of rod-like structures.

Figure 1 and Fig. 2 show nanorods obtained under a controlled current of 0.14 mA cm^{-2}. Figure 1 is an overall image of the products. The mean transverse diameter of a Cu nanorod is equal to *ca*. 30 nm, while the mean longitudinal length varies from 400 nm to 1 μm. The two typical copper nanorods shown in Fig. 2 are about 30 nm in diameter. A higher yield of nanorods was obtained at a current density of 0.3 mA cm^{-2}. The shape of the nanorods (Fig. 3) obtained at this current density are different from those obtained at a current density of 0.14 mA cm^{-2}, (Fig. 1). There is evidence that the current applied during the production plays and important role in the synthesis of copper nanorod by this method.

A microemulsion is a thermodynamically stable dispersion of two immiscible liquids consisting of microdomains of one or both liquids stabilized by an interfacial film of sur-

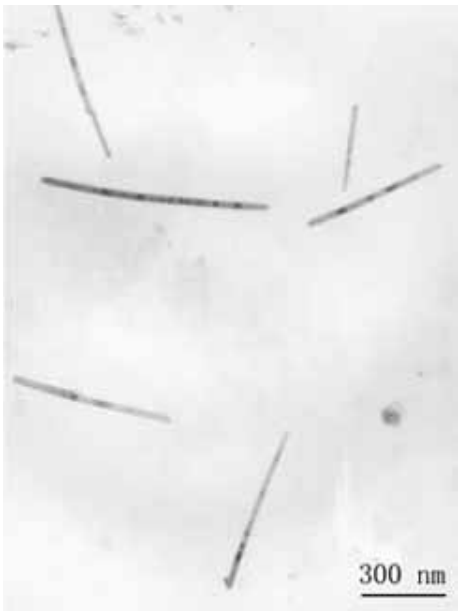

Fig. 1. TEM images of Cu nanorods obtained at a constant current of 0.14 mA cm^{-2} for 30 min. Mean diameter 30 nm. Mean lingth 500 nm.

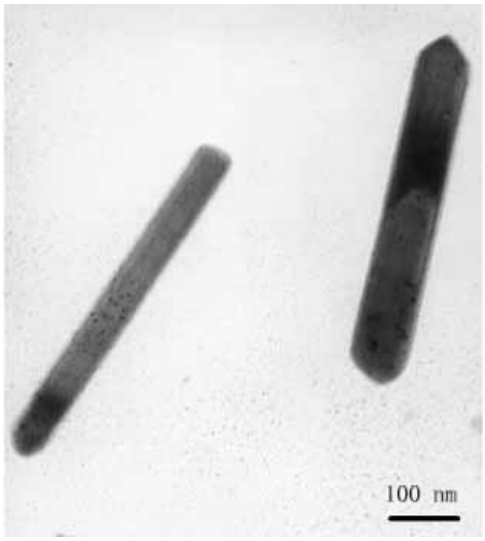

Fig. 2. Morphologies of two as-prepared Cu nanorods obtained at a constant current of 0.14 mA cm^{-2} for 30 min.

Fig. 3. TEM images of Cui nanorods obtained at a constant current of 0.3 mA cm^{-2} for 30 min.

face active molecules. The microstructure of a quaternary microemulsion CTAB/*n*-pentanol/*n*-hexane/water has been investigated in detail.[16] In such a system, the water-in-oil microemulsion acts as a microreactor. The system used in this work was a five-componenet system: CTAB/CT_4ABr/acetone/cyclohexane/water, which is more complicated than the one previously discussed. Under continuous ultrasonication, the cyclohexane phase was dispersed as small droplets surrounded by a monolayer of surfactant in the continuous liquid phase. The copper nanoparticles can then move into the small droplets. The role of acetone is to facilitate the incorporation of cylindrical-shaped-inducing co-surfactant into the CTAB micellar framework. Cyclohexane then acts as a stabilizer to protect the copper from further reaction.

As a result, copper nanorods have been successfully synthesized using a simple but efficient electrochemical method. Further experiments are to be carried out to investigate other factors controlling the shape of the obtained nano-materilas. High yields of the product should also be achieved by carefully controlling the experiment conditions.

Acknowledgements: The authors thank the Special Funds for the Major State Basic Research Projects (G19990650) and Chinese National Science Fund (20173033) for support of this research.

ИЗВОД

СИНТЕЗА НАНОШТАПИЋА ОД БАКРА ЕЛЕТРОХЕМИЈСКИМ ПУТЕМ

XUEGENG YANG[a], SHENHAO CHEN[a,b], SHIYONG ZHAO[a], DEGANG LI[a] and HOUYI MA[a]

[a]*Department of Chemistry, Chandong University, Jinan 250100, PR China and* [b]*State Key Laboratory for Corrosion and Protection of Metals, Shenyang 110015, PR China*

Наноштапићи од бакра добивени су коришћењем електрохемијске методе контролисане струје. Површински активна средства у електролиту током синтетске процедуре служе једновремено и као калуп и као стабилизатор. Слике добијене електронским микроскопом показују да је производ углавном материјал који има штапићасту структуру. Примењене густине струја током електрохемијског таложења имају утицаја и на облик и на принос бакарних наноштапића.

(Примљено 28. марта 2003)

REFERENCES

1. M. T. Reetz, W. Helbing, S. A. Quaiser, U. Stimming, N. Breuer, R. Vogel, *Science* **267** (1995) 367
2. R. L. V. Wal, *Chem. Phys. Lett* **324** (2000) 217
3. Y. Li, J. Liu, Y. Wang, Z. L. Wang, *Chem. Mater.* **13** (2001) 1008
4. J. S. Lee, G. H. Gu, H. Kim, W. S. Jeong, J. Bae, J. S. Suh, *Chem. Mater.* **13** (2001) 2387
5. B. E. Baker, M. J. Natan, H. Zhu, T. P. Beebe, *Supermol. Sci.* **4** (1997) 17
6. F. Kim, J. H. Song, P. Yang, *J. Am. Chem. Soc.* **124** (2002) 14316
7: C. J. Murphy, N. R. Jana, *Adv. Mater*. **14** (2002) 80
8. M. T. Reetz, W. Helbig, *J. Am. Chem. Soc*. **116**(1994) 7401
9. S. Y. Zhao, S. B. Lei, S. H. Chen, H Y. Ma, S Y. Wang, *Colloid Polym. Sci.* **278** (2000) 682
10. S.Y. Zhao, S. H. Chen, S. Y. Wang, S. B. Lei, Z. L. Quan, *Thin Solid Films* **360** (2000) 56
11. Y. Y. Yu, S. S. Chang, C. L. Lee, C. R. C. Wang, *J. Phys. Chem. B* **101** (1997) 6661
12. S. S. Chang, C. W. Shih, C. D. Chen, W. C. Lai, C. R. C. Wang, *Langmuir* **15** (1999) 701
13. M. B. Mohamed, K. Z. Iamail, S. Link, M. A. El-Sayed, *J. Phys. Chem. B* **102** (1998) 9370

14. *Handbook of Microemulsion Science and Technology*, Promod Kumar and K. L. Mittal, Eds., M. Dekker, New York, 1999, p. 849
15. M. P. Pileni, B. W. Ninham, T. Gulik-Krzywicki, J. Tanori, I. Lisiecki, A. Filankembo, *Adv. Mater.* **11** (1999) 1358
16. M. Giustini, G. Palazzo, G. Colafemmina, M. D. Monoca, M. Giomini, A. Ceglie. *J. Phys. Chem. B* **100** (1996) 3190.

J.Serb.Chem.Soc. 68(11)849–857(2003)
JSCS – 3106

UDC 547.291+542.943:54–44+546.226–323
Original scientific paper

Comparison of formic acid oxidation at supported Pt catalyst and at low-index Pt single crystal electrodes in sulfuric acid solution

AMALIJA V. TRIPKOVIĆ, KSENIJA DJ. POPOVIĆ and JELENA D. LOVIĆ

ICTM – Center for Electrochemistry, University of Belgrade, Njegoševa 12, P. O. Box 473, 11001 Belgrade, Serbia and Montenegro

(Received 4 April, revised 9 July 2003)

Abstract: The oxidation of formic acid was studied at supported Pt catalyst (47.5 wt%. Pt) and a low-index single crystal electrodes in sulfuric acid. The supported Pt catalyst was characterized by the TEM and HRTEM techniques. The mean Pt particle diameter, calculated from electrochemical measurements, fits well with Pt particle size distribution determined by HRTEM. For the mean particle diameter the surface averaged distribution of low-index single crystal facets was established. Comparison of the activities obtained at Pt supported catalyst and low-index Pt single crystal electrodes revealed that Pt(111) plane is the most active in the potential region relevant for fuel cell applications.

Keywords: formic acid oxidation, Pt single crystals, supported Pt catalyst, particle size, surface distribution of crystallographic sites.

INTRODUCTION

Simple organic compounds, such as methanol, formaldehyde and formic acid have been extensively studied as fuels for fuel cells. Formic acid is relatively benign and non-explosive which makes it facile in handling and distribution, as compared to hydrogen. On the other hand, it has a lower energy content with respect to hydrogen or methanol. Recent data have shown, however, that formic acid fuel cells are attractive alternatives for small portable fuel cell applications.[1]

In contrast to the limited informations on formic acid properties as a fuel, many results have been reported concerning electrocatalytic oxidation of formic acid from the fundamental viewpoint. Formic acid was studied on polycrystalline[2] and single crystal Pt electrodes.[3–7] There is an agreement that platinum is initially a good catalyst, but the metal surface is rapidly poisoned by the strongly adsorbed intermediates identified by spectroscopic studies.[8,9]

The efforts have been made to enhance oxidation rates of formic acid on platinum by adding a variety of surface modifiers (adatoms). The increase in the reactivity induced by adatoms has been accounted for by a "third body effect", *i.e.*, the third body prevents poison to form on the surface.[10–13]

Despite the simplicity of the formic acid oxidation with only two electrons involved, the reaction proceeds through two parallel paths on platinum[14] leading to direct formation of CO_2 and to the formation of CO_{ad}, which poisons the electrode surface. Both paths are structure sensitive.[15]

There are only a few papers reported so far dealing with formic acid oxidation on Pt-based nanoparticle catalyst,[16,17] *i.e.*, on the high surface area catalysts for anode application in the direct oxidation formic acid fuel cells.

However, the problem with CO poisoning at potentials relevant for fuel cells remains still open as in a case of methanol oxidation.

The present paper aims to examine the electrocatalytic properties of supported Pt catalyst (47.5 wt% Pt) in electrochemical oxidation of formic acid in sulfuric acid solution and to compare the results with the data obtained at low-index single crystal platinum electrodes. This approach was based on the TEM, HRTEM and electrochemical measurements, which allowed the correlation between the size of Pt nanoparticles and the surface distribution of (111), (100) oriented facets and low-coordinated (110) edge and corner sites.

EXPERIMENTAL

Commercially available Pt-based catalyst (47.5 wt% Pt) provided by Tanaka Precious Metals Group supported on high surface area carbon was used. The catalyst was characterized by the transmission electron microscopy (TEM) and by high resolution transmission electron microscopy (HRTEM) techniques. TEM and HRTEM images of the electrode as well as the histogram of the particle size distribution are shown in Fig. 1 (a –c). TEM analysis (a) shows that the distribution of metal particle on the carbon support is reasonably uniform. Typical highly faceted cubooctahedral nanoparticles are shown in part (b). The histogram of the particle size distribution (c) reveals that the average particle size is ranged between 2 nm and 6 nm.

The catalytic acitivty of the catalyst was determined by using the thin-film rotating disk (RDE) method. The catalyst was ultrasonically dispersed in Millipore water and a drop of this suspension was placed onto a polished glassy carbon disk (Sigradur G) diameter 6.7 mm, resulting in metal loading of 20 μg cm^{-2}. After drying in nitrogen at room temperature, the deposited catalyst layer was covered with 20 μl of a diluted aques Nafion solution leading to thickness of ≈ 0.2 μm. Finally, the electrode was immersed in nitrogen purged electrolyte.

In order to verify that the Nafion film used to attach the catalyst particles onto the glassy carbon RDE does not impose additional film diffusion resistance the polarization curves for the hydrogen oxidation reaction, (HOR), in a solution saturated with H_2 were recorded on supported Pt catalyst in sulfuric acid solution (Fig. 2). The Levich-Koutecky plot inferred from the diffusion limiting currents at 0.3 V is shown as an inset in Fig. 2.

As the value of $B\ c_0 = 6.51 \times 10^{-2}$ mA cm^{-2} $rpm^{-1/2}$ closely agrees with the theoretical value of 6.54×10^{-2} mA cm^{-2} $rpm^{-1/2}$, assumed from the Levich equation:

$$j_0 = 0.62\, nFD^{2/3}\, \nu^{-1/6}\, c_0\omega^{1/2} = B\, c_0\, \omega^{1/2} \qquad (1)$$

it appears that there is no significant mass transfer resistance through the Nafion film.

The catalytic activity was measured either by recording the potentiodynamic (sweep rate 50 mV s^{-1}) or quasi steady-state (sweep rate 1 mV s^{-1}) polarization curves.

Formic acid (Merck, p.a.) was added to the solution while the electrode was held at ≈ 0.05 V. The reference electrode was a saturated calomel electrode (SCE). All potentials are referred to the reversible hydrogen electrode (RHE) in the same electrolyte. Current densities in Figs. 3 – 6 are given on real surface

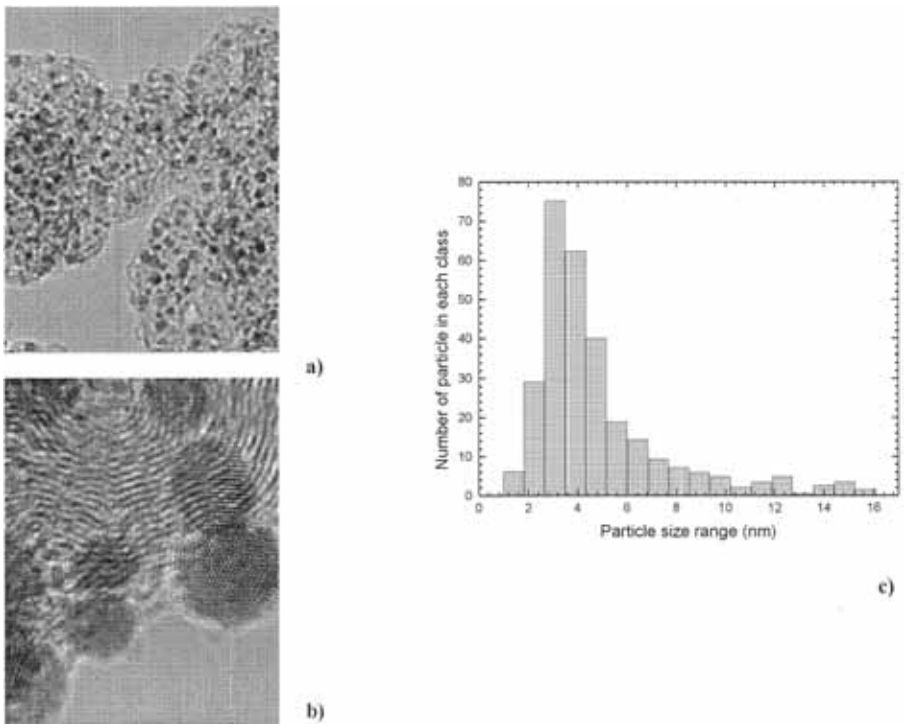

Fig. 1. TEM image of Pt nanoparticles on a carbon black support (a); HRTEM image of generally facetted shapes of nanoparicles (b); particle size distribution (c).

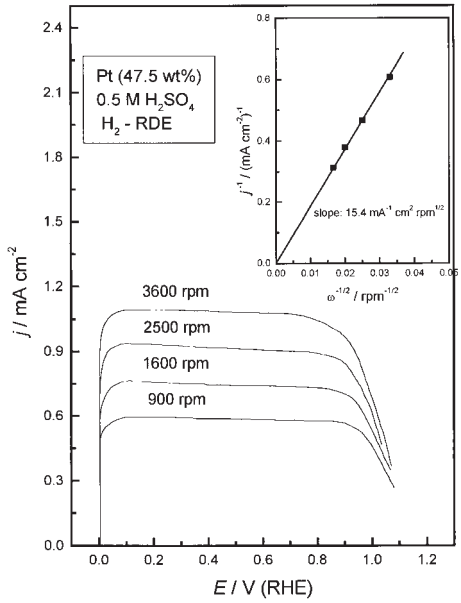

Fig. 2. Polarization curves for the HOR on Pt supported catalyst in 0.5 M H_2SO_4. Inset: plot of $1/j$ *vs.* $\omega^{-1/2}$.

area scale.

RESULTS AND DISCUSSION

Basic voltammograms

Figure 3 illustrates the voltammograms of the supported Pt catalyst (a) and low-index single crystal Pt electrodes (b), (only hydrogen adsorption/desorption region), in sulfuric acid solution. The potential region of hydrogen adsorption/desorption on supported Pt catalyst accompanied with bisulfate desorption/adsorption is separated from the reversible/irreversible oxide formation by the double layer potential region. The features in the hydrogen region could be rationalized on the basis of hydrogen electrochemistry at low-index single crystal platinum electrodes in the same acidic solution. The H-desorption peak at $E \approx 0.15$ V can be correlated with the Pt(110) sites. The more positive H-desorption peaks at $E \approx 0.3$ V suggests the presence of Pt(100) related facets. The broad and featureless H-desorption occurring over the potential range $0.05 \text{ V} < E < 0.35$ V, below the Pt(110) and Pt(100) peaks, indicates the presence of Pt (111) correlated sites. This

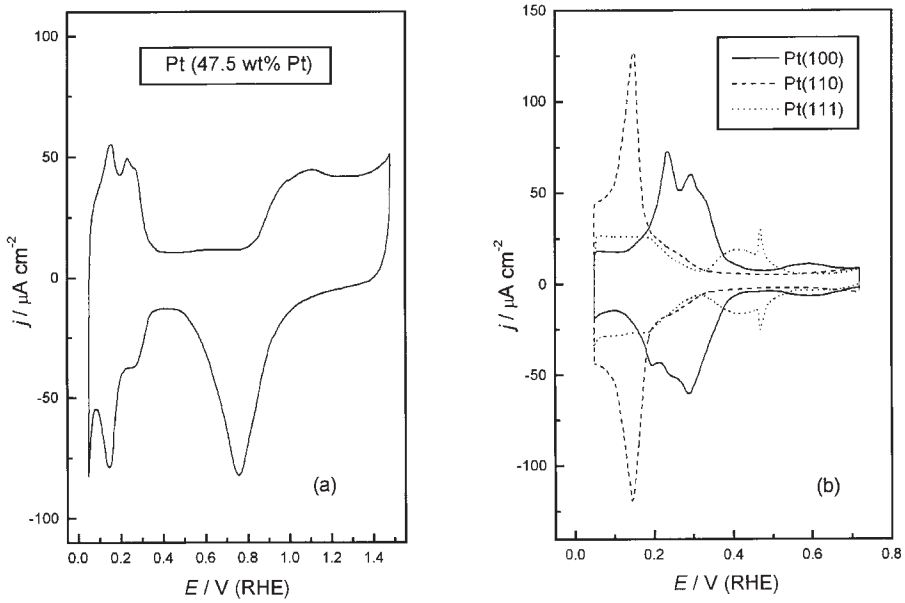

Fig. 3. Cyclic voltammograms for Pt supported catalyst (a) and Pt low-index single crystal electrodes (b) in 0.5 M H_2SO_4. $\nu = 50$ mV s^{-1}; $T = 295$ K.

observation is consistent with the fact that the nanostructured platinum was composed of low coordination – number single crystals.[18]

Basic voltammogram for supported catalyst (a) was used for an estimation of the real surface area (S), mass specific surface area (S_1) and diameter of Pt particles (d).

The hydrogen adsorption charge (Q_H) in the potential region $0.05 \text{ V} < E < 0.4$ V was

determined as $Q_H = 0.5(Q_{total} - Q_{DL})$, where Q_{total} is a total charge transfer in the hydrogen adsorption/desorption region and Q_{DL} is a capacitive charge from both double layer charging and a capacitance of the high surface area carbon support. Assuming that $Q_H = 0.21$ mC cm^{-2} corresponds to a monolayer of adsorb hydrogen[19] the value for real surface area is estimated as $S = 4.6$ cm^2. This value normalized by mass of Pt gives mass specific surface area $S_1 = 66$ m^2 g^{-1}. Assuming that the Pt particles are spherical the partials diameter calculated by using the equation $d = 6\times10^3/\rho S_1$, where $\rho = 21.4$ g cm^{-3} and S_1 is mass specific surface area is $d = 4.3$ nm. This value fits well with particle size distribution obtained by HRTEM.

Formic acid oxidation

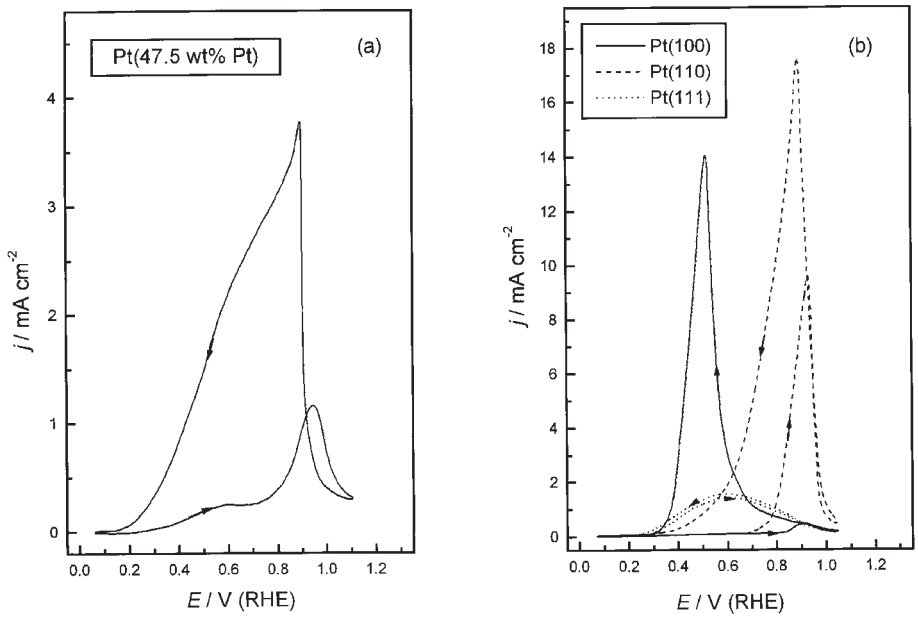

Fig. 4. Cyclic voltammograms for the oxidation of 0.5 HCOOH on Pt supported catalyst (a) and on Pt low-index single crystal electrodes (b) in 0.5 M H_2SO_4. $\nu = 50$ mV s^{-1}; $T = 295$ K.

Potentiodynamic measurements. The polarization curves for formic acid oxidation on supported Pt (a) and a low-index platinum electrodes are presented in Fig. 4 (a and b, respectively).

The fraction commences at the surface still partially covered by H_{ad} species and proceeds further through the double layer region with a relatively slow kinetics. Then it becomes faster in the potential region related to the adsorption of oxygen-containing species, giving a current maximum at $E \approx 0.95$ V. Upon sweep reversal an increase of the activity is seen which is followed by a gradual decrease as the overpotentials decrease.

The polarization curve for formic acid oxidation on supported Pt catalyst has similar shape as the curve obtained on a polycrystalline Pt bulk electrode[2] suggesting that there is

no unexpected surface composition of the nanoparticles compared with a bulk electrode.

A brief interpretation of the voltammograms given in Fig. 4b shows that both Pt (110) and Pt (100) are completely blocked with poisoning species during the positive sweep up to high potentials where these species can be oxidized. Upon reversal of the sweeps, the reaction attains high rates on both planes. On the contrary, the Pt (111) surface shows a negligible poisoning effect over the whole potential region where the reaction occurs. This observation is supported by the almost overlapping of the sweeps recorded in both directions of potential scanning.

By comparing the shape of voltammograms on the Pt(*hkl*) electrodes and on supported Pt catalyst, it could be suggested that formic acid is oxidized predominantly at the (111) oriented sites up to $E \approx 0.7$ V, in the positive going sweep, while the peak of $E \approx 0.95$ V, as well as the large increase of the currents in the negative direction correspond to oxidation at the (110) and (100) facets.

This interpretation is supported by the relationship between Pt particle size and the different surface sites (crystal facets, edges, corners) done by Kinoshita[20,21] on the basis of the theoretical analysis of ideal geometric structures, which are representative of small Pt particles. The space lattice of platinum is face-centered cubic and Pt particles are generally represented as cubooctahedral structures consisting of Pt atoms arranged in (111) and (100) crystallographic faces bounded by edge and corner atoms. The concentration of surface atoms at the different crystallographic sites vary with the change of particle size. For an average Pt particle diameter of 4.3 nm, calculated in this work, the surface-averaged distribution amounts: ≈ 65 % (111) sites, ≈13 % (100) sites and 22 % corner and edge sites (which may be correlated with (110) sites).

The data given in Table I displaying the activities of Pt supported catalyst and single crystal Pt electrodes at $E = 0.5$ V show that supported Pt catalyst is more active than both the Pt(100) and the Pt(110) electrodes but less active than the Pt(111) electrode.

In order to obtain a better understanding of formic acid oxidation, the reaction is studied from its early stage to the potentials of interest for electrocatalysis.

Figure 5 shows the onset of formic acid oxidation in sulfuric acid and the basic voltammogram for supported Pt catalyst (a). The reaction commences in the hydrogen adsorption/desorption region at $E \approx 0.15$ V and, in the case of sulfuric acid, the onset of the reaction could not be associated with OH^- anions adsorption.

The first sweep up to $E = 0.55$ V (b) shows an increase of the specific current density with potential and its decrease upon reversal of the scan. The decrease of the oxidation currents in the second sweep compared with those recorded in the first sweep indicates a poisoning effect. This surface blocking is caused by the presence of (110) and (100) oriented sites which are very sensitive to "poison" adsorption.

Upon sweep reversal at $E = 0.75$ V (c) a small hysteresis in the oxidation currents occurs with some increased activity observed during the negative going sweep. This feature remains unchanged during further scanning suggesting the absence of a poisoning effect. Actually, it means that the some poison formed in the reaction can be oxidized up to $E =$

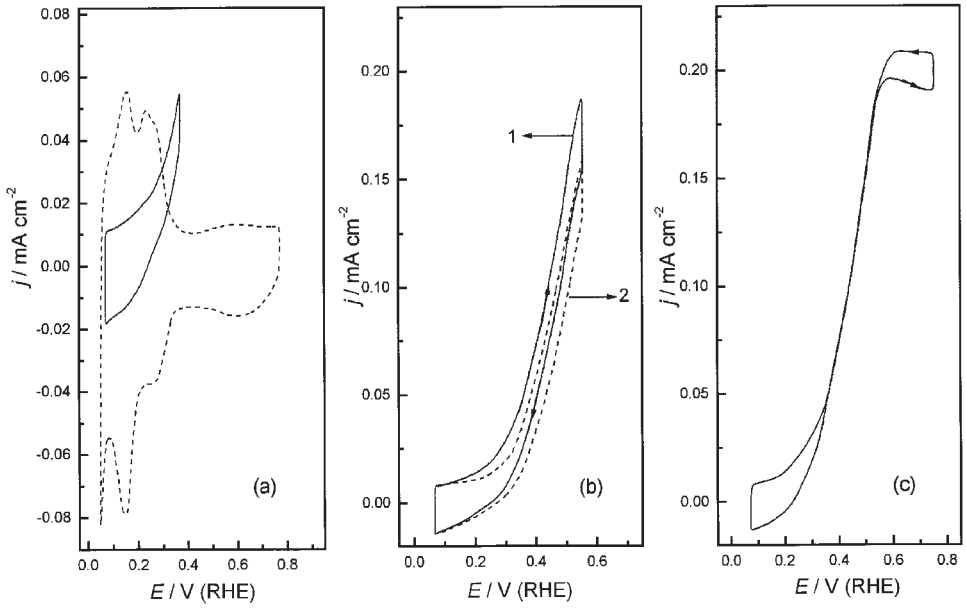

Fig. 5. Cyclic voltammogram for the oxidation of 0.5 M HCOOH up to different positive potential limits on a Pt supported catalyst in 0.5 M H_2SO_4. $\nu = 50$ mV s^{-1}; $T = 295$ K.

0.75 V. Most likely CO_{ad} is the dominant poison which cannot be removed from the nanostructured Pt catalyst until the potential exceeds at least 0.5 V while a sharp peak is seen at 0.76 V.[22]

From the viewpoint of the participation in the reaction of different oriented facets in the supported Pt catalyst it could be suggested that in the potential region up to $E = 0.75$ V the reaction takes place predominantly at the (111) oriented facets although the influence of (110) and (100) oriented sites could not be neglected.

TABLE I. Activities of Pt supported catalyst and Pt single crystal electrodes at $E = 0.5$ V

	Pt (47.5 wt% Pt)	Pt(111)	Pt(100)	Pt(110)
j / mA cm^{-2}	0.186	1.18	0.08	0.08

Quasi steady-state measurements. The quasi steady-state curve obtained in formic acid oxidation on supported Pt catalyst is given in Fig. 6.

The reaction follows a Tafel type equation in the potential region between 0.25 V and 0.55 V giving a well defined Tafel line with the slope ≈ 120 mV/dec. It should be pointed out that in this potential region formic acid oxidation takes place predominantly at the (111) oriented facets. This suggestion is confirmed by the quasi steady state curve for formic acid oxidation at the Pt(111) plane shown in the inset of Fig. 6, which has the same slope of ≈ 120 mV/dec in almost the same potential region. The Pt(111) electrode is also more active than supported Pt catalyst under the quasi steady-state conditions although less

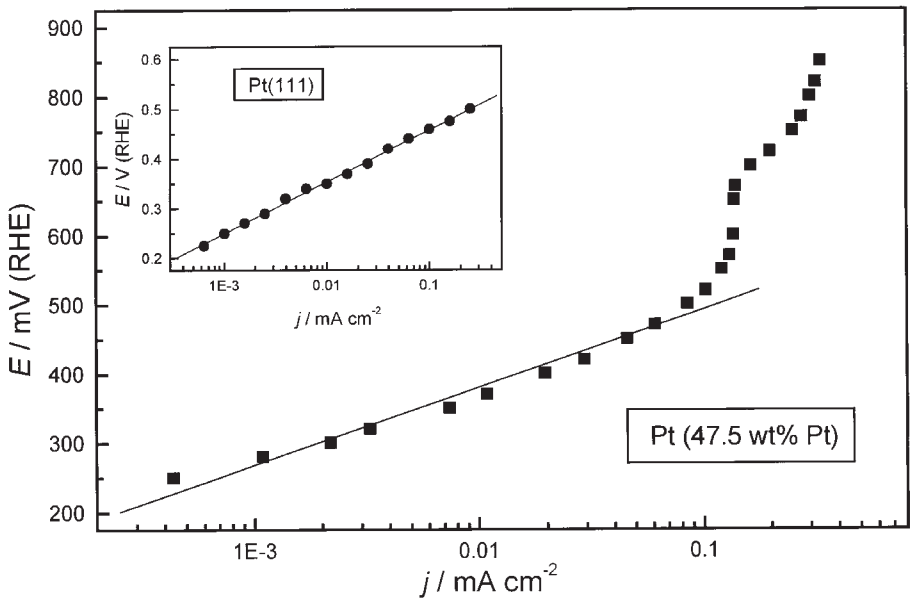

Fig. 6. Tafel plots for the oxidation of 0.5 M HCOOH in 0.5 M H_2SO_4 on Pt supported catalyst and on a Pt(111) surface (inset). $\nu = 1$ mV s^{-1}; $T = 295$ K.

pronounced compared with potentiodynamic conditions (Table I). At $E = 0.5$ V low-index (111) surface, in respect to supported Pt catalyst, is 3 times more active in steady-state measurements and 6 times in potentiodynamic measurements. It is an evidence that the true catalytic activity can be obtained only in steady-state measurements, while the activities observed in potentiodynamic experiments are transient in nature.

CONCLUSIONS

1. TEM and HRTEM analysis of supported Pt catalyst (47.5 wt % Pt) used have shown:

– a relatively uniform distribution of Pt nanoparticles on the carbon support

– cubooctahedral shape of the Pt nanoparticles

– an average Pt particle size between 2 nm and 6 nm.

2. The mean particle diameter $d = 4.3$ nm calculated in this work is in a good agreement with a particle size distribution determined by HRTEM.

3. For the mean particle diameter of 4.3 nm, the surface distribution amounts: 65 % (111) sites, 13 % (100) sites and 22 % corner and edge sites (which may be correlated with low coordination (110) sites.

4. Supported Pt catalyst is more active than (100) and (110) surfaces, but significantly less active than (111) surface in the potential region relevant for electrocatalytic consideration.

Acknowledgement: The authors are grateful to Dr. Nenad Marković for the TEM and HRTEM images,

obtained in the National Center for Electron Microscopy, Lawrence Berkeley National Laboratory, Berkeley. This work was supported by the Ministry of Science, Technology and Development of Serbia, Contract No. H-1796.

ИЗВОД

ПОРЕЂЕЊЕ ОКСИДАЦИЈЕ МРАВЉЕ КИСЕЛИНЕ НА Pt КАТАЛИЗАТОРУ НА НОСАЧУ И НА НИСКОИНДЕКСНИМ Pt МОНОКРИСТАЛИМА У СУМПОРНОЈ КИСЕЛИНИ

АМАЛИЈА В. ТРИПКОВИЋ, КСЕНИЈА Ђ. ПОПОВИЋ и ЈЕЛЕНА Д. ЛОВИЋ

ИХТМ – Центар за електрохемију, Универзитет у Београду, Његошева 12, п. пр. 473, 11000 Београд

Оксидација мравље киселине испитивана је на Pt катализатору нанетом на активни угаљ (47,5 мас % Pt) и на ниско-индексним Pt монокристалним електродама у сумпорној киселини. Први катализатор је окарактерисан коришћењем техника трансмисионе електронске микроскопије ниске (TEM) и високе резолуције (HRTEM), при чему је одређена дистрибуција, величина и облик наночестица Pt. Средњи пречник наночестица, израчунат из електрохемијских мерења, сагласан је расподели величина честица добијеној HRTEM анализом. На основу средњег пречника наночестица дата је просечна дистрибуција (111), (100) и (110) места на површини катализатора на носачу. Овај катализатор је активнији у оксидацији мравље киселине од монокристалних Pt електрода оријентације (100) и (110), али је мање активан од Pt(111) електроде у области потенцијала релевантној за примену у горивном спрегу.

(Примљено 4. априла, ревидирано 9. јула 2003)

REFERENCES

1. M. Weber, J. T. Wang, S. Wasmus, R. F. Savinell, *J. Electrochem. Soc.* **143** (1996) L158
2. A. Capon, R. Parsons, *J. Electroanal. Chem. Interfacial Electrochem.* **44** (1973) 1
R. R. Adžić, A. V. Tripković, W. O'Grady, *Nature* **296** (1982) 137
4. A. Tripković, K. Popović, R. R. Adžić, *J. Chim. Phys.* **88** (1991) 1635
5. J. Clavilier, R. Parsons, R. Durand, C. Lamy, J. M. Leger, *J. Electroanal. Chem. Interfacial Electrochem.* **124** (1981) 321
6. C. Lamy, J. M. Leger, *J. Chim. Phys. – Chim. Biol.* **88** (1991) 1649
7. T. Iwasita, X. H. Xia, E. Herrero, H. D. Liess, *Langmuir* **12** (1996) 4260
8. A. Bewick, K. Kunimatsu, B. S. Pons, *J. Electroanal. Chem.* **160** (1984) 147
9. B. Beden, F. Hahn, S. Juanto, C. Lamy, J. M. Leger, *J. Electroanal. Chem.* **225** (1987) 215
10. M. Watanabe, M. Horiuchi, S. Moto, *J. Electroanal. Chem. Interfacial Electrochem.* **250** (1988) 117
11. M. D. Macia, E. Herrero, J. M. Feliu, A. Aldaz, *J. Electroanal. Chem.* **500** (2001) 498
12. H. A. Gasteiger, N. Marković, P. N. Ross Jr., E. J. Cairns, *Electrochim. Acta* **39** (1994) 1825
13. R. R. Adžić, A. V. Tripković, N. M. Marković, *J. Electroanal. Chem.* **150** (1983) 79
14. R. Parsons, T. Van der Noot, *J. Electroanal. Chem.* **257** (1988) 9
15. C. Lamy, J. M. Leger, C. Clavilier, R. Parsons, *J. Electroanal. Chem.* **150** (1983) 71
16. N. M. Marković, H. A. Gasteiger, P. N. Ross Jr, X. Jiang, I. Villegas, M. J. Weaver, *Electrochim. Acta.* **40** (1995) 91
17. V. Climent, E. Herrero, J. M. Feliu, *Electrochim. Acta* **44** (1988) 1403
18. P. Stonehart, *J. Appl. Electrochem.* **22** (1992) 995
19. B. B. Damaskin, D. A. Petrii, V. V. Batrakov, *Adsorption of Organic Compound on Electrodes*, Plenum Press, New York, London, 1971
20. K. Kinoshita, *J. Electrochem. Soc.* **137** (1990) 845
21. K. Kinoshita, *Electrochemical Oxygen Technology*, Wiley, New York, 1992

22. J. Jiang, A. Kucernak, *J. Electroanal. Chem.* **520** (2002) 64.

J.Serb.Chem.Soc. 68(11)859–870(2003)
JSCS – 3107

UDC 547.261+66.087.3:669.231–034+669.25–034
Original scientific paper

Electrochemical oxidation of methanol on Pt_3Co bulk alloy

S. LJ. GOJKOVIĆ[#]

Faculty of Technology and Metallurgy, University of Belgrade, Karnegijeva 4, P. O. Box 3503, 11120 Belgrade, Serbia and Montenegro

(Received 15 July 2003)

Abstract: The electrochemical oxidation of methanol was investigated on a Pt_3Co bulk alloy in acid solutions. Kinetic parameters such as transfer coefficient, reaction orders with respect to methanol and H^+ ions and energy of activation were determined. It was found that the rate of methanol oxidation is significantly diminished by rotation of the electrode. This effect was attributed to the diffusion of formaldehyde and formic acid from the electrode surface. Stirring of the electrolyte also influenced the kinetic parameters of the reaction. It was speculated that the predominant reaction pathway and rate determining step are different in the quiescent and in the stirred electrolyte. Cobalt did not show a promoting effect on the rate of methanol oxidation on the Pt_3Co bulk alloy with respect to a pure Pt surface.

Keywords: methanol, electrochemical oxidation, Pt_3Co alloy, direct methanol fuel cell.

INTRODUCTION

Methanol oxidation is an important electrochemical reaction from both practical and fundamental aspects because it is the anodic reaction in direct methanol fuel cells (DMFC) and a prototype of the oxidation of small organic molecules. The main features of the reaction and also the main obstacles for its application are the high overpotential needed in order to oxidize methanol at a measurable rate and the deactivation of all electrocatalysts with time. Methanol oxidation has been extensively investigated since the early 70's with two main topics: identification of the reaction intermediates, poisoning species and products, and modification of Pt surface in order to achieve higher activity at lower potentials and better resistance to poisoning. The results have been reviewed by several authors.[1–5]

Intermediates that have been identified by infrared spectroscopy,[6–10] electrochemical thermal desorption mass spectroscopy (ECTDMS)[11,12] and differential electrochemical mass spectrometry (DEMS)[13–15] are (C, O) species, which can be linearly or bridge bonded CO_{ads},[6–11] and (C, H, O) species, suggested to be CHO_{ads}[15] and COH_{ads}.[10,13,14] Evidence of the methoxy CH_3O_{ads} intermediate was also found.[9] The main reaction product is CO_2,[16] although significant amounts of formaldehyde[17,18] formic acid[16] and

[#] Serbian Chemical Society active member.

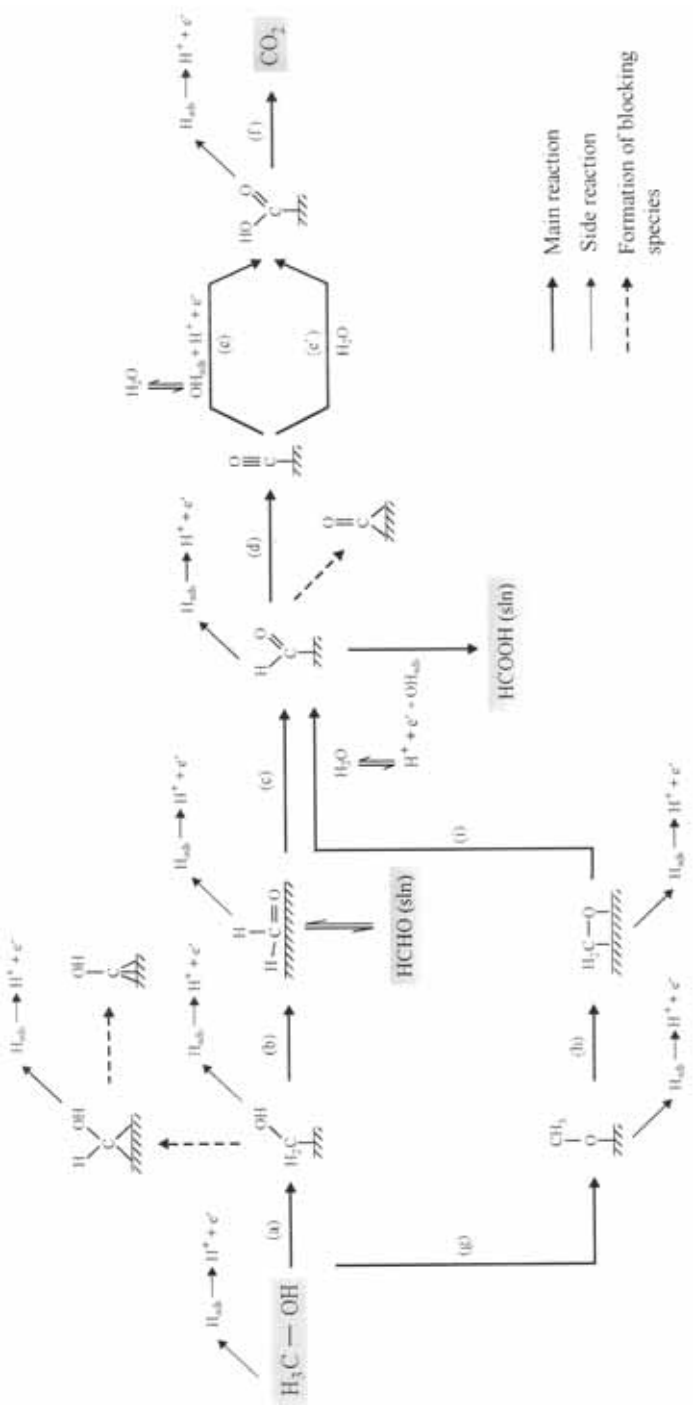

Fig. 1. Reaction pathways of methanol oxidation on a Pt surface.

methyl formate[18,19] were also detected. Some of the possible reaction steps for methanol oxidation that can be envisaged from the above mentioned intermediates and the products are given in Fig. 1.

Platinum is the most active metal for dissociative adsorption of methanol, but the potential where it adsorbs OH species, which are necessary for the oxidation of adsorbed methanol residues, is too high for the application of a single Pt electrocatalyst in a DMFC. Consequently, bimetal catalysts have been developed among which Pt–Ru was proved to be the best choice until now. However, Pate *et al.*[20] recently reported that the activity of a carbon supported Pt–Co catalyst approches that of a Pt–Ru electrocatalyst at elevated temperatures. In the present paper, methanol oxidation was investigated on well deffined smooth bulk Pt_3Co alloy in acid solutions. The kinetic parameters and energy of activation of the reaction were determined in a quiescent and in a stirred electrolyte. A mass transfer effect on the reaction kinetics was found and correlated with a possible reaction pathway.

EXPERIMENTAL

A thermally prepared Pt_3Co alloy electrode (prepared and characterized at Lawrence Berkeley National Laboratory, Berkeley, CA) was used in this study. A bulk composition of 75 % Pt was determined by means of X-ray fluorescence spectroscopy.

A disk electrode (0.127 cm^2 geometric surface area) was fabricated from the alloy and used in a rotating disk assembly (Tacussel). Prior to the experiment, the electrode surface was polished with an aqueous suspension of 0.05 μm Al_2O_3, then rinsed and ultrasonicated for 5 min in high purity water. In order to prevent possible changes in the surface composition of the alloy, the usual potential cycling of the electrode in the supporting electrolyte was not performed. Instead, the electrode was set into the methdnol containing electrolyte under potential control and a positive going potential sweep at 1 mV s^{-1} was immediately started. The starting potential was just at the beginning of hydrogen evolution and its value was adjusted for each supporting electrolyte concentration (*e.g.*, +20 mV *vs*. SHE in 0.1 M $HClO_4$ solution).

A standard glass cell was used with a Pt spiral as the counter electrode and a saturated calomel electrode as the reference electrode. All the potentials reported in this paper are expressed on the scale of the standard hydrogen electrode (SHE). The electrolyte contained 0.02 to 1 M $HClO_4$ as a supporting electrolyte and 0.01 to 1 M CH_3OH. All solutions were prepared with high purity water (Millipore, 18 MΩ cm resistance). The electrolyte was deaerated by bubbling with N_2, which had previously been purified by passing through an ammonium-metavanadate solution. When the polarization curves were recorded on a stationary electrode, the stream of N_2 was passed over the electrolyte in order to have complete quiescent conditions. The cell was thermostated at 25.0 to 45.0 ºC. A potentiostat PAR 273A and an X–Y recorder Philips PM 8143 were used in all experiments.

RESULTS

The cyclic voltammogram of the Pt_3Co alloy in 0.1 M $HClO_4$ solution in the potential window relevant to methanol oxidation is given in Fig. 2. No current indicating dissolution of Co was observed, which nominated the alloy as a potential anode catalyst. Hydrogen adsorption/desorption peaks are present on the voltammogram but they do not have fine structure as on pure Pt. This demonstrates that alloying with Co not only reduces the number of Pt atoms on the electrode surface but also changes its ability for underpotential deposition of hydrogen atoms. This is in accordance with the results of Marković *et al.*[21] who compared voltammograms of Pt_3Co and Pt materials prepared in the same way in the same laboratory.

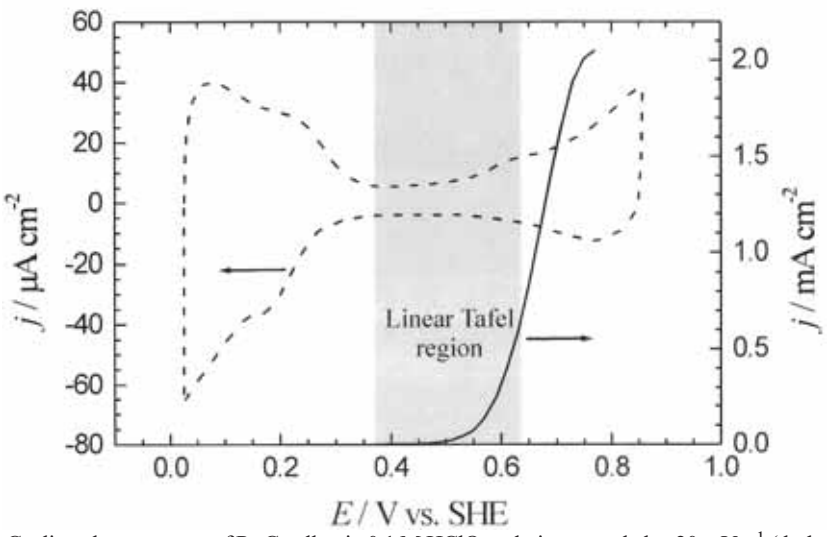

Fig. 2. Cyclic voltammogram of Pt_3Co alloy in 0.1 M $HClO_4$ solution recorded at 20 mV s^{-1} (dashed line) and the polarization curve for methanol oxidation in 0.1 M $HClO_4$ + 0.1 M CH_3OH solution recorded at 1 mV s^{-1} (solid line).

The polarization curve for the oxidation of 0.1 M methanol in 0.1 M $HClO_4$ is also presented in Fig. 2. The reaction starts at ≈ 0.37 V, which is in the double layer region of Pt and reaches a maximum rate at ≈ 0.75 V when the electrocatalyst is substantially oxidized. These two characteristic potentials are the same as on a pure Pt electrocatalyst,[22] which means that, at least at room temperature, Co does not improve the electrocatalytic properties of Pt.

It was reported earlier[23] that the open circuit potential of a Pt electrode in a methanol containing solution was more negative on a stationary electrode than on a rotating one. Also it was established[22,24] that the methanol oxidation current on Pt decreased when the electrode was rotated. The same phenomena were observed on the Pt_3Co electrode and investigated in details in this work. Figure 3 presents the Tafel plots for methanol oxidation on a stationary disk electrode and on a disk electrode rotating at 1000 rpm in electrolytes containing 0.01 to 1 M methanol in 0.1 M $HClO_4$ at 30 ºC. Several characteristics of these Tafel plots deserve attention. Methanol oxidation is strongly supressed by the rotation of the electrode. No significant influence of the rotation rate of the electrode was found, *i.e.*, the current densities on the electrode rotating between 500 and 2000 rpm were the same within experimental error. The difference between the reaction rate in a quiescent and in a stirred solution is much more pronounced in the electrolytes with low methanol concentration than in more concentrated solutions. The onset of the reaction in the stirred electrolyte is shifted towards more positive potentials compared to the quiescent electrolyte. Well defined linear Tafel regions were obtained in both cases, but with different slopes. In the quiescent electrolytes, the Tafel slope changed from 75 to 90 mV dec^{-1} when the methanol concentration was increased from 0.01 to 1 M. It should be noted that a Tafel

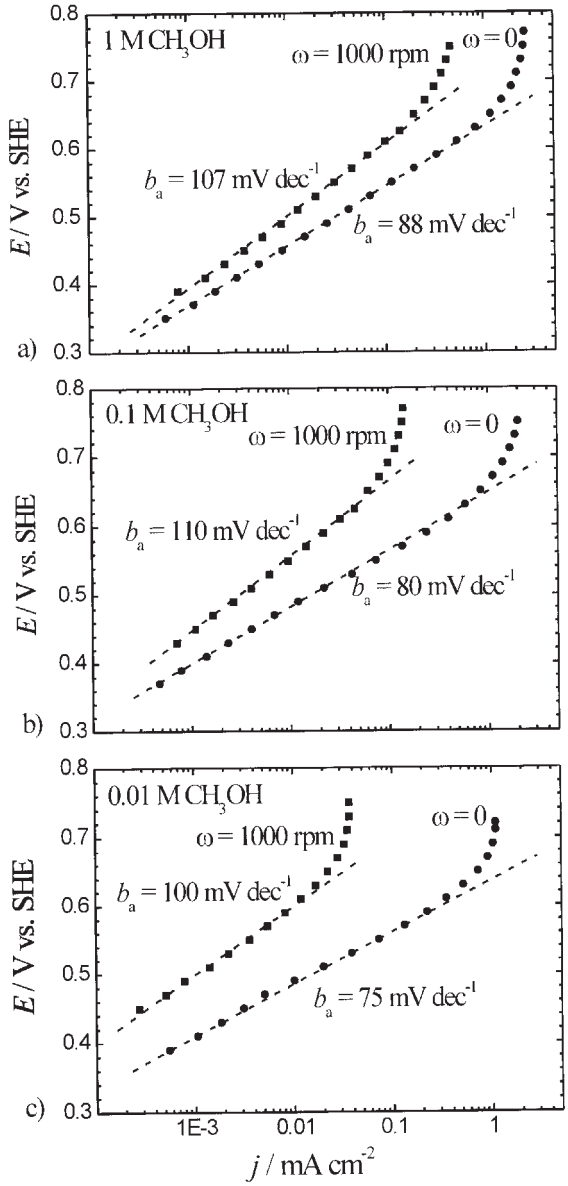

Fig. 3. Methanol oxidation in quiescent and stirred electrolytes controlytes containing 0.1 M $HClO_4$ and different concentration of methanol at 30 ºC.

slope of 90 mV dec^{-1} was also obtained on a pure Pt surface in 0.1 M methanol solution.[22] However, in the stirred electrolytes, the Tafel slope was 100–110 mV dec^{-1} without systematic dependence on the methanol concentration. The end of the Tafel-like behavior at ≈ 0.64 V concides with the plateau of the first step in the oxidation of the catalyst (Fig. 2). At more positive potentials when the catalyst is more oxidized, probably to $Pt(OH)_2$, the increase of the methanol oxidation rate with potential becomes slower and finally a

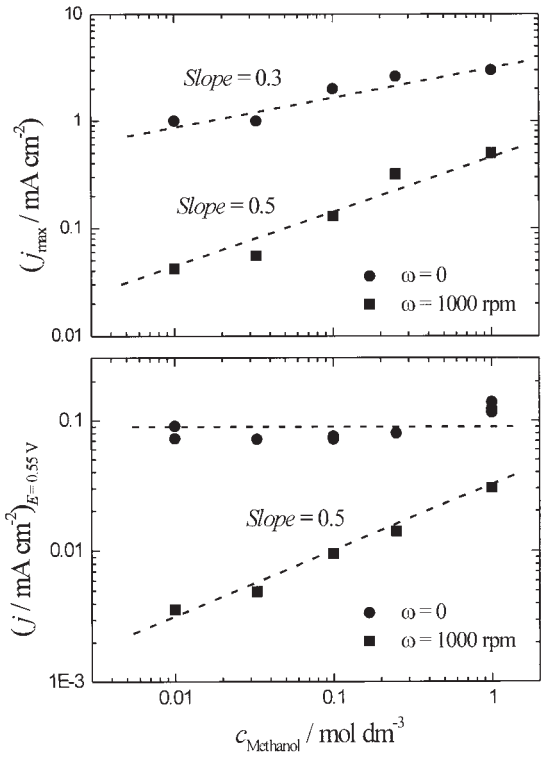

Fig. 4. Dependence of the methanol oxidation rate on the methanol concentration in quiescent and stirred electrolytes containing 0.1 M $HClO_4$ at 30 ºC. Top – maximum current densities and bottom – current densities in the Tafel region.

maximum current density is reached, which is followed by a decrease in the reaction rate (not shown in Figs. 2 and 3).

The influence of the methanol concentration on the reaction rate is summarized in Fig. 4 where the current densities at 0.55 V (approximately in the middle of the linear Tafel region) and the maximum current densities in both quiescent and stirred electrolytes are plotted as a function of methanol concentration. The reaction order with respect to methanol is 0.5 in the stirred electrolyte and the same value was calculated from the maximum current values. In the quiescent electolytes the reaction rate is independent of the methanol concentration in the Tafel region and only slightly dependent at the maximum of the polarization curve. The potentials of the maximum on the polarization curves slightly increased with increasing methanol concentration, both in the quiescent and in the stirred electrolytes.

The influence of the concentration of H^+ ions was investigated in electrolytes containing 0.1 M methanol and different concentration of $HClO_4$ at 30 ºC. The Tafel slopes in the stirred electrolytes were about 110 mV dec^{-1}, irrespective of the $HClO_4$ concentration, while in the quiescent electrolytes its value increased form 75 mV dec^{-1} in 0.02 M to 105 mV dec^{-1} in 1 M $HClO_4$. Increasing the concentration of $HClO_4$ led to a decrease in the methanol oxidation rate. The current densities at 0.55 V are plotted as a function of $HClO_4$ concentration in Fig. 5. The influence of H^+ ion concentration on the reaction rate is similar

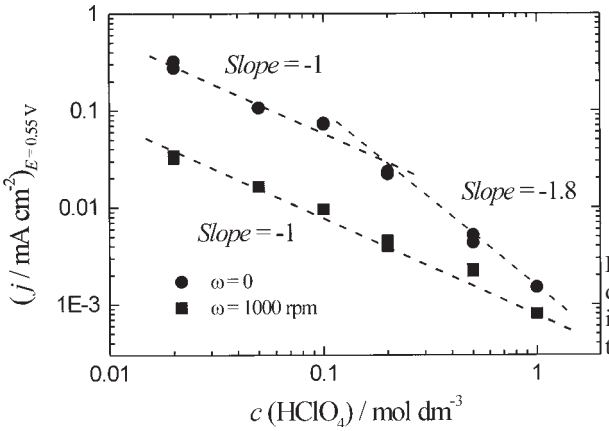

Fig. 5. Dependence of the methanol oxidation rate on the concentration of $HClO_4$ in quiescent and stirred electrolytes containing 0.1 M methanol at 30 °C.

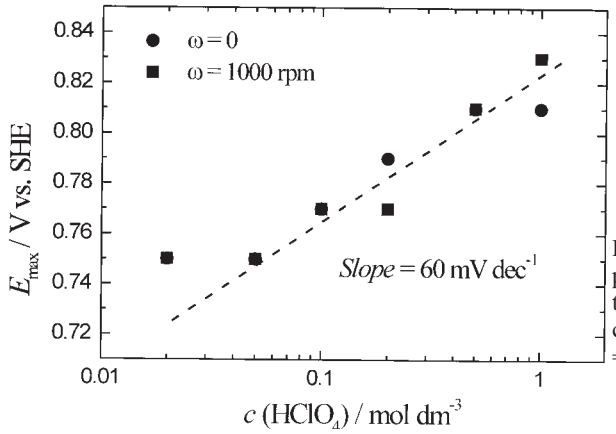

Fig. 6. Potential of the maximum of the polarization curve for methanol oxidation at 30 °C as a function of $HClO_4$ concentration. Methanol concentration = 0.1 M.

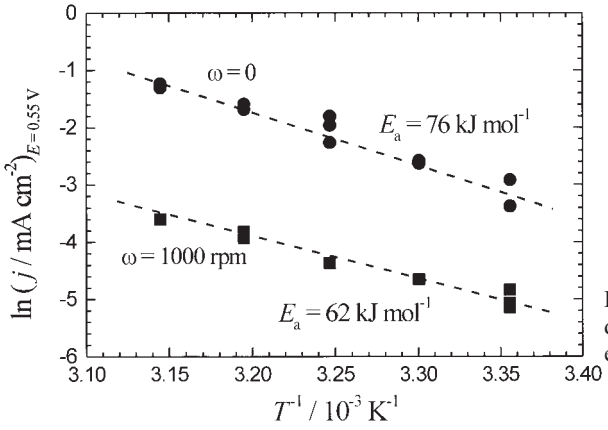

Fig. 7. Arrhenius plots for methanol oxidation in 0.1 M $HClO_4$ + 0.1 M CH_3OH electrolyte.

in both the quiescent and stirred electrolytes, with the exception that in the first case the decrease in the current densities becomes steeper when the concentration of $HClO_4$ is higher than 0.1 M. The reaction order with respect to H^+ ions was calculated to be above –1. The potentials where the polarization curves reach their maximum are also dependent on the $HClO_4$ concentration. Although the potentials of the maximum were not very reproducible, they were shifted toward more positive values with increasing $HClO_4$ concentration and as shown in Fig. 6, a line with a slope of 60 mV dec^{-1} can be drawn, irrespective of the rotation of the electrode.

Polarization curves for methanol oxidation in an electrolyte containing 0.1 M methanol and 0.1 M $HClO_4$ were recorded in the temperature range from 25 to 45 ºC. No significant shift in the onset of the methanol oxidation with temperature was observed. Over the entire temperature range, Tafel plots with slopes of 80 mV dec^{-1} were obtained. The corresponding Arrhenius plots for 0.55 V in the quiescent and stirred electrolytes are given in Fig. 7. An activation energy of about 76 kJ mol^{-1} was estimated for the quiescent electrolyte and 62 kJ mol^{-1} for the stirred electrolyte.

DISCUSSION

Methanol oxidation on Pt_3Co bulk alloy is similar to that on pure Pt electrocaalyst. The reaction begins when hydrogen is desorbed from the electrode surface and attains a maximum rate when the Pt is significantly covered by an oxide, probably $Pt(OH)_2$. Cobalt did not show a promoting effect on the potential of the onset of methanol oxidation.

Being a very slow reaction, the rate of methanol oxidation should not be limited by the mass transfer of methanol from the electrolyte toward the electrode surface. A simple calculation shows that the limiting diffusion current density for the oxidation of 0.1 M methanol in a quiescent electrolyte should be about 50 mA cm^{-2}, which is 25 times higher than the maximum current density observed in this solution (Fig. 3b). On the contrary, agitation of the electrolyte provoked a pronounced decrease in the current densities over the entire potential region. This indicates that some intermediate which can diffuse away from the electode is involved in the reaction mechanism.

Before discussing this hypothesis, possible artifacts that could produce such an unusual effect of the electrode rotation on the methanol oxidation current have to be mentioned. The first possibility is some impurity in the electrolyte the adsorption of which is facilitated on the rotating electrode. The supporting electrolyte used in this work was $HClO_4$ which could contain traces of Cl^- ions. However, Biegler[24] reported the same phenomenon, although his experiments were performed in H_2SO_4 solutions and additional purification of the electrolyte had no influence on the effect. In this work, when the polarization curve was being recorded on a rotating electrode, the current increased when the rotation was stopped and decreased when the rotation was started again. This reversible effect of the rotation is also inconsistent with the influence of impurities. Recently Iwashita[5] pointed the necessity of thoroughly eliminating traces of oxygen in the electrolyte because the peroxide species produced

during oxygen reduction on Pt can oxidize adsorbed organic residues. However, the amount of oxygen in the electrolyte in this work was estimated to be $< 10^{-6}$ M which is too low to act as a scavenger for some reactive intermediate in the oxidation of methanol. Moreover, Wasmus and Vielstich[25] showed that oxygen in the electrolyte can enhance the catalytic properties of Pt towards the oxidation of CO and methanol, because oxygen containing species are required for the removal of poisoning species formed during methanol oxidation. However, this effect was established when pure oxygen was bubbled through the electrolyte.

Hence, it seems that the lower current densities in the stirred electrolyte is genuine to methanol oxidation on Pt and similar electrocatalysts and that the phenomenon originates from a weakly adsorbed intermediate. Desorption of carbon monoxide can be ruled out, because CO_{ads} is a rather stable species that can survive removal of the electrode from the electrolyte, its transfer into a UHV chamber and re-immersion in the electrolyte.[3] According to the reaction scheme in Fig. 1, other species that can diffuse away from the electrode are formaldehyde and formic acid. Since both of them were detected in the electrolyte,[16–18] it is likely that they are responsible for the lower reaction rate when the electrode is rotated. The difference between the current density on a stationary electrode and that of a rotating one is more than an order of magnitude in electrolytes with a low methanol concentration, which is much larger than the difference in the number of electrons transferred when methanol is completely oxidized to CO_2 and only partially to HCOH. This is an indication that the intermediate which diffuses away from the electrode surface is formed before the occurrence of the rate determining step (rds).

It is rather difficult to identify the rds in such a complex reaction as methanol oxidation where numerous intermediates, steps and pathways are possible (see Fig. 1). However, the negative reaction order with respect to H^+ ion concentration can be attributed to the participation of OH_{ads} in the rds. Thus, the chemical steps

$$CHO_{ads} + OH_{ads} \rightarrow HCOOH \tag{1}$$

or

$$CO_{ads} + OH_{ads} \rightarrow COOH_{ads} \tag{2}$$

might be suggested as the possible rds. They should result in a Tafel slope of about 60 mV dec^{-1}, while the experimentally observed values were 75 to 90 mV dec^{-1} in the quiescent electrolytes. An explanation of this discrepancy cannot be proposed at the moment, except the complexity of the reaction mechanism with several adsorbed species, the surface coverage of which can be potential dependent and influence the Tafel behavior.

If step (1) is the rds, the desorption of HCOH should be the main cause of the current drop in stirred electrolyte, and if step (2) is the rds then both the desorption of HCOH and HCOOH could be responsible for this effect. On a stationary electrode, the diffusion of these species from the electrode surface is slow and a high coverage of CHO_{ads} of CO_{ads} is achieved, which is indicated by the zero reaction order with respect to methanol. However,

when the diffusion of HCOH and HCOOH is enhanced by rotation, the surface coverage of the participant in the rds is dimished to a medium value which results in a one-half reaction order with respect to methanol. The Tafel slope under these conditions is about 110 mV dec^{-1} and also energy of activation is slightly changed. This leads to the assumption that the rds might be different in the stirred electrolyte. According to the scheme in Fig. 1, two pathways are conceivable for methanol oxidation. The first one is (a)–(f) and the other is (g)–(i)–(d)–(f). They take place in parallel up to the CHO_{ads} intermediate, after which they merge into a single reaction sequence. Since the pathway (g)–(i)–(d)–(f) circumvents formaldehyde as an intermediate, it could be proposed that in the stirred electrolyte where HCOH leaves the vicinity of the electrode, pathway (g)–(i)–(d)–(f) becomes significant and even takes over the whole reaction. Under these conditions the elekctrochemical step

$$CH_3O_{ads} \rightarrow CH_2O_{ads} + H^+ + e^- \quad (3)$$

could be slow. The negative reaction order with respecxt to the concentration of H^+ ions is in accordance with this assumption because the formation of CH_3O_{ads} is dependent on the H^+ concentration:

$$CH_3OH \rightleftharpoons CH_3O_{ads} + H^+ + e^- \quad (4)$$

A reaction order with respect to methanol of 1/2 and a Tafel slope of 110 mV dec^{-1} indicate that the surface coverage of CH_3O_{ads} has a medium value and that it is independent of the potential.

The maximum on the polarization curve for for methanol oxidation is in the potential region where Pt is substantially oxidized. A role of $Pt(OH)_2$ in the deactivation of the Pt surface is indicated by the dependence of the potential of the maximum on the H^+ concentration. The formation of PtOH from $Pt(OH)_2$

$$PtOH + H_2O \rightleftharpoons Pt(OH)_2 + H^+ + e^- \quad (5)$$

follows the same dependence of a 60 mV per tenfold increase in the H^+ concentration as the maximum on the polarization curve of methanol oxidation (Fig. 6). $Pt(OH)_2$ is less active for the adsorption of methanol and this step becomes rate determining at more positive potentials, which results in the insensitivity of the reaction rate on the potential.

CONCLUSIONS

Cobalt does not show a promoting effect on the rate of methanol oxidation on Pt_3Co bulk alloy with respect to a pure Pt surface. However, this statement should be reconsidered on nanoscale alloy particles.

The methanol oxidation rate is significantly diminished by rotation of the electrode in electrolytes containing a low concentration of methanol. This was ascribed to the diffusion of formaldehyde and formic acid from the electrode surface. Mass transfer effects on the reaction rate should also be investigated on nanoscale electrocatalysts. This is important because in the porous structure of gas diffusion electrodes all catalyst particles are not

evenly available to the fuel and some of them can operate at low methanol concentrations. In the optimization of the fuel flow in DMFC, one should be aware of a possible negative effect of convection on the methanol oxidation current.

The dependence of the methanol oxidation kinetics on the stirring of the electrolyte can help in the postulation of the reaction pathway. On the basis of the kinetic parameters of methanol oxidation and its dependence on the stirring of the electrolyte, it was speculated that the reaction on Pt_3Co bulk alloy follows parallel pathways. In the quiescent electrolyte, the pathway which includes formaldehyde and formic acid is predominant. When the electrolyte is stirred, this reaction pathway is suppressed and the reaction occurs *via* CH_3O_{ads} as the intermediate.

Acknowledgements: The author is grateful to P. N. Ross, N. M. Marković and V. Stamenković from the Materials Science Division, Lawrence Berkeley National Laboratory, Berkeley, USA, for supplying the alloy used in this work and their kind contribution to its preparation and characterization. This work was financially supported by the Ministry of Science, Technology and Development of the Republic of Serbia, Contract No. 1796.

ИЗВОД

ЕЛЕКТРОХЕМИЈСКА ОКСИДАЦИЈА МЕТАНОЛА НА ЛЕГУРИ Pt_3Co

С. Љ. ГОЈКОВИЋ

Технолошко-металуршки факултет, Универзитет у Београду, Карнегијева 4, п. пр. 3503, 11120 Београд

Електрохемијска оксидација метанола је испитивана на легури Pt_3Co у киселим растворима. Одређени су кинетички параметри реакције: коефицијент прелаза, редови реакције по метанолу и H^+ јону и енергија активације. Утврђено је да се брзина реакције значајно смањује када електрода ротира. Тај ефекат је приписан дифузији формалдехида и мрављe киселине са површине електроде. Мешање електролита такође утиче на кинетичке параметре реакције. Дискутована је могућност да су доминантан реакциони пут и спори ступањ у механизму реакције различити у мирном и мешаном електролиту. Присуство кобалта у легури није утицало на повећање брзине оксидације метанола у поређењу са чистом платином.

(Примљено 15. јула 2003)

REFERENCES

1. R. Parsons, T. VanderNoot, *J. Electroanal. Chem.* **257** (1988) 9
2. S. Wasmus, A. Kuver, *J. Elelctroanal. Chem.* **461** (1999) 14
3. T. Iwashita in *Advances in Electrochemical Science and Engineering, Vol. 1*, H. Gerisher, C. Tobias, Eds., VCH, 1990
4. T. D. Jarvi, E. M. Stuve, in *Electrocatalysis*, J. Lipkowski, P. N. Ross, Eds., Wiley-VCH, New York, 1998
5. T. Iwashita, *Electrochim. Acta* **47** (2002) 3663
6. B. Beden, C. Lamy, A. Bewick, K. Kunimatsu, *J. Electroanal. Chem.* **121** (1981) 343
7. P. A. Christensen, A. hamnett, G. L. Troughton, *J. Electroanal. Chem.* **362** (1993) 207
8. T. Iwasita, F. C. Nart, *J. Electroanal. Chem.* **317** (1991) 291
9. M. I. S. Lopes, B. Beden, F. Hahn, J. M. Leger, C. Lamy, *J. Electroanal. Chem.* **313** (1991) 323
10. X. H. Xia, T. Iwashita, F. Ge, W. Vielstich, *Electrochim. Acta* **41** (1996) 711
11. W. Vielstich, P. A. Christensen, S. A. Weeks, A. Hamnett, *J. Electroanal. Chem.* **242** (1987) 327
12. S. Wilhelm, T. Iwashita, W. Vielstich, *J. Electroanal. Chem.* **238** (1987) 383
13. J. Willsau, O. Wolter, J. Heitbaum, *J. Electroanal. Chem.* **185** (1985) 163

14. T. Iwashita, W. Vielstich, E. Santos, *J. Elecroanal. Chem.* **229** (1987) 367
15. J. Wilsau, J. Heitbaum, *Electrochim. Acta* **31** (1986) 943
16. T. Iwashita, W. Vielstich, *J. Electroanal. Chem.* **201** (1986) 403
17. C. Korzeniewski, C. Childers, *J. Phys. Chem. B* **102** (1998) 489
18. K. Ota, Y. Nakagava, M. Takahashi, *J. Electroanal. Chem.* **179** (1984) 179
19. Y. Jusys, J. Kaiser, R. J. Behm, *Electrochim. Acta* **47** (2002) 3693
20. T. Page, R. Johnson, J. Hormes, S. Noding, B. Rambabu, *J. Electroanal. Chem.* **485** (2000) 34
21. U. A. Paulus, A. Wokaun, G. G. Schere, T. J. Schmidt, V. Stamenković, N. M. Marković, P. N. Ross, *Electrochim. Acta* **47** (2002) 3787
22. S. Lj. Gojković, T. R. Vidaković, *Electrochim. Acta* **47** (2001) 633
23. D. M. Dražić, V. Dražić, *Electrochim. Acta* **11** (1966) 1235
24. T. Biegler, *Aust. J. Chem.* **26** (1973) 2571
25. S. Wasmus, W. Vielstich, *J. Appl. Electrochem.* **23** (1993) 120.

J.Serb.Chem.Soc. 68(11)871–881(2003)
JSCS – 3108

UDC 546.76+546.226–325+541.13:536.5
Originacal scientific paper

Electrochemistry of active chromium. Part III. Effects of temperature

J. P. POPIĆ[#] and D. M. DRAŽIĆ[#*]

Institute of Chemistry, Technology and Metallurgy - Center for Electrochemistry, Njegoševa 12, P. O. Box 473, 11001 Belgrade, Serbia and Montenegro (e-mail: dmdrazic@eunet.yu)

(Received 21 August 2003)

Abstract: It was shown that the temperature in the range 20 – 65 ºC has considerable effects on the electrochemical anodic dissolution of chromium in the active potential range as well as on the electrochemical hydrogen evolution reactions on bare and oxide covered chromium surfaces. Also, the chemical dissolution of chromium is strongly affected. The apparent energy of activation for anodic dissolution is 63.1 kJ mol^{-1}, for hydrogen evolution on a bare Cr surface 19.5 kJ mol^{-1}, for the same reaction on an oxide covered surface 44.0 kJ mol^{-1} and for the chemical ("anomalous") dissolution 66.9 kJ mol^{-1}. The temperature dependences of the total corrosion rate, and the electrochemical corrosion rate alone, are presented in polynomial forms with the appropriate constants obtained by the best fit of the experimental data. For the hydrogen evolution reaction on both bare and oxide covered chromium, the Volmer-Heyrovsky reaction mechanism with the second step as rate determining was proposed.

Keywords: chromium, anodic dissolution, anomalous dissolution, hydrogen evolution, sulfuric acid, effect of temperature, energy of activation.

INTRODUCTION

In a series of papers published elsewhere,[1–3] it was shown that chromium in sulfuric acid corrodes in a complex manner, forming simultaneously Cr(II) and Cr(III) ions, dissolving simultaneously electrochemically and anomalously (chemically) and of being the substrate for three different hydrogen evolution reaction, hydronium ions discharge and chemical evolution on bare chromium surfaces, and hydronium ions discharge at oxide covered chromium surfaces. All these reactions are pH dependent being faster in more acidic solutions. It was shown that the mechanism of the anodic dissolution reaction follows the same pattern as the mechanism of the electrochemical dissolution of some transition metals (Fe, Co, Ni),[4] while the chemical dissolution is in accordance with the mechanism proposed by Kolotyrkin and coworkers.[5,6] In this work the influence of temperature on the abovementioned processes in the temperature range 20 – 65 ºC for a chromium electrode in an aqueous sulfuric acid solution of pH 1.0 was studied.

Serbian Chemical Society active member.
* Author for correspondence.

EXPERIMENTAL

The experiments were performed with metallic Cr (Merck, p.a.). The electrodes were made in a form of a piece of metal sealed in epoxy resin (exposed surface 2 cm^2). All the experiments were performed in an aqueous mixtures of 0.1 M Na_2SO_4 + H_2SO_4, (pH 1.0), Merck p.a. chemicals and doubly distilled water were used for the preparation of the solutions. An all glass three compartment electrochemical cell with a Pt foil as the counter electrode and a saturated calomel reference electrode (SCE) was used. The cell was thermostated in a water bath with a ±1 ºC temperature control. All the potentials are referred to the SCE which was situated outside the water bath (*i.e.*, its tempeature was equal to the room temperature (22 ± 2 ºC). The soltuions were continuously deaerated with purified nitrogen. The potential scan rate of the Cr electrode was 2 mV s^{-1}, which was thought to be sufficiently slow to be able to consider the polarization curves as having been obtained under a quasi-steady state condition. Prior to the measurements, the electrodes were activated by cathodic polarization at – 0.9 V for 90 s, since the spontaneous formation of the open circuit potential of the electrode, which had previously been in contact with air, was at about – 0.45 V, which corresponds to the passive state of the chromium surface.[1]

A Hewlett-Packard HP8452A spectrophotometer was used for the determination of chromium ion concentration and a stoppered cuvette was used in order to eliminate possible oxidation of Cr(II) ions by air oxygen. Care was also taken during removal of the samples from the cell, which had a stopcock at the bottom enabling the solution samples to be passed directly into the cuvette. Details concerning the difficulties involved in the spectrophotometry of Cr(II) ions and mixtures of Cr(II) and Cr(III) ions have been presented elsewhere.[1] Some of the corrosion rates were determined gravimetrically by weight-loss measurements.

RESULTS AND DISCUSSION

Hydrogen evolution on bare chromium surface

The cathodic polarization curves recorded at different temperatrues in the range 20 – 65 ºC for a sulfuric acid solution of pH 1.0 are depicted in Fig. 1. As can be seen increasing the temperature increases the hydrogen evolution rate, while the Tafel slopes are *ca.* – 120 mV dec^{-1}. The exchange current density at 20 ºC was *ca.* 1×10^{-7} A cm^{-1}, while the variation of the Tafel slope with temperature was practically within the theoretically expected range (118 mV dec^{-1} for 20 ºC and 135 mV dec^{-1} for 65 ºC, respectively). The exchange

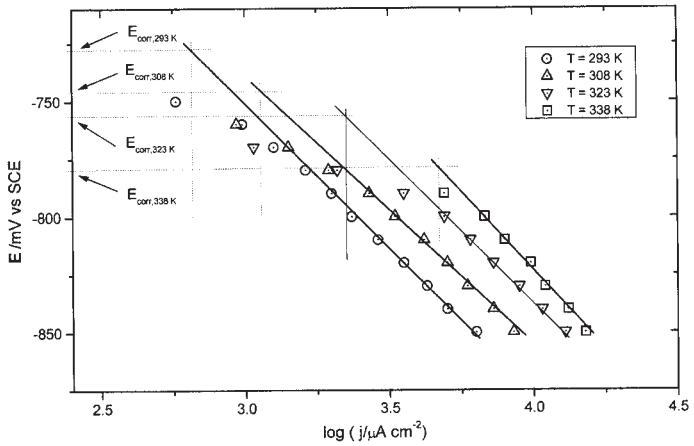

Fig. 1. Cathodic polarization curves for Cr in an aqueous 0.1 M Na_2SO_4 + H_2SO_4 (pH 1.0) solution at different temperatures.

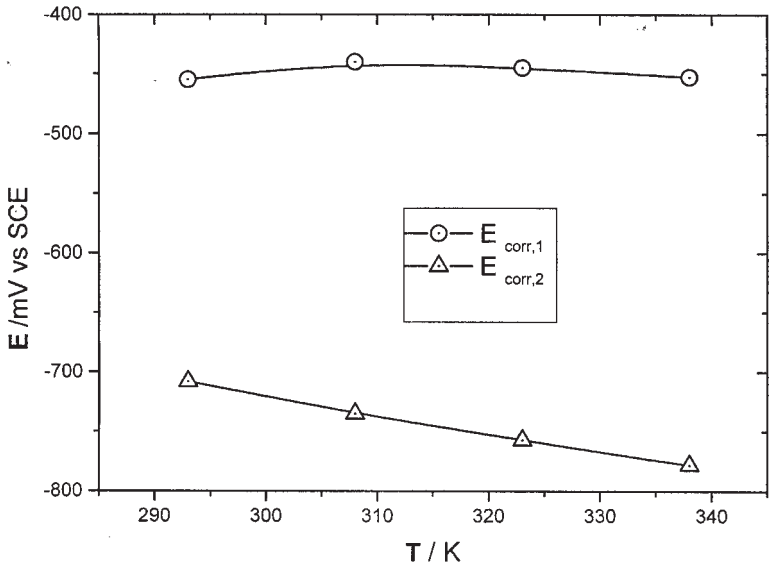

Fig. 2. Corrosion potentials of non-activated ($E_{corr,1}$) and activated ($E_{corr,2}$) Cr as a function of temperature.

current density is in accord with data presented in the literature.[7,8] The corrosion potential of activated chromium, $E_{corr,2}$, changes with temperature, becoming more negative with $dE_{corr,2} / dT \approx -0.8$ mV K^{-1} (see Fig. 2) which is similar to that observed by Wilde and Hodges.[9] Since both the cathodic and anodic Tafel slopes are about 120 mV dec^{-1}, this change of the corrosion potential in the negative direction with the increasing of temperature implies that the temperature has a larger effect on the anodic reaction than on the catodic one. This will be confirmed later with data presented in Fig. 3. The electrochemical corrosion current densities, $j_{corr,el}$, were obtained by extrapolation of Tafel lines to the corrosion potential, while the total corrosion rates were calculated from the gravimetric (weight-loss) measurements, $j_{tot,g}$, or from the solution analysis, $j_{tot,an}$, and they are presented in Fig. 3. As can be seen, the total corrosion rates, *i.e.*, the equivalent current densities, for all temperatures are much larger than the electrochemical corrosion current densities. For some reason, not quite clear as yet, the analytical results were systematically smaller than the gravimetric ones. This point has already been discussed in our previous paper.[2] Nevertheless, the much larger total corrosion rates than the electrochemical ones doubtlessly point to the existence of a considerable chemical dissolution of chromium, as shown elsewhere.[3] The room temperature total corrosion rate was *ca.*3.5 – 5.3 (depending whether the analytical or gravimetric data were used) times faster than the electrochemical one, which is in fair agreement with our previous results.[1] This difference increases with increasing temperature, as can be seen in Fig. 2, representing the obtained electrochemical and total corrosion current densities at different temperatures. At 65 ºC, the total corrosion rate from the gravimetric data is about 15 times faster than the electrochemical corrosion rate. At the same time, this means that the anomalous dissolution rate at this temperature is 14 times faster than the electrochemical one.

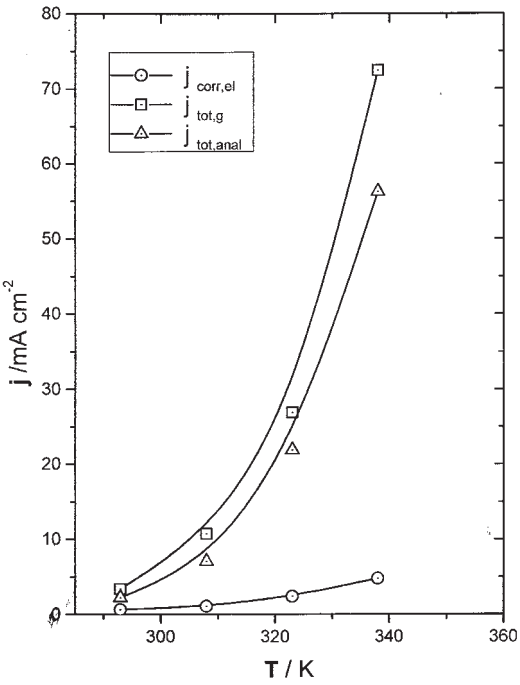

Fig. 3. Total corrosion current densities obtained gravimetrically (□) or analytically (Δ) and electrochemically obtained corrosion current densities (○) at different temperatures.

Figure 4 depicts the dependences of the logarithms of the current densities as a function of the reciprocal temperature (Arrhenius plots) for determination of the apparent energies of activation for the cathodic hydrogen evolution reaction at – 800 mV (squares), the anodic dissolution reaction at – 680 mV (circles) and the anomalous chromium dissolution reaction (triangles). The apparent energy of activation for the cathodic hydrogen evolution is 19.5 kJ mol^{-1}. It is interesting to point out that the apparent energy of activation at the same potential for hydrogen evolution at a Fe electrode under similar conditions was *ca*. 27 kJ mol^{-1} while the exhange current density was much higher, *ca.* 10^{-6} A cm^{-2}.[10] Also, Kita[11] quotes 1.6×10^{-6} A cm^{-2} as the mean literature value for this exchange current density. Since the decrease of 8.1 kJ mol^{-1} in the energy of activation for Cr should *increase* the reaction rate by *ca.* 7 times but the exchange current density for Cr is *ca*. 10 times *smaller* than for Fe, it is obvious that the difference in the exchange current densities between Cr and Fe is not due only to the effect of the enthalpy of activation, *i.e.*, to the differences in the enthalpies of adsorption of H on Fe and Cr. In fact, according to the M–H bond strengths used by Trasatti,[12] this value is *ca.* 289 kJ mol^{-1} for Fe and for Cr somewhat larger, 312 kJ mol^{-1}. Two special cases as analyzed by Trasatti[12] could be considered: (*i*) a slow discharge of protons whereby an increase of the M–H bond energy should *decrease* the energy of activation and (*ii*) a slow electrochemical desorption or slow recombination with a potential dependent coverage[11] for which increase of the M–H bond energy should *increase* the energy of activation. Since our experimentally determined apparent energies of activation and exchange current densities cannot be attributed to either of these cases as common to both metals, it seems obvious that one should conclude that,

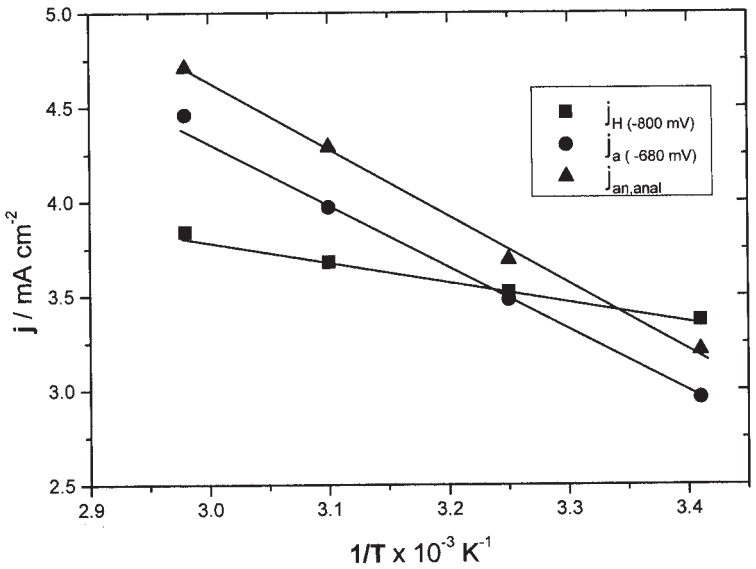

Fig. 4. Arrhenius plots for a Cr electrode in a solution of pH 1. (■) – Hydrogen evolution at – 800 mV; (●) – anodic Cr dissolution at – 680 mV; (▲) chemical ("anomalous") Cr dissolution.

staying within the framework of the postulated possible mechanisms for electrochemical hydrogen evolution, the mechanism and slow step are *different* for Fe and Cr. This conclusion is not in accordance either with the suggestions of Trasatti[12] based on the volcano curve analysis that for both Fe and Cr the electrochemical desorption steps should be rate determining, or with the suggestion of Krishtalik also based on the volcano curve analysis that for both metals a slow proton discharge is the rate determining reaction. The only difference between these two authors is the method of calculating the M–H bond strengths. However, neither of these proposals was able to solve the problem of the mechanisms of hydrogen evolution. Krishtalik and coworkers[13,14] discussed the problem of the unexpectedly high separation factors (> 10) for Fe, Cr and Mn. They considered the fact that at the surfaces of these metals chemical ("anomalous" hydrogen evolution in terms of Kolotyrkin and coworkers[5,6]) hydrogen evolution occurs simultaneously with the electrochemical hydrogen evolution and proposed as the rate determining step for the later reaction electrochemical desorption, but with the participation of H_2O molecules instead of H_3O^+ ions, as is usually done. In our opinion also this proposal cannot solve the previously discussed inconsistency between the apparent energies of activation and exchange current densities for Fe and Cr. Therefore, it seems that this controversy should be considered as still being unresolved. To our knowledge there have been no attempts in the literature to use the temperature dependence of the hydrogen evolution reaction on different metals for the purpose of the elucidation of reaction mechanisms. Perhaps more work on the study of the temperature dependence of the hydrogen evolution reaction on different metals would help in this respect.

Anodic dissolution of chromium

The anodic polarization curves for chromium in sulfuric acid of pH 1.0 recorded at different temperatures are presented in Fig. 5. The shapes of the polarization curves are similar except that the curves are shifted to higher current densities with increasing temperature, which is to be expected. The same is the case with the passivation current densities.

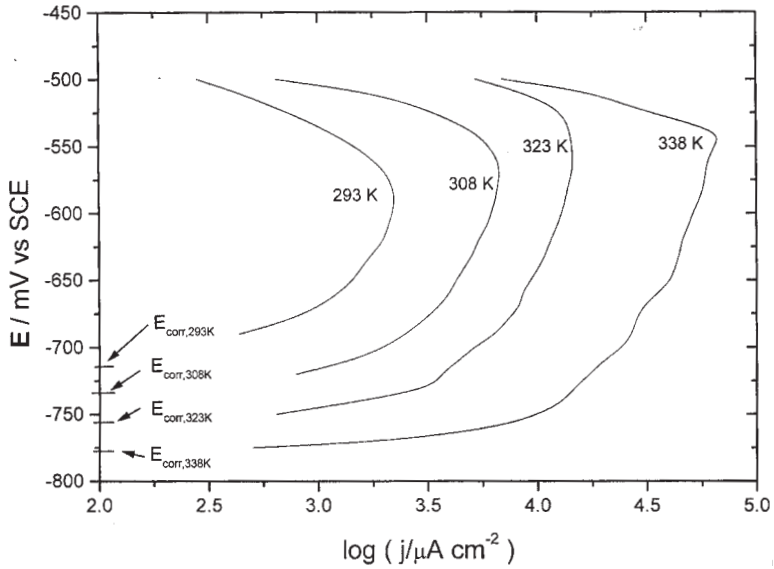

Fig. 5. Anodic polarization curves for a Cr electrode in a solution of pH 1 at different temperatures.

The Arrhenius plot for – 680 mV shown in Fig. 4 (circles) gives an apparent energy of activation for the anodic active dissolution of $E_a = 63.1$ kJ mol^{-1}. This indicates that the anodic reaction is more temperature dependent than the cathodic one, which also explains the change in the negative direction of the corrosion potential with temperature.

Corrosion rates

The corrosion rates presented in Fig. 3 depend considerably on temperature. These parabolic dependences can be represented by the third order polynoms. The best fit for the electrochemical corrosion rates is given by the polynom:

$$j_{corr,el} = 9.3\times10^{-6}\,T^3 + 9.8\times10^{-4}\,T^2 - 0.046T + 1.09 \quad (1)$$

and for the total corrosion rate obtained from the analytical (UV spectroscopy) data:

$$j_{tot,anal} = 4.8\times10^{-4}\,T^3 - 0.028T^2 + 0.764T - 5.64 \quad (2)$$

These empirical equations can be used to calculate the electrochemical corrosion rate or the total corrosion rate for any temperature within the studied temperature range, and to estimate the corrosion rates at temperatures lying to some extent outside the mentioned temperature limits with fair proximity.

It should be mentioned here that in the literature dealing with corrosion in acids some authors use the term "energy of activation of the corrosion process" and make efforts to determine its numerical value, assuming that the Arrhenius equation and its approach to determine the energy of activation of a chemical reaction can be directly applied to the corrosion process as well. Even though the experimentally determined electrochemical corrosion rates for different temperatures when plotted as an Arrhenius plot often give an almost straight line dependence, the energies of activations calculated from such diagrams have no theoretical meaning. Namely, according to the transition state theory of chemical kinetics,[15] the term energy of activation can be used only for simple elementary reactions. For successive, complex reactions, since the temperature dependence of the overall reaction rate also follows the Arrhenius equation, the use of term "apparent energy of activation" is recommended instead, to indicate immediately that one is dealing with a complex successive reaction. The real energies of activation of each individual step in a successive reaction and the apparent energy of activation of the overall reaction are correlated in a defined way, according to the mechanism of the successive reaction. But this energy of activation is related to *one reaction*, even though it could be a successive one. On the other hand, corrosion process, as often named, is by definition, the result of the simultaneous occurrence of at least two opposite reactions, *e.g.*, cathodic hydrogen evolution, oxygen reduction or something similar and anodic metal dissolution. Each of these independent electrochemical reactions has its own apparent energy of activation, which are unrelated. If in a parallel cathodic reaction the simultaneous reduction of oxygen occurs under diffusion control, which is most commonly the case with corrosion in acid solutions open to air, the interpretation of the temperature dependence of the corrosion rate using the Arrhenius equation and a kind of quasi energy of activation becomes totally senseless. Therefore we prefer to present the measured temperature dependences of the corrosion rates in polynomial forms (Eqs. (1) and (2)).

Chemical dissolution of chromium

As shown in Fig. 1, the overall corrosion rates, j_{tot}, at all temperatures used in these experiments are much higher than the electrochemical corrosion rates, $j_{corr,el.}$. As elaborated in more detail elsewhere,[3] this difference is due to the chemical dissolution of chromium, by the direct reaction of water molecules with Cr atoms from the electrode surface which is potential independent. These differences between the total dissolution rates determined analytically, $j_{tot,anal}$, and the electrochemical corrosion rates, $j_{corr,el.}$, are plotted for different temperatures in Fig. 4 (triangles). From the slope the apparent activation energy can be estimated to be 66.9 kJ mol^{-1}. This high energy of activation implies that the influence of temperature on the chemical dissolution reaction is rather large and contributes more to the overall corrosion rate at higher temperatures than in the lower temperature range. One should bear in mind this fact when attempting to use corrosion data colected at room temperature for prediction of the corrosion behavior of chromium at higher temperatures. It is very probable that similar differences in the effects of temperature exist in the

case of the corrosion of other metals which corrode both electrochemically and chemically (*e.g.*, Fe, Ni, Mn, *etc.*[5,6]), but we do not know of any serious experimental study of this type, except the work of Kolotyrkin and Florianovich,[5] from whose data for a Cr electrode in 0.05 M sulfuric acid dependence of the total corrosion rates, including the chemical one, on temperature is also considerable but somewhat lower than observed by us.

Hydrogen evolution on oxide covered chromium

As shown elsewere,[3] slow sweep rate cyclic voltammograms for a chromium electrode in sulfuric acid of pH 1.0 show unusual behavior in the reverse parts of the scan. Namely, registered current instead of being always anodic in the potential range between the corrosion potential, $E_{corr,2}$, and the positive limit of the potential scan, changes its sign two times in this potential range forming another corrosion potential, $E_{corr,1}$, and a cathodic peak, which is not the oxide reduction peak. An example for a sweep rate of 2 mV s^{-1} is shown in Fig. 6. It depicts an enlarged part of the reverse scans of the cyclic voltammograms recorded at different temperatures. As can be seen, the cathodic currents increase with increasing temperature, but the positions of the corrosion potentials, $E_{corr,1}$, and the cathodic peaks do not ehange. It was shown[3] that these cathodic currents are due to chatodic hydrogen evolution on the oxide covered chromium, and that the corrosion potential $E_{corr,1}$, is controlled by this hydrogen evolution reaction and the anodic dissolution of passive chromium. From the initial portions of the cathodic currents, Tafel plots can be constructed for different temperatures which are shown in Fig. 7. They show Tafel slopes of *ca.* – 60 mV dec^{-1} and increase of the current densities with temperature. The inset to Fig. 7 presents the Arrhenius plot at –520 mV from which an apparent energy of

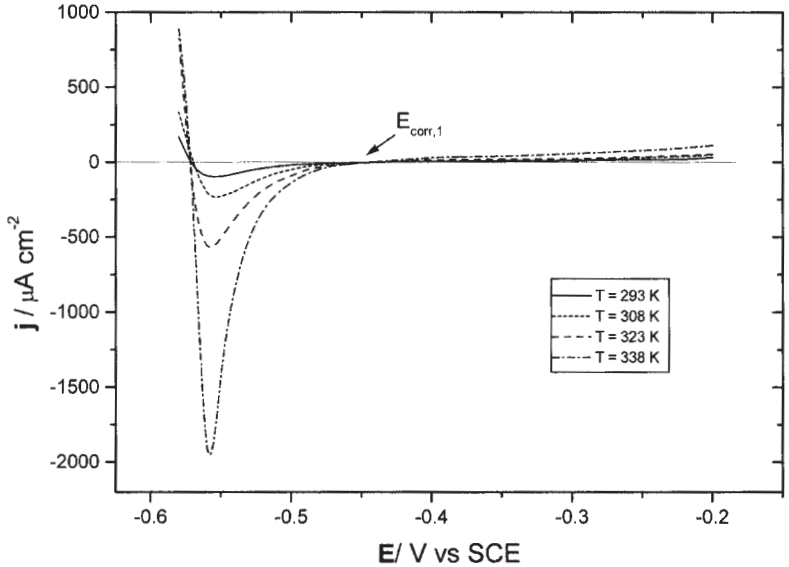

Fig. 6. Reverse parts of the voltammogram scans (2 mV s^{-1}) for a Cr electrode in a solution of pH 1 at different temperatures.

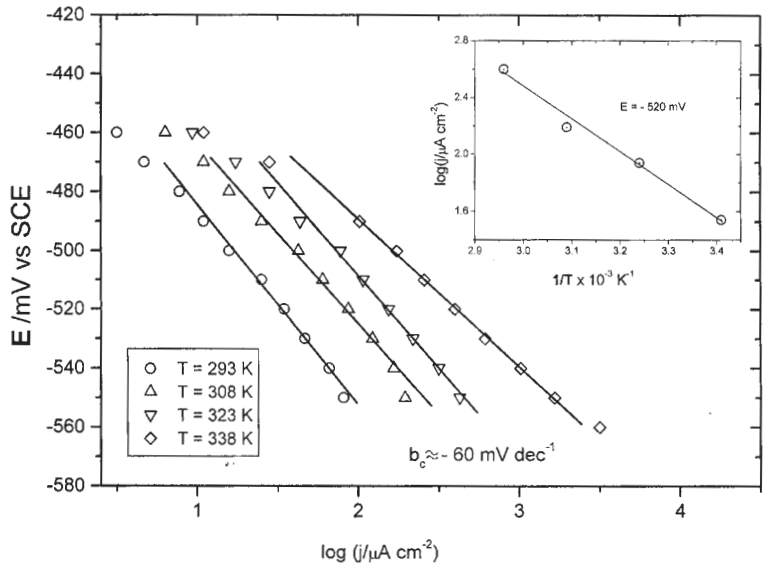

Fig. 7. Cathodic Tafel plots from the data in Fig. 6 for different temperatures. Inset: Arrhenius plot at –520 mV).

activation of 44.0 kJ mol^{-1} can be calculated. This is much higher than the energy of activation for hydrogen evolution on a bare surface (19.5 kJ mol^{-1}). Bearing in mind that it was shown earlier[3] that at room temperature the slopes of these Tafel lines gradually change their slopes from *ca.* –120 mV dec^{-1} for pH 3 to – 60 mV dec^{-1} for pH 1, and that the energy of activation for the hydrogen evolution is double that for a bare surface indicate differences in the reaction mechanism of the hydrogen evolution reaction, even though the first order reaction kinetics with respect to the H^+ ion concentration undoubtedly shows that both these cathodic reactions (*i.e.*, on the bare and on oxide covered chromium) start with the discharge of H^+ ions from the solution. Extrapolation of the Tafel lines for H_2 evolution on a bare Cr surface to –500 mV to compare with a Tafel line for an oxide covered surface shows that the rate of H_2 evolution on a bare surface would be 3–4 times slower at this potential. Since the energy of activation for the oxide covered surface is twice as large as that on the bare surface, this higher rate on the oxide covered surface can be explained only by a large difference in the pre-exponential factors in the Arrhenius equation for these two reactions. This could be so only if the entropy of activation is considerably different, and this could be true if either the reaction mechanisms are different, or that the entropy of adsorption of H atoms onto a bare surface is much larger than onto an oxide covered surface. All these findings could be rationalized so that the hydrogen evolution on Cr in both cases follows the Volmer-Heyrovsky mechanism

$$H^+ + e^- \rightleftharpoons H_{ads} \quad (3)$$

$$H_{ads} + H^+ + e^- \rightarrow H_2 \quad (4)$$

with a surface coverage of adsorbed hydrogen close to one, $\theta_H \rightarrow 1$ with the second step being the rate determining one. This is similar to the case of the hydrogen evolution reaction on iron[4] which also adsorbs considerable amount of hydrogen (hydrogen embrittlement). Since an oxide surface adsorbs hydrogen more weakly than a metallic phase, the slope of –60 mV dec^{-1} on the oxide covered surface for pH 1.0 could be a cosequence of a decrease of the surface coverage to the $\theta_H = 0.2 – 0.8$ range when under Temkin conditions of adsorption[16] Tafel slope should have a value of *ca.* – 60 mV dec^{-1}, as was experimentally observed (see Fig. 7).

CONCLUSIONS

– Corrosion of activated metallic chromium in aqueous sulfuric acid solutions of pH 1.0 consists of two simultaneous corrosion processes, an electrochemical corrosion and chemical dissolution (*i.e.*, corrosion). In the temperature range 20 – 65 ºC, the dependence of the total corrosion rate on temperature can be expressed by the equation:

$$j_{\text{tot,anal}} = 4.8\times10^{-4}\, T^3 – 0.028\, T^2 + 0.764\, T – 5.64$$

while the dependence of the electrochemical corrosion on temperature by the equation

$$j_{\text{corr,el}} = 9.3\times10^{-6}\, T^3 + 9.8\times10^{-4}\, T^2 – 0.046\, T + 1.09\ .$$

– The hydrogen evolution reaction, the anodic dissolution reaction and the chemical dissolution reaction of chromium on activated chromium in sulfuric acid solution of pH 1.0 in the temperature range 20 – 65 ºC follow the Arrhenius equation dependence with an apparent energy of activation of 19.5 kJ mol^{-1}, 63.1 kJ mol^{-1} and 66.9 kJ mol^{-1}, respectively.

– The hydrogen evolution reaction on an oxide covered chromium has an apparent energy of activation of 44 kJ mol^{-1}.

– Kinetic analysis of the obtained data suggests that the hydrogen evolution reaction on both bare and oxide covered chromium follow the Volmer-Heyrovsky mechanism with slow Heyrovsky reaction and stronger adsorption of atomic H on the bare Cr surface than on the oxide covered surface. This means that in the second case the Langmuir type adsorption on metallic Cr changes to Temkin type adsorption, resulting eventually in a change of the Tafel slope from –120 to –60 mV dec^{-1} in the later case.

Acknowledgement: This work was financially supported by the Ministry of Science, Technology and Development of the Republic of Serbia (Grant No. 1397).

NOMENCLATURE

$E_{\text{corr,1}}$ – Corrosion potential of passivated Cr
$E_{\text{corr,2}}$ – Corrosion potential of activated Cr
$j_{\text{corr,el}}$ – Electrochemical corrosion current density
$j_{\text{tot,anal}}$ – Total dissolution rate from analytical data
$j_{\text{an,anal}}$ – "Anomalous" (chemical) dissolution rate from analytical data
$j_{\text{tot,g}}$ – Total disolution rate from gravimetric data

ИЗВОД

ЕЛЕКТРОХЕМИЈА АКТИВНОГ ХРОМА. ДЕО III. УТИЦАЈ ТЕМПЕРАТУРЕ

Ј. П. ПОПИЋ и Д. М. ДРАЖИЋ

Институт за хемију, технологију и металургију - Центар за електрохемију, Његошева 12, п. пр. 473, 11001 Београд

Показано је да се на Cr електроди у раствору 0,1 M Na_2SO_4 + H_2SO_4 (pH 1,0) са повишењем температуре значајно убрзавају реакције анодног растварања Cr, хемијског растварања Cr, катодног издвајања водоника на голој металној површини, као и на површини хрома превученој оксидом. За анодно растварање добијена је привидна енергија активнације E_a = 63,1 kJ mol^{-1}, за хемијско растварање хрома E_a = 66,9 kJ mol^{-1}, за издвајање водоника на голом хрому E_a = 19,5 kJ mol^{-1} и издвајање водоника на хрому прекривеном оксидом E_a = 44,0 kJ mol^{-1}. Температурна функција укупне брзине корозије и електрохемијске брзине корозије приказане су као полиноми трећег реда са одговарајућим коефицијентима одређеним фитовањем експерименталних података. Предложено је на основу ових резултата да је механизам издвајања водоника и на голој и на оксидом превученој површини хрома механизам Фолмер-Хејровски, са другим ступњем као спорijим.

(Примљено 21. августа 2003)

REFERENCES

1. D. M. Dražić, J. P. Popić, *J. Serb. Chem. Soc.* **67** (2002) 777
2. D. M. Dražić, J. P. Popić, *Corrosion NACE*, (accepted)
3. J. P. Popić, D. M. Dražić, *Electrochim. Acta* (submitted)
4. D. M. Dražić in *Modern Aspects of Electrochemistry*, Vol. 19, B. E. Conway, J. O'M. Bockris and R. E. White Eds., Plenum Press, New York, 1989, Chapter 2
5. Ya. M. Kolotyrkin, G. M. Florianovich, *Zashch. Metal.* **1** (1965) 7
6. Ya. M. Kolotyrkin, G. M. Florianovich, *Elektrokhimiya* **9** (1973) 988
7. Kho Hgok Ba, Nguen Dyk Vi, *Elektrokhimiya* **4** (1968) 990
8. A. Bélanger, A. K. Vijh, *J. Electrochem. Soc.* **121** (1974) 225
9. B. E. Wilde, F. G. Hodge, *Electrochim. Acta* **14** (1969) 619
10. Lj. M. Vračar, D. M. Dražić, *J. Electroanal. Chem.* **265** (1989) 171
11. H. Kita, in *Encyclopedia of Electrochemistry of the Elements*, A. J. Bard, Ed., Vol IX A, Marcel Dekker, New York, 1982, pp. 413–555
12. S. Trasatti, *J. Electroanal. Chem.* **39** (1972) 163
13. T Sh, Korkashvili, V. M. Tsionski, L. I. Krishtalik, *Elektrokhimiya* **15** (1979) 1383
14. V. M. Tsionski, T. Sh. Korkashvili, *Elektrokhimiya* **16** (1980) 451
15. H. Eyring, S. H. Lin, *Basic Chemical Kinetics*, Wiley-Interscience, New York, 1980
16. E. Gileadi, B. E. Conway, in *Modern Aspects of Electrochemistry*, J. O'M. Bockris and B. E. Conway, Eds., Butterwoths, London, 1964, Chapter 5.

J.Serb.Chem.Soc. 68(11)883–892(2003)
JSCS – 3109

UDC 577.175.8+616.15:543.544+66.061
Original scientific paper

High-performance liquid chromatographic determination of famotidine in human plasma using solid-phase column extraction

DRAGICA ZENDELOVSKA[1] and TRAJČE STAFILOV[2*]

[1]Institute of Preclinical and Clinical Pharmacology and Toxicology, St. Cyril and Methodius University, Medical Faculty, 50 Divizija bb, 1000 Skopje, Republic of Macedonia and [2]Institute of Chemistry, Faculty of Science, St. Cyril and Methodius University, P. O. Box 162, 1001 Skopje, Republic of Macedonia (e-mail: trajcest@iunona.pmf.ukim.edu.mk)*

(Received 17 April 2003)

Abstract: A rapid, specific and sensitive high-performance liquid chromatographic method for the determination of famotidine in human plasma has been developed. Famotidine and the internal standard were chromatographically separated from plasma components using a Lichrocart Lichrospher 60 RP selec B cartridge for solid-phase separation with a mobile phase composed of 0.1 % (v/v) triethylamine in water (pH 3) and acetonitrile (92:8, v/v). UV detection was set at 270 nm. The calibration curve was linear in the concentration range of 10.0 – 350.0 ng mL^{-1}. The method was implemented to monitor the famotidine levels in patient samples.

Keywords: famotidine, high-performance liquid chromatography, solid-phase extraction.

INTRODUCTION

The description of the selective histamine H_2-receptor blockade by Black in 1970 was a landmark in the history of pharmacology and set the stage for the modern approach to the treatment of acid-peptic disease, which until then had relied almost entirely on acid neutralization in the lumen of the stomach. The most prominent effects of H_2-receptor antagonists are on basal acid secretion; less profound but still significant is the suppression of stimulated (feeding, gastrin, hypoglycemia, or vagal stimulation) acid production.[1] Famotidine is a well known histamine H_2-receprot antagonist and highly effective and useful in the treatment of peptic ulcers. The absorption is rapid but incomplete in the gastro-intestinal tract with peak concentrations in the plasma occurring about 2 h after oral administration. Famotidine is weakly bound, about 15 to 20 %, to plasma proteins. Most of the drug is eliminated unchanged in the urine, but a small amount of famotidine is metabolised in the liver to famotidine S-oxide.[2] Therefore, the determination of famotidine concentrations in biological samples is of particular interest in pharmacokinetic studies.

Several high-performance liquid chromatography methods have been developed for measuring the famotidine concentration in pharmaceutical preparations.[3–7] A number of assay methods for famotidine in biological fluids have been reported.[8–17] Some authors have investigated the possibility of the determination of famotidine in plasma or urine after its separation and concentration by liquid–liquid extraction using ethyl acetate as the solvent[8,9] or a two-step liquid extraction using diethyl ether and ethyl acetate.[10] However, the disadvantage of these methods employing liquid–liquid extraction of famotidine from biological fluids with ethyl acetate is that they give highly variable and relatively low recoveries (20–60 %) and therefore some authors suggested solid-phase extraction for sample pre-treatment.

Many investigators have performed the separation of famotidine from plasma with solid-phase extraction on different cartridges such as silica and C_{18}-bonded silica.[11–13] Sample preparation performed on this kind of solid-phase cartridges unsatisfactory values for the recovery and poor separation of famotidine from the interfering plasma matrix.

Also, the isolation of the drug and elimination of endogenous plasma interferences with strong cation exchanger (SCX) solid-phase cartridges has been reported.[14–16]

Zhong *et al.*[14,15] proposed methods for the separation of famotidine from plasma samples using an SCX cartridge for solid-phase extraction and its determination with normal-phase liquid chromatography/tandem mass spectrometry[14] and column switching technique with UV detection.[15]

Guo *et al.*[17] proposed the direct injection of plasma samples to determine famotidine in plasma using the HPLC column switching technique. This method involves direct injection of plasma to an extraction column for sample clean-up followed by switching onto an analytical column. The only disadvantages of this method is the high reagent consumption and a HPLC system with two pumps.

The aim of this work was develop a solid-phase extraction method for the elimination of plasma endogenous interferences on the determination of famotidine in human plasma. Namely, continuing our work on the development of solid-phase extraction methods for the separation of drugs from the plasma endogenous interferences,[16,18] in this paper a new method for the determination of famotidine in plasma samples using the solid-phase extraction technique on RP-select B cartridges is proposed. In order to fulfil the aim, the method was first developed for the separation of and determination of famotidine concentrations using the internal standard method by optimising the experimental parameters and determining the linearity for the investigated drug. Then, the method for the determination of famotidine concentrations was validated by evaluating recovery, selectivity, linearity, precision and accuracy. Finally, the method was used for the determination of famotidine in patient plasma samples.

EXPERIMENTAL

Reagents and chemicals

Famotidine and the internal standard (I.S.) 3-[({2-[(aminoiminomethyl)amino]-4-thiazolyl}-methyl)thio]-propanamide, were kindly supplied by Select Chemie (Switzerland) and KRKA Pharmaceuticals (Slovenia), re-

spectively. Acetonitrile and methanol were purchased from Across Organics (Belgium), *o*-phosphoric acid, potassium dihydrogen phosphate, sodium carbonate, acetic acid, sodium hydroxide and triethylamine were obtained from Merck (Germany). All used reagents were of analytical grade except acetonitrile and methanol, which were HPLC grade. Cartridges for solid-phase extraction were purchased from Merck (Germany).

Chromatographic system

The HPLC analysis was carried out on a Perkin-Elmer liquid chromatography system (USA) consisting of a pump LC series 200, autosampler LC ISS Series 200, diode array detector LC 235 C and column oven model 101. The chromatographic system was controlled by the software package Turbochrom Version 4.1. plus and the UV-spectrometric data are produced by the program TurboScan Version 2.0. The analytical column was LichroCart Lichrospher 60 RP-select B, 250 × 4 mm I.D., 5 μm particle size with a matched guard column (Merck, Germany). The mobile phase consisted of 0.1 % triethylamine (pH 3 adjusted with a very small amount of *o*-phosphoric acid) – acetonitrile (92:8, v/v). The mobile phase was filtered, degassed with helium and delivered at a flow-rate 1.2 mL min^{-1}. All experiments were carried out at ambient temperature, approximately 25 ºC.

Preparation of standard solutions and plasma samples

Stock solutions of famotidine and I.S. were prepared at a concentration 1000 μg mL^{-1} by dissolving appropriate amounts in 0.1 % (v/v) acetic acid. These solutions were stored at 4 ºC and no change in stability over a period of 1 month was observed. The working solutions were prepared by diluting appropriate portions of these solutions with distilled water.

Human plasma was prepared from heparinized whole blood samples. The blood samples were collected from healthy volunteers and stored at –20 ºC. After thawing, the samples were spiked daily with working solutions of famotidine and internal standard.

Sample preparation

A solid-phase extraction vacuum manifold (Merck) was used for the sample preparation. Satisfactory values of the recovery of famotidine and the I.S. were obtained with a single extraction using a RP select B solid phase cartridge (200 mg) for the isolation of the drugs from the plasma samples. Before analysis the plasma samples (0.9 mL) spiked with 100 μl of I.S. (20 μg mL^{-1}) were buffered with 1 mL of 0.1 mol L^{-1} Na_2CO_3 solution (pH 10 adjusted with NaOH). The cartridge was conditioned sequentially using 2 mL of methanol and 2 mL of water. The buffered plasma sample was introduced onto the cartridge under vacuum at 5 psi. Water (4 mL) was used to rinse the cartridge. The analytes were eluted with 2 mL methanol. The eluate was evaporated to dryness under N_2 for about 20 min at 40 ºC. After redissolving the residue in 150 μL of 0.017 mol L^{-1} CH_3COOH, a volume of 120 μL was injected into the HPLC system.

Extraction recovery

Recovery studies were performed by analysing plasma samples spiked with famotidine at two concentration levels. Three replicate samples for each concentration were extracted and chromatographed. The extraction recoveries were calculated by comparing the peak height of famotidine and internal standard obtained for plasma samples ($n = 3$ for each level for famotidine, $n = 6$ for internal standard) with those resulting from the direct injection ($n = 3$, working solutions) of the theoretical amount of either famotidine or internal standard (= 100 % recovery).

Assay validation for famotidine

Linearity. Five calibration solutions of famotidine were prepared by serial dilution of the stock solution and spiking them into drug-free human plasma. The standard samples were prepared according to the procedures as unknown samples. The calibration curve was constructed by analysing a series of plasma calibration samples spiked with famotidine to obtain concentrations ranging from 10.0 to 350.0 ng mL^{-1}. The chromatograms were evaluated on the basis of the famotidine/I.S. ratios of the peak heights. The regression equation was calculated by the least-squares method.

Precision, accuracy and reliability

The intra- and inter-day precision was determined by analysing the spiked plasma samples of each concentration used for the construction of the calibration curve on three different days. The mean, standard deviations, RSD of the intra- and inter-day experiments were calculated.

The intra- and inter-day accuracy was determined by measuring plasma quality control samples of low, middle and high concentration levels of famotidine. The relative error of the mean predicted concentration compared with the nominal concentration was determined.

The reliability was tested on a second HPLC column of the same type by determining the linearity, precision and accuracy. The linearity was performed at five concentration points for famotidine in human plasma in the concentration range from 10.0 to 350.0 ng mL^{-1}. Intra-dey precision and accuracy were determined by measuring three series of plasma quality control samples.

Stability evaluation

The stability of famotidine in plasma was investigated using spiked samples at two different concentration levels prepared in duplicate. The spiked samples were analysed after different storage conditions: immediately, after staying in an autosampler for 2 and 24 h, after one and two freeze/thaw cycles and after one month sorage at –20 ºC. The stability was determined by comparing the nominal concentration of famotidine in the samples analysed immediately with those analysed after different storage conditions.

RESULTS AND DISCUSSION

Method development

A series of studies were conducted in order to develop a convenient and easy-to-use method for the quantitative analysis of famotidine in human plasma. Several HPLC method variables with respect to their effect on the separation of famotidine and internal standard from the matrix were investigated. In the extensive preliminary experiments, various column packings including C8, C18 and RP-select B of different lengths and particle sizes were tested. The results of this investigation showed that when the separation was performed on C8 and C18 columns the investigated drugs showed peak tailing. The peak tailing may be attributed to hydrogen bonding between the free silanols of the stationary phase and the amino groups of the investigated drugs. The final choice of the stationary phase giving satisfying peak shape, resolution and run time was a Lichrocart Lichrospher 60 RP-select B, 250 × 4 mm I.D. (5 μm, particle size). Also, a series of aqueous mobile phases with different pH values in combination with different modifiers including acetonitrile, methanol and triethylamine (TEA) with different volume fractions were tested. The elution was monitored over the whole UV region and the wavelength of 270 nm exhibited the best detection.

The amount of organic modifier present in the mobile phase will influence analytes that are retained predominantly by adsorption onto the stationary phase. Figure 1 shows the results that were obtained when the mobile phase contained 0.1 % (v/v) TEA and acetonitrile in the concentration range from 5 % to 15 % with the pH adjusted to 3 with a very small amount of concentrated *o*-phosphoric acid. This data was used to determine an optimal amount of organic modifier that should be used for the separation of famotidine and the I.S. The best results (good separation between two peaks, short time of analysis) were obtained when the percentage of acetonitrile in the mobile phase was 8 %.

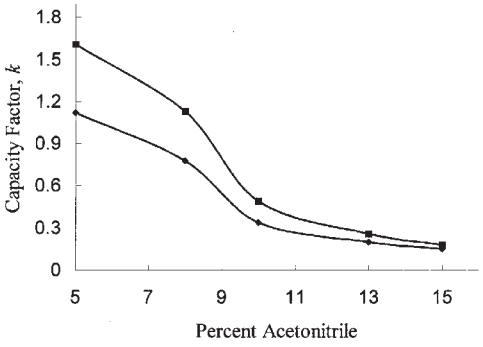

Fig. 1. The effect of the organic modifier concentration on the retention of the analytes (◆–famotidine, ■–internal standard).

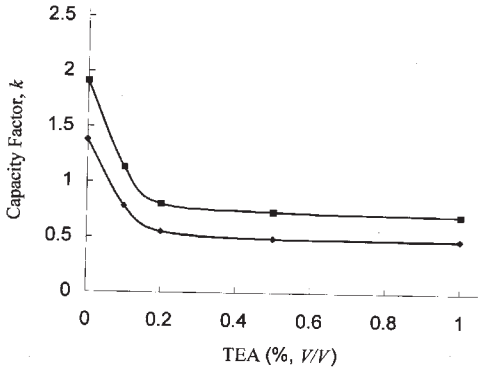

Fig. 2. The effect of the TEA concentration on the retention of the analytes (◆–famotidine, ■–internal standard).

An additional study was also done to check the effect that the percentage of TEA in the mobile phase had on the retention of the analytes. Figure 2 show the results obtained when the percentage of TEA was varied in the range of 0.0 % to 1.0 %. With increasing percentage of TEA in the mobile phase the retention of all the analytes decreased. Actually, TEA acts like an organic modifier. The best results (good separation between the two peaks, short time of analysis) was obtained when the percentage of TEA in the mobile phase was 0.1 %.

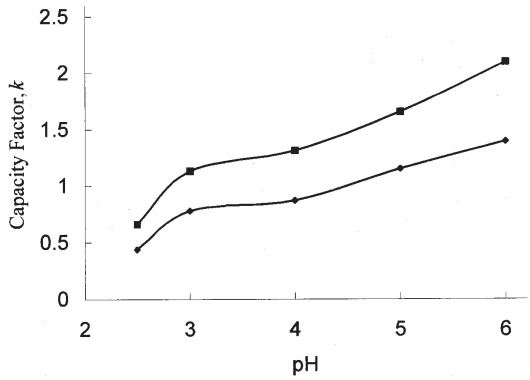

Fig. 3. The effect of the pH of the mobile phase on the retention of the analytes (◆–famotidine, ■–internal standard).

Also, the effect of pH on the retention of the analytes and their separation was observed over the pH range 2.5–6.0 using 0.1 % TEA solution. The obtained results are shown in Fig. 3, which it can be seen that the retention of famotidine and I.S. decreased with decreasing pH of the mobile phase. A good separation of the investigated drugs and short time of analysis were obtained when the pH of the mobile phase was 3.

From these data it was determined that mobile phase containing 0.1 % TEA and 8 % acetonitrile with a pH of 3 would provide good retention of famotidine and the internal standard as well as an acceptable runtime for the separation of less that 8 min.

Typical chromatograms of standard solutions of famotidine and internal standard pro-

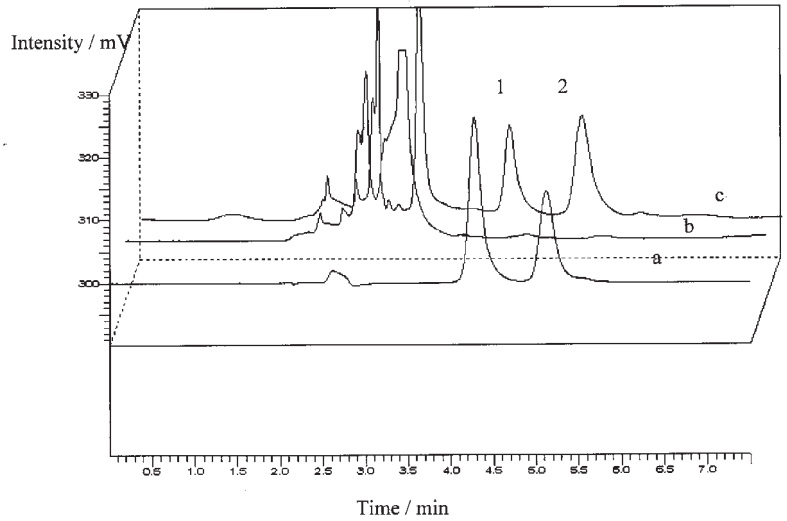

Fig. 4. Chromatograms of standard solutions (a) of famotidine (2 μg mL^{-1}) and I.S. (1 μg mL^{-1}); 1-famotidine, 2-internal standard, blank (b) and spiked plasma (c) sample containing 200 ng mL^{-1} of famotidine and I.S.

duced by the developed HPLC method are shown in Fig. 4a The retention time of famotidine and of the internal standard are 4.2 and 5.1 min, respectively.

In addition, different cartridges for solid phase extraction (C18, TSC, SCX and RP-select B) were tested in order to determine the satisfactory values of the recovery of famotidine and internal standard. The results from this investigation shows that solid-phase extraction without any pre-treatment of the plasma sample results in poor separation of the investigated drugs from the plasma endogenous interference of the plasma.

TABLE I. Absolute recoveries of famotidine from spiked plasma samples

γ/ng mL^{-1}	Mean recovery / %			
	TSC	RP-select B	C18	SCX
Famotidine				
250.0	103.9	101.5	96.3	89.6
500.0	102.1	101.7	100.4	95.3
Internal standard				
500.00	100.4	99.8	94.3	96.7

γ* – Mass concentration

Therefore, in order to improve the extraction procedure, the plasma samples were buffered at volume ratio of 1:1 with 0.1 mol L^{-1} solutions of Na_2CO_3 (pH 10), KH_2PO_4 (pH 3) or citric acid (pH 2.5) before being introduced onto the cartridges for solid-phase extraction. It was found that satisfactory values of the recovery of famotidine and I.S. were obtained when the plasma samples were buffered with Na_2CO_3 solution and extracted using TSC, C18 and

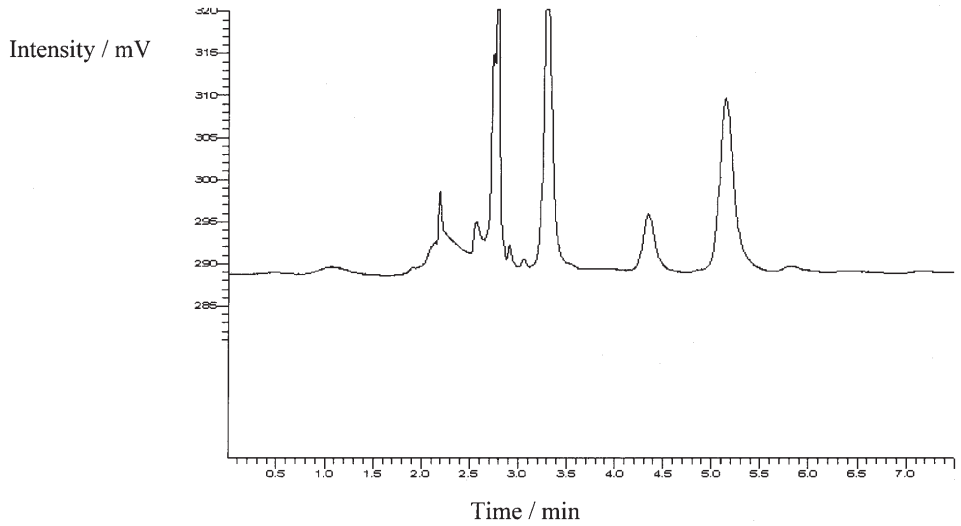

Fig. 5. Chromatogram of a patient plasma sample after oral administration of 40 mg of famotidine.

RP-select B cartridges. Also, satisfactory values for the recovery of famotidine and I.S. were obtained when plasma samples, buffered with citric acid, were extracted with SCX columns. The results from this investigation are given in Table I. On the other hand, solid-phase extraction on TSC and C18 columns gave an interfering peak at the retention time of the internal standard. Interfering peaks were found at the retention times of investigated analytes except when the solid-phase extraction was performed on RP-select or SCX cartridges. Therefore, in this study, the determination of famotidine in plasma samples was performed after their preparation with Na_2CO_3 solution and extraction on RP select B cartridges.

Typical chromatograms of the blank human plasma (b) and plasma sample spiked with famotidine and internal standard (c) are shown in Fig. 4. No interfering peaks were found at the retention times of the investigated analytes.

The developed HPLC method was used for the analysis of plasma samples of patients after oral administration of famotidine. Typical chromatograms of the plasma samples of patients prepared according the procedures for sample preparation after a single 40 mg oral dose of famotidine are shown in Fig. 5.

Method validation

Linear detector response for the peak-height ratios of famotidine to internal standard was observed in the concentration range from 10.0 to 350.0 ng mL^{-1} with a correlation coefficient of 0.9999. The respective regression equation for famotidine obtained after sample preparation using solid-phase extraction was: $y = 0.0047\ \gamma - 0.0068$.

Under the employed experimental conditions, the lower limit of detection was 4 ng mL^{-1} at a signal-to-noise ratio of 3. The limit of quantification was defined as the lowest amount detectable with a precision of less than 15 % ($n = 5$) and an accuracy of ± 15 % ($n = 5$). The limit of quantification was found to be 10 ng mL^{-1}.

TABLE II. Intra- and inter-day precision data

Famotidine nominal concentration ng mL^{-1}	Intra-day		Inter-day	
	Mean (n = 3) observed concentration/ng mL^{-1}	Relative standard deviation/%	Mean (n = 6) observed concentration/ng mL^{-1}	Relative standard deviation/%
10.0	9.64	3.32	10.85	6.45
50.0	49.81	1.14	48.78	4.35
100.0	102.8	1.61	99.66	3.75
200.0	199.3	1.10	197.8	2.13
350.0	349.6	0.53	354.1	1.51

The results of the study of the validation of the method are presented in Tables II and III. The intra- and inter-day variations of the method throughout the linear range of concentrations are shown in Table II. The intra- and inter-day reproducibilities expressed as relative standard deviation (RSD) were found to be 0.53–6.45 %, indicating good precision of the proposed method. The indication of the accuracy was based on the calculation of the relative error of the mean observed concentration as compared to the nominal concentration. The accuracy data are presented in Table III. The relative errors at all three studied concentrations are less than 8.8 % and it is obvious that the method is remarkably accurate which ensures that reliable results can be obtained.

TABLE III. Intra- and inter-day accuracy data

Famotidine nominal concentration ng mL^{-1}	Intra-day		Inter-day	
	Mean (n = 3) observed concentration/ng mL^{-1}	Relative error/%	Mean (n = 6) observed concentration/ng mL^{-1}	Relative error/%
30.0	30.96	3.21	31.29	4.29
80.0	77.23	–3.46	79.62	–0.47
150.0	158.4	5.60	153.4	1.42

The reliability was tested using a second HPLC column of the same type by determining the linearity, precision and accuracy. The linearity test was performed at five concentration points for famotidine in human plasma in the concentration range from 10.0 to 350.0 ng mL^{-1}. The regression equation was: $y = 0.0047\ \gamma - 0.0155$, with a correlation coefficient of 0.9992. The relative standard deviations at all three studied concentrations of famotidine were less than 2.82 %. The relative errors ranged from 0.6 to 6.07 % of the nominal concentrations of the investigated drug. As can be seen, the results of this assessment are very similar to those obtained by the previous investigation on the first HPLC column. That means that this HPLC method for the determination of famotidine in spiked human plasma samples is reliable.

The results from the stability studies show that relative errors for the two different concentrations studied ranged from 0.14 to 11.4 % and it is obvious that famotidine added to plasma is stable under different storage conditions.

CONCLUSIONS

The developed HPLC method employing solid-phase extraction for sample preparation, is simple and convenient for the determination of famotidine in plasma samples. The typical assay time is about 8 min. Famotidine and the internal standard have been successfully separated. The proposed method is simply, rapid and provides efficient clean up of the complex biological matrix and high recovery of famotidine. The validation data demonstrate good precision and accuracy, which proves the reliability of the proposed method. Finally, the method has been implemented to monitor famotidine levels in clinical samples.

ИЗВОД

ОДРЕЂИВАЊЕ ФАМОТИДИНА У ЉУДСКОЈ ПЛАЗМИ МЕТОДОМ ТЕЧНЕ ХРОМАТОГРАФИЈЕ ВИСОКОГ РАЗЛАГАЊА КОРИШЋЕЊЕМ ЕКСРАКЦИЈЕ У КОЛОНИ СА ЧВРСТОМ ФАЗОМ

ДРАГИЦА ЗЕНДЕЛОВСКА и ТРАЈЧЕ СТАФИЛОВ

Институт за преклиничку и клиничку фармакологију и токсикологију, Медицински факултет, Универзитет "Св. Ћирило и Методије", 50 Дивизија бб, 1000 Скопје и Институ за хемију, Природно-математички факултет, Универзитет "Св. Ћирило и Методије", п. пр. 162, 1001, Скопје, Република Македонија

Развијена је брза, специфична и осетљива метода за одређивање фамотидина у људској плазми коришћењем течне хроматографије високог разлагања. Фамотидин и интерни стандард су хроматографски развојени од других компонената плазме помоћу Lichrocart Lichrospher 60 RP select B патроне за сепарацију помоћу чврсте фазе, уз коришћење 0,1 % (v/v) триетиламина у води (pH 3) и ацетонитрила (92:8 %, v/v) као покретне течне фазе. UV детекција је вршена на 270 nm. Калибрациони дијаграм је линеаран у области концентација 10,0 – 350,0 ng mL^{-1}. Метода је примењена за праћење нивоа концентрације фамотидина у узорцима узетим од пацијената.

(Примљено 17. априла 2003)

REFERENCES

1. *Goodman and Gilman's, The Pharmacological Basis of Therapeutics*, 10th ed., McGraw Hill, New York, 2001. pp. 1009–1011
2. *Martindale, The Extra Pharmacopeia*, 31st ed., Royal Pharmaceutical Society, London 1996, pp. 1218–1220
3. *European Pharmacopeia*, 4th ed., Council of Europe, Strasbourg, 2002
4. C. Ho, H. M. Huang, S. Y. Hsu, C. Y. Shaw, B. L. Chang, *Drug. Dev. Ind. Pharm.* **25** (1999) 379
5. N. Beaulieu, S. J. Graham, R. W. Sears, E. G. Lovering, *J. Pharm. Biomed. Anal.* **7** (1989) 1705
6. R. Ficarra, P. Ficarra, M. L. Calabro, *Farmaco* **42** (1987) 307
7. S. E. Biffar, D. J. Mazzo, *J. Chromatogr.* **363** (1986) 243
8. T. C. Dowling, R. F. Frye, *J. Chromatogr. B.* **10** (1999) 239
9. Y. Imai, S. Kobayashi, *Biomed. Chromatogr.* **6** (1992) 222
10. S. Wanwimolruk, A. R. Zoest, S. Z. Wanwimolruk, C. T. Hung, *J. Chromatogr.* **572** (1991) 227
11. L. Cvetković, L. Zupančić-Kralj, J. Marsel, *J. Pharm. Biomed. Anal.* **9** (1991) 207
12. M. Bologna, L. Biordi, T. Napolitano, G. Carlucci, *Int. J. Clin. Pharmacol. Res.* **8** (1989) 335
13. W. C. Vincek, M. L. Constanzer, G. A. Hessey, W. F. Bayne, *J. Chromatogr.* **338** (1985) 438
14. L. Zhong, R. Eisenhandler, K. C. Yeh, *J. Mass Spectrom.* **36** (2001) 736
15. L. Zhong, K. C. Yeh, *J. Pharm. Biomed. Anal.* **16** (1998) 1051
16. D. Zendelovska, S. Simeska, S. Petrov, P. Milosevski, *Acta. Pharm.* **52** (2002) 113

17. P. Guo, L. M. Ye, B. Lu, Y. J. He, Z. W. Li, *Yao. Xue. Xue. Bao.* **25** (1990) 622
18. D. Zendelovska, T. Stafilov, M. Stefova, *J. Chromatorg. B* **788** (2003) 199.

J.Serb.Chem.Soc. 68(11)893–901(2003)
JSCS – 3110

UDC 669.783+678.8+66.046.51:669.71.018
Original scientific paper

The effects of microalloying with silicon and germanium on microstructure and hardness of a commercial aluminum alloy

VESNA MAKSIMOVIĆ[1#], SLAVICA ZEC[1#], VELIMIR RADMILOVIĆ[2] and MILAN T. JOVANOVIĆ[1#]

[1]*Department of Materials Science, Vinča Institute of Nuclear Sciences, 11001 Belgrade, Serbia and Montenegro and* [2]*Department of Materials Science and Engineering, University of California, Berkeley, U.S.A.*

(Received 1 April, revised 26 June 2003)

Abstract: The effect of small additions of Si and Ge on the microstructure and hardness was investigated during aging of a commercial 2219 aluminum alloy. It was found that for the same level of microalloying in alloy 2219SG (containing Si and Ge), a maximum hardness was achieved 3 times faster than in alloy 2219S (without Ge). The accelerated precipitation kinetics is a consequence of the presence of fine Si–Ge particles, serving as heterogeneous precipitation sites for θ" strengthening particles.

Keywords: Al–Cu–Si–Ge alloys, Al alloy 2219, Si–Ge precipitate, heterogeneous precipitation, precipitate strengthening.

INTRODUCTION

There are several parameters which control the structure and properties of Al–Cu based alloys during the process of aging, such as: type (coherent or non-coherent), size, distribution and volume fraction of strengthening phase particles in the Al-based matrix. To promote a dense and homogeneous distribution of fine coherent precipitates, small amounts of Si, Mn, Be, Sn, Ag and Cd were added to an Al–Cu alloy.[1–5] Results of Hornbogen and co-workers[6,7] clearly demonstrated that in Al–Si–Ge alloys much finer Si–Ge precipitates (almost an order of a magnitude) may be achieved than in Al–Si and Al–Ge binary alloys. Very recently, Mitlin *et al.*[8–11] tried to modify the reaction of precipitation in Al–Cu alloy by the simultaneous addition of small amounts of Si and Ge (in total of 1 to 2 at.%) with the idea to control the kinetics of aging. Significant effects of strengthening have been achieved by this process through precipitation of θ' phase on finely dispersed Si and Ge particles. Due to the low concentration of Si and Ge additions, this concept of alloying may be regarded as microalloying.

Serbian Chemical Society active member.

It should be mentioned that the effect of Si and Ge on the reaction of precipitation was studied using an experimental quarternary Al–Cu–Si–Ge alloy.[8–11] However, elements such as Zr, V, Ti, Mn and Fe are always present in commercial aluminum alloys in order to control the grain size and to increase the temperature of recrystallization.[12] The effect of these elements on the chemical composition of the present phases and alloy properties must not be neglected.

The aim of this paper is to study the effect of small additions of Si and Ge on: (a) the microstructure and hardness, and (b) kinetics of precipitation of alloys based on a commercial 2219 aluminum alloy.

EXPERIMENTAL

A commercial 2219 aluminum alloy (fully corresponding to ASTM standard), produced by Kaiser Aluminum, was used as a starting material. In the next step the chemical composition of this alloy was modified since the total concentration of Si and Ge was anticipated to be about 0.5 at.%, with the Si/Ge ≈ 1 relation. Two experimental alloys were produced by this microalloying process, *i.e.,* one alloy (designated as 2219S) with higher concentration of Si than the standard ASTM alloy and another alloy with additions of both Si and Ge (designated as 2219SG). Spectrophotometry was used to determine the chemical composition of these alloys, which is shown in Table I. Concentration of most important elements is emphasized by framing.

TABLE I. The chemical composition of investigated alloys (mass %)

Element	2219 ASTM	2219 [at.%]	2219SC [at.%]
Cu	5.8–6.8	5.91 [2.52]	5.90 [2.52]
Ge	–	–	0.69 [0.26]
Si	max 0.2	0.51 [0.49]	0.28 [0.27]
Fe	max 0.3	0.24	0.26
Mn	0.2–0.4	0.28	0.29
Mg	max 0.02	0.01	0.01
Zn	max 0.1	0.05	0.06
Ti	0.02–0.1	0.08	0.08
Zr	0.1–0.25	0.12	0.13
V	0.05–0.15	0.09	0.09
Cr	–	0.007	0.007

Melting, microalloying with "master-alloys" (Al-12 mass % Si and Al-50 mass % Ge) and casting were performed in a one-chamber vacuum induction furnace "Degussa". Pouring was done in a graphite crucible.

After machining, ingots of 1 kg in weight each, were homogenized for 48 h at 500 ºC and hot-rolled from the starting thickness of 27 mm to a thickness of 2 mm. After hot-rolling, the heat treatment of samples was as follows:

a) annealing at 500 ºC for 24 h

b) water-quenching

c) holding at room temperature for 9 days (natural aging)

d) artificial aging at 190 ºC in the interval from 10 min to 300 h.

Rockwell macrohardness was measured using the B scale (1/16" diametar of ball, 100 kg load). Microstructural characterization was performed by the light microscope "Ziess Axiovert 25", scanning electron microscope (SEM) "JEOL JSM-5300" equipped with energy dispersive spectroscope (EDS), X-ray dif-

fraction equipment "Siemens D500" and transmission electron microscope (TEM) "JEOL 200 CX" operated at 200 kV. For light microscopy and SEM, samples were etched in a Keller solution consisting of 2 ml HF (48 %), 3 ml HCl (conc.), 5 ml HNO_3 (conc.) and 190 ml H_2O. Samples for TEM were thinned to electron transparency using a "Fischione" twin-jet apparatus. The electrolyte was 25 % solution of nitric acid in methanol and the thinning was carried out at –25 ºC at a voltage of 13 V that yielded a current of 50 mA. Only two sets of samples were studied by TEM: (a) aged for shorter times (corresponding to the maximum of hardness), and (b) aged for longer times (150 h).

RESULTS AND DISCUSSION

Microstructural investigation

Light microscopy. The microstructure of quenched samples is shown in Fig. 1 a,b.It is obvious that quenching did not produce a homogeneous microstructure which normally corresponds to the supersaturated solid solution. The presence of several phases of different morphology may be seen in the matrix of both alloys. The most prominent phase which appears in both alloys is in the form of light, plate-like particles with rounded edges, being larger in alloy 2219SG (about 20 μm in size). In addition, rod-like particles formed in parallel rows can be seen in the microstructure of 2219SG alloy (Fig. 1b).

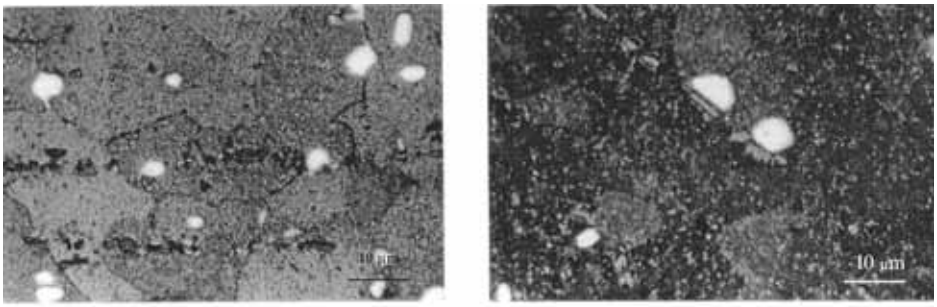

Fig. 1. Light microscopy. Microstructure of quenched samples. (a) Alloy 2219S; (b) alloy 2219SG.

SEM and EDS analysis. Microstructural details after quenching are shown in Fig. 2a,b, whereas results of EDS analysis of denoted particles are given in Table II. Results of Table II show that the thin and long particle (denoted as A) in alloy 2219S (Fig. 2a) consists of several elements, and it is likely that the chemical composition is similar to the phase of the type (Fe, Mn, Cu)$_3Si_2Al_{15}$ which appears in complex Al alloys.[13] On the other side, the chemical analysis of plate-like particle (B) in alloy 2219SG (Fig. 2b) suggests that it has a chemical composition close to that of a Al_7Cu_2Fe phase. The chemical composition of globular particles (C), appearing in both alloys, corresponds to the equilibrium Al_2Cu phase.

X-Ray diffraction. X-Ray diffraction patterns of quenched samples of both alloys are shown in Fig. 3a,b. In alloy 2219S (Fig. 3a), the existence of two phases was found, *i.e.*, an Al-based solid solution and the equilibrium θ phase (Al_2Cu). Apart from these two phases, peaks corresponding to a tetragonal lattice with parameters a = 0.6336 nm and c = 1.487 nm, were detected in a diffraction pattern of the 2219SG alloy (Fig. 3b). The appearance of these peaks fits quite well with the presence of the Al_7Cu_2Fe phase.

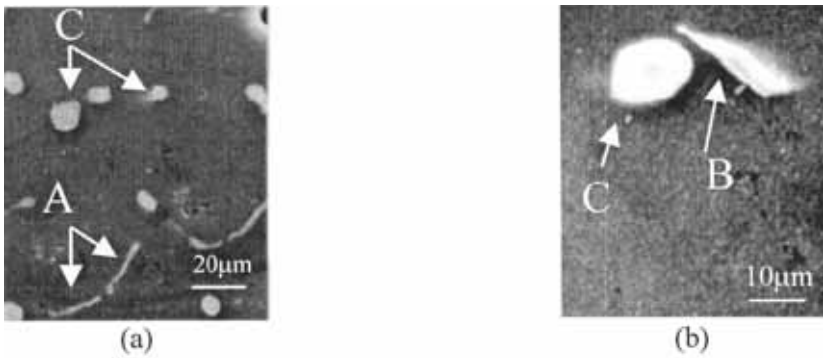

(a) (b)

Fig. 2. SEM micrographs. Microstrucrture of quenched samples. (a) Alloy 2219S; (b) alloy 2219SG. A – $(Fe, Mn, Cu)_3Si_2Al_{15}$ phase; B – Al_7Cu_2Fe phase; C – Al_2Cu phase.

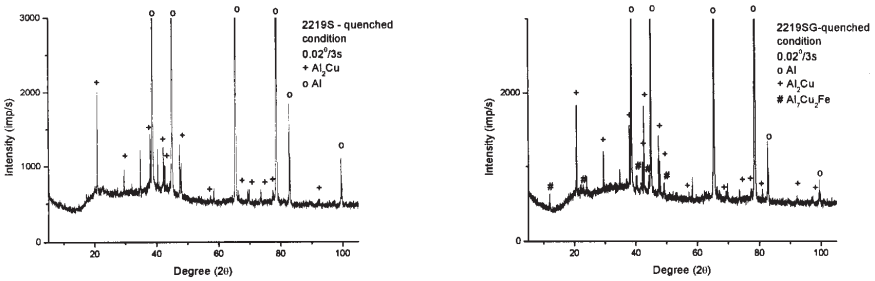

(a) (b)

Fig. 3. X-Ray diffraction of quenched samples. (a) Alloy 2219S; (b) alloy 2219SG.

TABLE II. Chemical analysis (EDS) of particles in quenched samples.

Alloy	Particle morphology	Element	mass %	at.%
2219S	Thin, long	Al	87.13	93.48
	(A)	Si	1.07	1.03
		Mn	2.40	1.19
		Fe	4.95	2.40
		Cu	4.46	1.90
	Globular	Al	71.65	87.89
	(C)	Cu	28.35	12.11
2219SG	Plate-like	O	0.95	1.59
	(B)	Al	73.04	86.88
		Mn	0.84	0.41
		Fe	5.56	2.75
		Cu	19.60	8.37
	Globular	Al	69.32	86.89
	(C)	Cu	30.68	13.11

Taking into account reflection of X-ray diffraction, it was found that a difference in the lattice parameters of the supersaturated solid solution of the two alloys exists, which indicates a different extent of supersaturation, especially considering Cu atoms. Lattice parameters of the Al-based supersaturated solid solution and the estimation of Cu concentration in this solid solution are given in Table III.

TABLE III. Lattice parameter of supersaturated Al solid solution and concentration of Cu solute atoms

Alloy	Lattice parameter a_{av} nm	*SE* x10^4	Concentration of Cu mass %
2219S	0.403887	7.8726	> 4.97
2219SG	0.404072	6.7123	≈ 4.3

**SE* – Standard error of the mean data

Concentration of Cu in the supersaturated solid solution was calculated using literature data for the binary Al–Cu system.[14] According to these data the amount of Cu (in mass %) varies from zero (for the lattice parameter $a = 0.40490$ nm) to 4.97 (for the lattice parameter $a = 0.40387$). The solubility of Cu in the solid solution of binary Al–based alloy at 500 ºC (which is the annealing temperature in this work) is about 4.4 mass %.[15] The results on concentration of Cu in the supersaturated solid solution should be regarded only as an approximate calculation, since the investigated materials are not binary Al–Cu alloys, but systems with rather complex chemical composition. Nevertheless, the enhanced concentration of Cu in the solid solution of 2219S alloy may be explained by the overall concentration of Si, considering that increased concentration of Si promotes the higher solubility of Cu in the Al-based solid solution.[16]

The results of X-ray diffraction and EDS analysis show that after quenching, besides the supersaturated solid solution (the matrix), some other phases are observed, *i.e.*:

$$\text{2219S alloy: water-quenching} \rightarrow \alpha_{S.S.S.} + Al_2Cu\ (\theta) + (Fe, Mn, Cu)_3Si_2Al_{15} \quad (1)$$

$$\text{2219SG alloy: water-quenching} \rightarrow \alpha_{S.S.S.} + Al_2Cu\ (\theta) + Al_7Cu_2Fe \quad (2)$$

where $\alpha_{S.S.S.}$ is the supersaturated solid solution of Al. (Fe, Mn, Cu)$_3$Si$_2$Al$_{15}$ and Al$_7$Cu$_2$Fe phases do not appear together in these alloys, the fact already established in some complex Al alloys.[13]

Change of hardness during aging. Change of hardness of 2219S and 2219SG alloys as a function of aging time at a constant temperature is shown in Fig. 4. Alloy 2219SG exhibits rapid hardening (up to 1 h) and a maximum at about 65 HRB is reached after 8 h of aging. During longer aging times hardness decreases approaching the level of about 50 HRB, which indicates that over-aging prevails as the operating process. Comparing to 2219SG, hardness of 2219S alloy slightly decreases at the beginning of aging which may be ascribed to reversion, *i.e.*, to the dissolution of GP zones formed during the previous process of artificial aging.[17] Maximum hardness at about 50 HRB (17 % less than the maximum of alloy 2219SG), is reached after 24 h, which is three times longer than for alloy 2219SG. After this maximum, the hardness of alloy 2219S significantly decreases with prolonged aging.

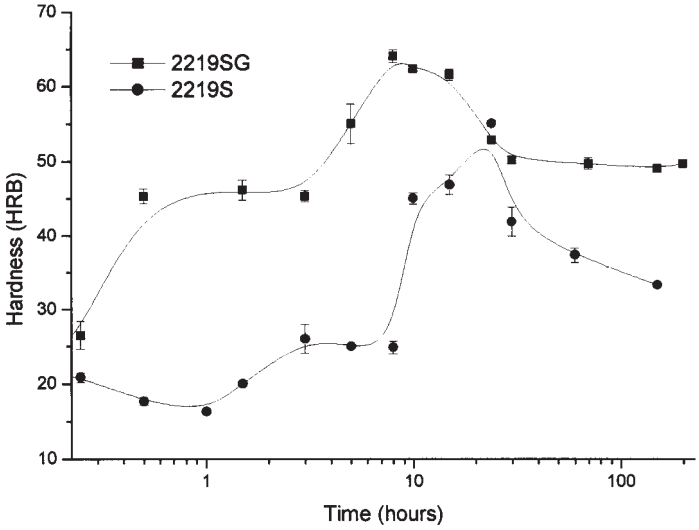

Fig. 4. Change of hardness during aging at 190 ºC.

Transmission electron microscopy. The microstructure of alloy 2219SG aged at the maximum hardness (after 8 h of aging) is shown in Fig. 5a,b. A selected area diffraction pattern (SADP) taken along the [001] matrix zone axis is characterized by weak streaks originating from coherent θ" particles (Fig. 5a). Edge-on θ" particles with diameters less than 100 nm are shown in Fig. 5b. The general sequence of the aging process of Al–Cu alloys is mostly described as: GP(1) zone → GP(2) zone or θ" → θ' → θ.[18] Maximum hardness on aging curves is associated with coherent precipitates, *i.e.*, θ" phase together with some θ' (the metastable form of the equilibrium θ phase, $CuAl_2$). In Al–4Cu–0.8Si–0.8Mg (mass %) alloy, the mixture of θ" and θ' phases at the maximum hardness was found at 130 ºC, whilst at 190 ºC only the θ' phase was associated with that maximum.[19] Weather the θ" and θ' mixture, or only

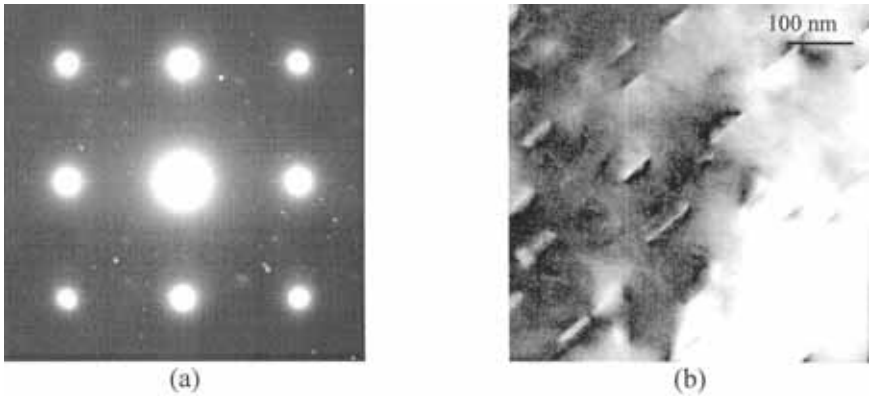

Fig. 5. TEM micrographs. Microstructure of alloy 2219SG aged at the maximum hardness (8 h at 190 ºC). (a) SADP along [001] matrix zone axis; (b) the bright field (BF) image showing θ" particles.

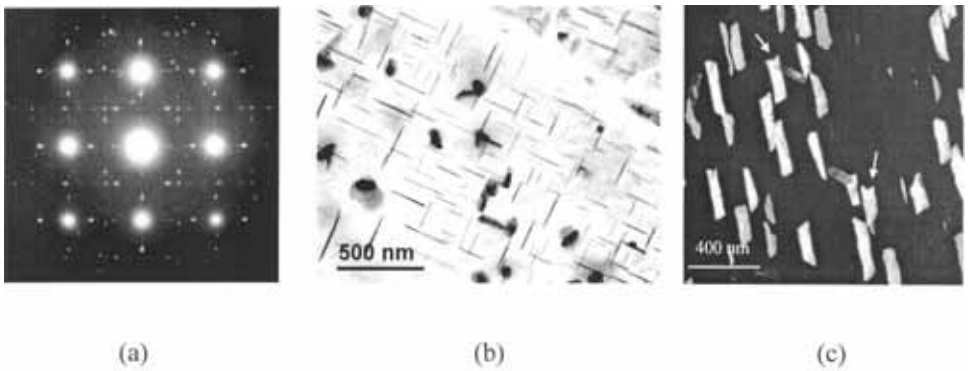

Fig. 6. TEM micrographs. Microstructure of over-aged alloy 2219SG (150 h at 190 ºC). (a) SADP along [001] matrix zone axis; (b) the bright field (BF) image showing θ' particles and rounded Si–Ge particles; (c) the dark-field (DF) image showing interaction of plate-like precipitates (θ') with Si–Ge particles (see arrows).

θ’ phase will be present at the hardness maximum depends on several parameters, such as concentration of copper, aging temperature and previous cold work. Microstructure after aging for 150 h is shown in Fig. 6a–c. SADP with additional spots corresponding to θ’ particles was taken along the [001] matrix zone axis (Fig. 6a). The bright-field image shows edge-on θ’ plates together with other equiaxed particles (Fig. 6b). The dark-field image which was obtained with the specimen tilted away from [011] matrix zone axis, shows that some θ’ phase precipitates interact with other precipitates, presumably Si–Ge particles (Fig. 6c). Since in an experimental alloy Al–0.5Si–0.5Ge (at.%) the appearance of Si–Ge particles was detected after 3 h of aging,[16] it is reasonable to suppose that these particles are also present in alloy 2219SG at the maximum hardness (although at a finer scale than after 150 h of aging) serving as nucleation sites for precipitation of θ” particles.

The microstructure of alloy 2219S after aging is shown in Fig. 7a,b for comparison. Figure 7a illustrates the bright-field image of the sample at the maximum hardness (after

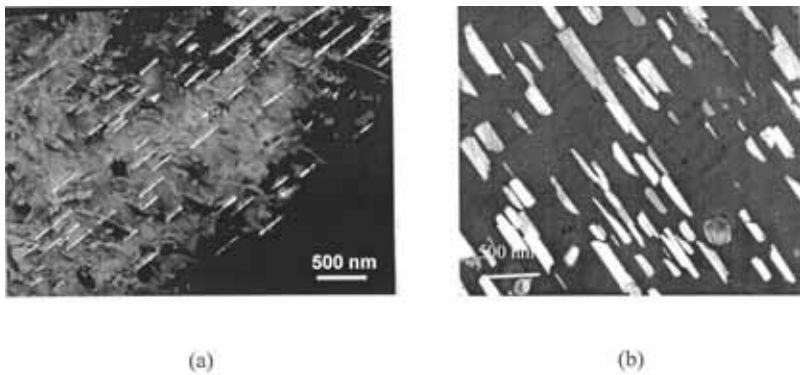

Fig. 7. TEM micrographs. DF image. Microstructure of alloy 2219S. (a) Aged at the maximum hardness (24 h at 190 ºC); (b) over-aged (150 h at 190 ºC).

24 h of aging) where thin edge-on θ' plates appear in the matrix, whereas Fig. 7b shows the dark-field image of θ' phase after aging for 150 h. It is clear that the limited over-aging after 150 h was controlled by the slow growth of θ' particles with diameters between 350 and 700 nm and thickness of about 100 nm.

Although there is some ambiguity on the issue whether not only θ'' phase, but a mixture of θ'' and θ' phases is present at the maximum hardness of alloy 2219SG, it is obvious that the addition of Ge in a commercial 2219 alloy promotes faster aging kinetics than in the alloy without Ge. Very fine Si–Ge precipitated particles were detected in the experimental quaternary Al–Cu–Si–Ge alloy aged at the maximum hardness (after 3 h).[16] Thus, it is reasonable to suppose that in the case of alloy 2219SG, Si–Ge particles are also present at th maximum hardness, although on much finer scale than after 150 h of aging. Accelerated aging kinetics in alloy 2219SG is a direct consequence of heterogeneous precipitation of Si–Ge particles representing energetically more favourable sites for precipitation of the θ'' phase. The significant effect of Ge addition on hardness is strongly confirmed by the fact that alloy 2219SG possesses higher hardness irrespective that the concentration of Cu, regarded as the most important hardening element, in this alloy is lower than in alloy 2219S (see Table III).

CONCLUSION

Applying microalloying, *i.e.*, by adding a very small amount of Ge to a commercial Al 2219 alloy and varying the concentration ratio of Si and Ge, changes of microstructure and hardness of two experimental alloys 2219S (without Ge) and 2219SG (with Ge) have been achieved.

After quenching, apart from the supersaturated solid solution, the equilibrium θ phase (Al_2Cu) is present in both alloys, as well as phases of the approximate chemical composition $(Fe, Mn, Cu)_3Si_2Al_{15}$ (2219S alloy) and Al_7Cu_2Fe (2219SG alloy).

Small addition of Ge promotes not only accelerated aging kinetics due to the presence of Si–Ge particles which serve as favourable sites for precipitation of fine coherent θ'' particles, but also increases the level of hardness compared to the alloy without Ge.

Acknowledgement: This investigation was a part of the project No. 1261 financed by The Ministry of Science, Technology and Development, Republic of Serbia. Authors are indebted to Miroslav Miljković from The University of Niš for provision of SEM facilities.

ИЗВОД

УТИЦАЈ МИКРОЛЕГИРАЊА СИЛИЦИЈУМОМ И ГЕРМАНИЈУМОМ НА МИКРОСТРУКТУРУ И ТВРДОЋУ КОМЕРЦИЈАЛНЕ ЛЕГУРЕ АЛУМИНИЈУМА

ВЕСНА МАКСИМОВИЋ[1], СЛАВИЦА ЗЕЦ[1], ВЕЛИМИР РАДМИЛОВИЋ[2] и МИЛАН Т. ЈОВАНОВИЋ[1]

[1]Лабораторија за материјале, Институт за нуклеарне науке "Винча", 11001 Београд, Србија и Црна Гора и [2]Department of Materials Science and Engineering, University of California, Berkeley, U.S.A.

Испитиван је утицај малих додатка Si и Ge на микроструктуру и тврдоћу за време старења комерцијалне легуре алуминијума 2219. Микролегирање утиче на микроструктуру легура и каљеном стању због различитог односа Si и Ge. Утврђено је да се при истом нивоу микролегирања максимум тврдоће у легури 2219SG (садржи Si и Ge) постиже три пута брже него у легури 2219S (без Ge). Убрзана кинетика таложења, последица је присуства Si–Ge талога који служе као места за хетерогено таложење θ" фазе која ојачава легуру.

(Примљено 1. априла, ревидирано 26. јуна 2003)

REFERENCES

1. S. P. Ringer, K. Hono, I. J. Polmear, T. Sakuraj, *Acta Metall.* **44** (1996) 1883
2. R. N. Wilson, *J. Inst. Metal.* **97** (1969) 80
3. J. Karov, W. V. Youdelis, *Mater. Sci. Technol.* **3** (1987) 1
4. J. M. Silcock, T. J. Heal, H. K. Hardy, *J. Inst. Metal.* **84** (1955) 23
5. J. D. Boyd, R. B. Nicholson, *Acta Metall.* **19** (1971) 1101
6. E. Hornbogen, A. K. Mukhopadahyay, E. A. Starke, Jr., *Z. Metallkd.* **83** (1992) 577
7. E. Hornbogen, A. K. Mukhopadahyay, E. A. Starke, Jr., *Script. Metall. Mater.* **27** (1992) 732
8. D. Mitlin, V. Radmilović, U. Dahmen, J. W. Morris, Jr., *Met. and Mat. Trans.* **32A** (2001) 197
9. V. Radmilović, U. Dahmen, J. W. Morris, will be submitted for Nature (2003)
10. V. Radmilović, U. Dahmen, B. Dracup, M. K. Miller, D. Mitlin, J. W. Morris, *Int. Conference on Aluminum Alloys*, Cambridge, 1–6 July (2002), UK
11. D. Mitlin, V. Radmilović, U. Dahmen, J. W. Morris, Jr., *Mater. Sci. Eng.* **A301** (2001) 232
12. J. E. Hatch, *Aluminum Properties and Physical Metallurgy*, (Russian translation) Moskva, Metallurgy, 1989, p. 215
13. L. F. Mondolfo, *Aluminum Alloys, Structure and Properties*, Butterworths, London, 1976, p. 208
14. W. P. Pearson, *A Handbook of Lattice Spacing and Structures of Metals and Alloys*, Pergamon Press, 1958, p. 328
15. H. Schuman, *Metalografija*, Beograd, TMF (1989) p. 531
16. D. Mitlin, *Ph. D. Thesis*, University of California, Berkeley, CA 94720 (2001)
17. D. A. Porter, K. E. Easterling, *Phase Transformations in Metals and Alloys*, Van Nostrad Reinhold (UK) Co. Ltd., 1983, pp. 291–308
18. J. W. Martin, *Precipitation Hardening*, Pergamon Press, Oxford, 1969, p. 142
19. W. Bonfield, *J. Mat. Sci.* **11** (1976) 1661.

J.Serb.Chem.Soc. 68(11)903–907(2003)
JSCS – 3111

UDC 669–492.2/.3–0.34.3:532.14:531–2
Original scientific paper

The apparent density as a function of the specific surface of copper powder and the shape of the particle size distribution curve

KONSTANTIN I. POPOV,[#] PREDRAG M. ŽIVKOVIĆ and SNEŽANA B. KRSTIĆ[#]

Faculty of Technology and Metallurgy, University of Belgrade, P. O. Box 3503, Karnegijeva 4, 11001 Belgrade, Serbia and Montenegro

(Received 2 June 2003)

Abstract: The relation between the specific surface and apparent density of copper powders electrodeposited from acid copper sulphate solutions is established. It is shown that the apparent density is inversly proportional to the specific surface of copper powder. The shape of the particle size distribution curve is also discussed.

Keywords: copper powder, apparent density of copper powder, specific surface of copper powder, particle size distribution of copper powder.

INTRODUCTION

Some properties, called decisive properties, charcterise the behaviour of copper powder. The most important of these are the specific surface and the apparent density.[1,2] These properties had not been related to the conditions of electrodeposition by any quantitative or semiquantitative relationships, until it was shown recently[3,4] that the specific surface, S_{sp}, of copper powder can be related to the deposition overpotential, η. The aim of this work was to relate the apparent density of copper powder, ρ, to the corresponding value of the specific surface, S_{Sp}, and, hence, to the deposition overpotential, η, and other deposition conditions.

DISCUSSION

Using the data of Calusaru,[1] it is possible to obtain the diagram given in Fig. 1, which indicates

$$\rho = \frac{K}{S_{Sp}} \tag{1}$$

where K is a constant, as the relation between the apparent density and the specific surface of a copper powder. This is confirmed by the plot in Fig. 2, which was obtained by

Serbian Chemical Society active member.

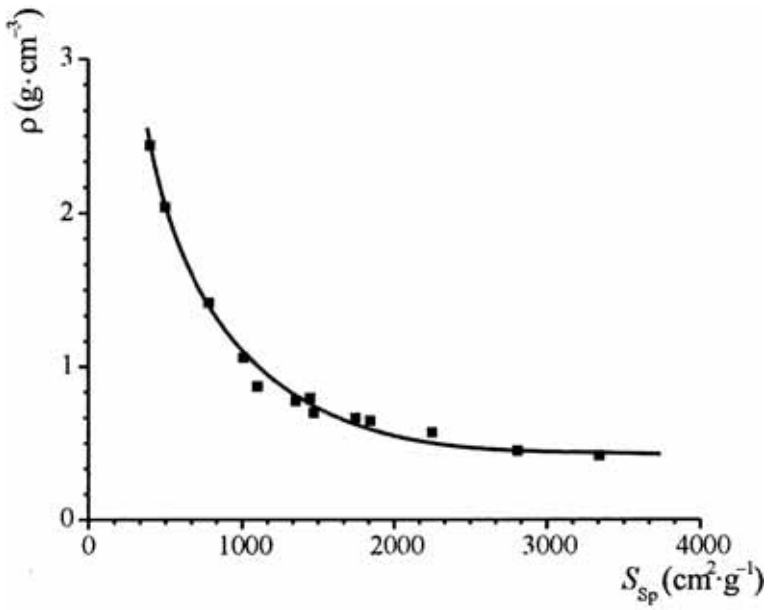

Fig. 1. The apparent density, ρ, of copper powder as a function of powder specific surface S_{Sp}.

replotting the data from Fig. 1 in the $\rho - 1 / S_{Sp}$ coordinates. From the slope of the straight line from Fig. 2, K = 1009 cm^{-1} is determined. The maximum difference between experimental value of the apparent density and the one calculated using Eq. (2) is 20 % and less then 10 % in other cases. Hence, Eq. (1) correlates the apparent density with the

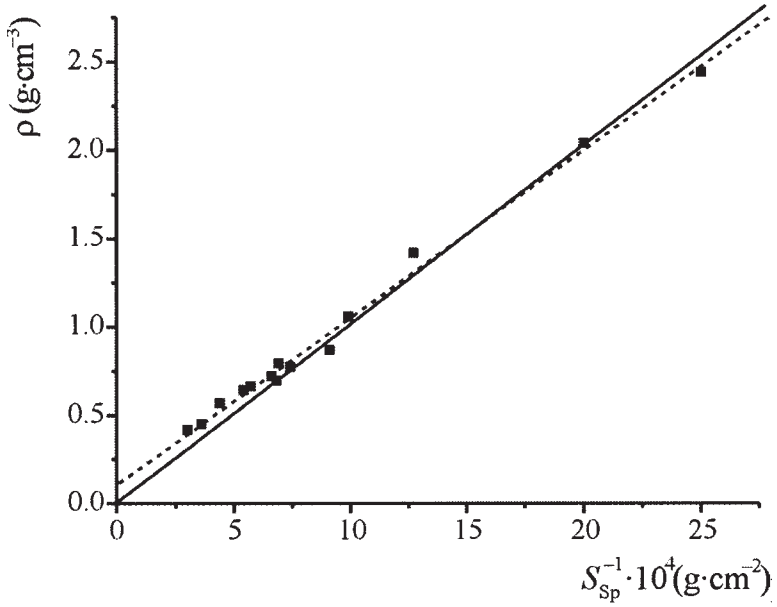

Fig. 2. $2\rho - 1/S_{Sp}$ dependence obtained by replotting the data from Fig. 1.

specific surface of a copper powder well. On the other hand, Eq. (1) can be rewritten in the form:

$$K = \rho \times S_{Sp} \tag{2}$$

which means that the value of K can be estimated using the values of the specific surface and apparent density of each particular powder.

It was shown in a previous paper[5] that copper powder could be treated as a homogeneous material the density of which is equal to the apparent density of the copper powder. The mass, m, of the volume, V, of the powder is given by:

$$m = \rho \times V \tag{3}$$

If S is the corresponding surface of the powder, Eq. (3) can be written as:

$$\frac{S}{V} = \frac{\rho \times S}{m} \tag{4}$$

or

$$\frac{S}{V} = \rho \times S_{Sp} \tag{5}$$

where:

$$S_{Sp} = \frac{S}{m} \tag{6}$$

It follows from Eqs. (2) and (5) that:

$$K' = \frac{S}{V} \tag{7}$$

Hence, the physical meaning of K is the surface per unit volume of copper powder. The values of S_{Sp} and ρ used for plotting Figs. (1) and (2) correspond to powders obtained under very different deposition conditions and K = 1009 cm^{-1} can be considered to be valid for any powder obtained by electrodeposition from a pure sulphate bath. It is interesting that this value is not valid for commercial copper powders.[6] It can be seen from Fig. 2 that the equation:

$$\rho = 0.12 + 944 \frac{1}{S_{Sp}} \tag{8}$$

valid for $S_{Sp} \geq 400$ cm^2/g, fits the data of Calusaru better. This plot is presented by the dashed line in Fig. 2. Substitution of ρ from Eq. (8) in Eq. (2) produces:

$$K' = 944 + 0.12\, S_{Sp} \tag{9}$$

meaning that K' increases slightly with increasing S_{Sp}.

It was shown in a previous paper[5] that the size H of the representative particle of a powder is given by:

$$H = \frac{6}{\rho S_{Sp}} \tag{10a}$$

or

$$H = \frac{6}{K} \tag{10b}$$

Hence, because of Eq. (2) and taking into account Eqs. (9) and (10a).

$$H = \frac{6}{944 + 012 S_{Sp}} \tag{11}$$

assuming the particles have a cubic shape. It follows from Eq. (11) that the size of the representative particle decreases slightly with increasing specific surface of the powder and deposition overpotential, which is in accordance with literature data.[1,6]

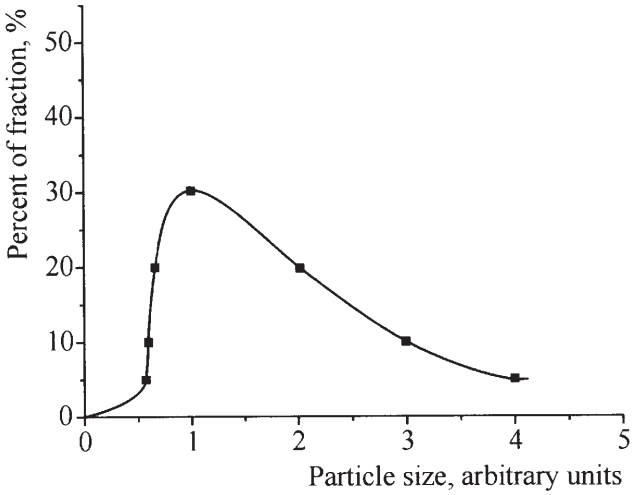

Fig. 3. The shape of the particle size distribution calculated using Eq. (15) and $H = 1$.

The shape of the particle size distribution curves can also be discussed.

The representative particle of a copper powder has the same specific surface as the powder,[5] meaning that the mass m of powder should have the same surface as mass m of the representative powder particles. It follows from the above fact that two equal portions of two fractions of the particles can have the same surface as the same quantity of representative powder particles. Hence,

$$S_1 + S_2 = 2S_r \tag{12}$$

or

$$S_{Sp1} + S_{Sp2} = 2S_{Sp} \tag{13}$$

where S_1, S_2 and S_r are the surfaces of mass m of particles 1, 2 and representative ones, respectively, and S_{Sp1}, S_{Sp2} and S_{Sp} are the corresponding values of specific surface. Taking into account Eq. (10a), Eq. (13) can be rewritten in the form:

$$\frac{1}{H_1}+\frac{1}{H_2}=\frac{2}{H} \tag{14}$$

assuming that ρ' is approximatly the same for all fractions as shown earlier,[7] where H_1 and H_2 are the sizes of the particles 1 and 2, respectively, and H is the size of the representative particle. It follows from Eq. (14) that:

$$H_1=\frac{H_2\times H}{2H_2-H} \tag{15}$$

which is valid for $H_2 > H$, if

$$H_1 < H < H_2 \tag{16}$$

Assuming that the large fraction of particles corresponds to the representative ones, it is now possible to calculate the shape of the particle size distribution curves, which is presented in Fig. 3. It is obvious that its shape is in perfect agreement with literature data.[1,6]

Acknowledgement: This work was supported by the Ministry of Sciences, Technology and Development of the Republic of Serbia under the research project "Electrodeposition of Metal Powders at a Constant and at a Periodically Changing Rate" (1806/2002).

ИЗВОД

НАСИПНА МАСА КАО ФУНКЦИЈА СПЕЦИФИЧНЕ ПОВРШИНЕ БАКАРНОГ ПРАХА И ОБЛИК ЗАВИСНОСТИ РАСПОДЕЛЕ ВЕЛИЧИНЕ ЧЕСТИЦА

КОНСТАНТИН И. ПОПОВ, ПРЕДРАГ М. ЖИВКОВИЋ и СНЕЖАНА Б. КРСТИЋ

Технолошко-металуршки факултет, Универзитет у Београду, п. пр. 35-03, Карнегијева 4, 11001 Београд

Утврђена је зависност између специфичне површине и насипне масе бакарног праха исталоженог електрохемијским поступком из киселог бакарног купатила. Показано је да је насипна маса обрнуто сразмерна специфичној површини бакарног праха. Размотрен је и облик зависности расподеле величина честица.

(Примљено 2. јуна 2003)

REFERENCES

1. A. Calusaru, *Electrodeposition of Metal Powders*, Elsevier, Amsterdam-Oxford-New York, 1979, p. 296
2. E. Peisseker, *J. of Powder Metallurgy and Powder Technology* **20** (1984) 27
3. K. I. Popov, N. D. Nikolić, Z. Rakočević, *J. Serb. Chem. Soc.* **67** (2002) 635
4. K. I. Popov, N. D. Nikolić, Z. Rakočević, *J. Serb. Chem. Soc.* **67** (2002) 769
5. K. I. Popov, N. D. Nikolić, Z. Rakočević, *J. Serb. Chem. Soc.* **67** (2002) 861
6. R. M. German, *"Powder Metallurgy Science"*, Metal Powde Industries Federation, Princeton, New Jersey, USA, 1994, p. 58
7. M. G. Pavlović, Lj. J. Pavlović, E. R. Ivanović, V. Radmilović, K. I. Popov, *J. Serb. Chem. Soc*. **66** (2001) 923.

J.Serb.Chem.Soc. 68(11)909(2003)

Errata

In the No. 8-9(2003) of this Journal the reference JSCS numbers in the upper left corner of all papers in this issue instead JSCS-3068–3078 should read JSCS-3077–3087, respectively.